# *Sco1* mouse models of human disease: a tool to investigate the role of mitochondria in the regulation of copper homeostasis

A Thesis Submitted to the College of Graduate and Postdoctoral Studies

in Partial Fulfillment of the Requirements

for the Degree of Doctor of Philosophy

in the Department of Biochemistry

University of Saskatchewan

Saskatoon

By

Zakery N. Baker

**PERMISSION TO USE**

In presenting this thesis in partial fulfillment of the requirements for a postgraduate degree from the University of Saskatchewan, I agree that the Libraries of this University may make it freely available for inspection. I further agree that permission for copying of this thesis in any manner, in whole or in part, for scholarly purposes may be granted by the professor or professors who supervised my thesis work or, in their absence, by the Head of the Department or the Dean of the College under which this thesis work was done. It is understood that any copying or publication or use of this thesis or parts thereof for financial gain shall not be allowed without my written permission. It is also understood that due recognition shall be given to me and the University of Saskatchewan in any scholarly use which may be made of any materials in my thesis.

Requests for permission to copy or to make other use of materials in this thesis in whole or part should be addressed to:

Dr. Scot C. Leary
Department of Biochemistry
Health Sciences Building, 107 Wiggins Road
University of Saskatchewan
Saskatoon, Saskatchewan S7N 5E5
Canada

OR

Dean
College of Graduate and Postdoctoral Studies
University of Saskatchewan
116 Thorvaldson Building, 110 Science Place
Saskatoon, Saskatchewan S7N 5C9
Canada

**ABSTRACT**

Copper is a vital micronutrient that impacts a variety of essential biochemical pathways within mammalian cells. Yet little is known about the homeostatic mechanisms that maintain intracellular copper levels or their relative importance across cell types. Recent evidence argues that copper handling pathways contained within the mitochondrion play an active role in the regulation of cellular copper homeostasis, as human patients with pathogenic mutations in the mitochondrial copper chaperone SCO1 exhibit tissue-specific deficits that are attributable in part to a severe copper deficiency. However, how the activity of mitochondrial copper handling pathways is functionally coupled to other cellular copper handling machinery and how this coupling impinges upon cellular copper sensing in general remains ill-defined. Developing an understanding of how the organelle is integrated into the functional framework that regulates copper homeostasis may be further challenged by the fact *SCO1* patients from three unique pedigrees present with drastically different, tissue-specific clinical phenotypes, suggesting that mitochondrial signalling through SCO1 to regulate copper homeostasis may exhibit cell type-specific features. To begin investigating these questions, we generated and characterized multiple transgenic *Sco1* models of human disease in which SCO1 function is perturbed in the heart and liver, two of the most affected tissues in *SCO1* patients. Deletion of *Sco1* in the liver was lethal and mice presented with a significant hepatopathy and hepatic steatosis. *Sco1* null hepatocytes had both an isolated COX deficiency as well as a severe copper deficiency, the latter of which was attributable to an increase in the degradation of the high-affinity copper transporter CTR1. Deletion of *Sco1* in the heart or striated muscle was also lethal with mice developing a dilated cardiomyopathy. Similar to the *Sco1* null livers, *Sco1* null hearts displayed a combined COX and copper deficiency; however, in the case of the *Sco1* null hearts, the copper deficiency was caused by the relocalization of CTR1 to intracellular vesicles rather than its degradation. To further examine the human condition, we also generated *Sco1* knock-in mice harbouring a G115S substitution, which in patients causes a fatal infantile hypertrophic cardiomyopathy. The heart of this knock-in mouse phenocopied the *Sco1* knockout heart, suggesting that both the null and knock-in models afforded one with the opportunity to investigate the underlying etiology of the associated human diseases. Collectively, my Ph.D. thesis data confirm that SCO1 fulfills an evolutionarily conserved role in maintaining cellular copper homeostasis and identify a novel role for the protein in regulating the function of the copper import machinery.

**ACKNOWLEDGMENTS**

I would like to thank my supervisor, Dr. Scot Leary, for all the help he has given me throughout my entire graduate program. The time and effort he put into push me to succeed and become a better scientist was invaluable to me getting to where I am today. I would also like to thank the members of the Leary lab, both past and present, for all the scientific discussions, technical help and general comradery; the members of my committee for taking the time to answer any questions and critically evaluate my progress; and all of our collaborators for donating their time and resources to advance our project. I would like to thank my parents for instilling in me a sense of curiosity and a drive to always continue learning, I would be nowhere without everything they have given me. Lastly, I would like to thank all my family and friends for the love and support they have given me and for believing in me when I didn't. PDMSBP.

## PERMISSION TO REPRODUCE

All previously published panels and figures contained within this document have been reproduced with permission from the journals in which they are published.

**Figure 1.2:** Schushan, M., Barkan, Y., Haliloglu, T., Ben-Tal, N. (2010). Cα-trace model of the transmembrane domain of human copper transporter 1, motion and functional implications. Proc. Natl. Acad. Sci. U.S.A. *107*, 10908-10913. doi: 10.1073/pnas.0914717107.

**Figure 3.1: Baker, Z.N.**, Cobine, P.A., and Leary, S.C. (2017). The mitochondrion: a central architect of copper homeostasis. Metallomics *9*, 1501–1512. doi:10.1039/c7mt00221a.

**Figures 4.1-4.8:** Hlynialuk, C.J.*, Ling, B.*, **Baker, Z.N.***, Cobine, P.A., Yu, L.D., Boulet, A., Wai, T., Hossain, A., El Zawily, A.M., McFie, P.J., et al. (2015). The mitochondrial metallochaperone SCO1 is required to sustain expression of the high-affinity copper transporter CTR1 and preserve copper homeostasis. Cell Rep. *10*, 933–943. doi:10.1016/j.celrep.2015.01.019

*co-first author

**Figures 4.9-4.20: Baker, Z.N.**, Jett, K., Boulet, A., Hossain, A., Cobine, P.A., Kim, B.-E., El Zawily, A.M., Lee, L., Tibbits, G.F., Petris, M.J., et al. (2017). The mitochondrial metallochaperone SCO1 maintains CTR1 at the plasma membrane to preserve copper homeostasis in the murine heart. Hum. Mol. Genet. 23, 4617–4628. doi:10.1093/hmg/ddx344.

**TABLE OF CONTENTS** **PAGE**

**PERMISSION TO USE** ..... i

**ABSTRACT** ..... ii

**ACKNOWLEDGEMENTS** ..... iii

**PERMISSION TO REPRODUCE** ..... iv

**LIST OF TABLES** ..... viii

**LIST OF FIGURES** ..... ix

**LIST OF ABBREVIATIONS** ..... xi

**1. INTRODUCTION** ..... 1

1.1 Copper in the human body ..... 1

1.1.1 Physiological roles of copper within the cell ..... 1

1.1.2 Import and export of copper across the plasma membrane ..... 2

1.1.3 Copper trafficking and storage within the cell ..... 7

1.1.4 Copper within the mitochondrion ..... 10

1.2 Assembly of COX $Cu_A$ site ..... 11

1.2.1 COX and the electron transport chain ..... 11

1.2.2 COX assembly factors ..... 15

1.2.3 Assembly of the $Cu_A$ site within COX2 ..... 17

1.2.4 The role of COX assembly factors in maintaining cellular copper homeostasis ..... 19

**2. RATIONALE AND OBJECTIVES** ..... 21

2.1 Rationale and Hypothesis ..... 21

2.2 Specific Objectives ..... 21

**3. MATERIALS AND METHODS** ..... 22

3.1 Generation of model organisms ..... 22

3.1.1 Generation and validation of tissue-specific *Sco1* knockout mice ..... 23

3.1.2 Generation and validation of *Sco1*$^{G115S/G115S}$ homozygous knock-in mice ..... 25

3.1.3 Animal husbandry and tissue collection ..... 25

3.2 Cell culture ..... 25

3.2.1 Generation of *Sco1* null mouse embryonic fibroblasts ..... 25

3.2.2 Transfection and retroviral transduction for protein overexpression ..... 26

3.3 Immunoblot Analysis.....26
3.3.1 Blue Native Polyacrylamide Gel Electrophoresis.....26
3.3.2 Denaturing Polyacrylamide Gel Electrophoresis.....26
3.3.3 Immunodetection of proteins.....28
3.4 Enzymatic Assays.....28
3.5 Elemental Analysis.....28
3.6 Lipid Analysis.....30
3.7 Immunohistochemistry, Immunofluorescence, and TEM imaging.....30
3.7.1 Tissue perfusion, fixation, and preparation.....30
3.7.2 Immunohistochemistry staining and imaging procedure.....30
3.7.3 Immunofluorescence protocol and imaging procedure.....31
3.8 Echocardiography.....32
3.9 Microarray and RT-PCR analysis.....32
3.10 Statistical Analysis.....33
**4. RESULTS**.....34
4.1 The role of SCO1 in maintaining cellular copper homeostasis in the murine liver.....34
4.1.1 Physiological characterization of liver-specific *Sco1* (*Sco1*$^{liv/liv}$) knockout mice.....34
4.1.1.1 Validation of liver-specific *Sco1* deletion.....34
4.1.1.2 Liver-specific deletion of *Sco1* is lethal with mice having a pronounced growth deficiency.....34
4.1.1.3 Livers from *Sco1*$^{liv/liv}$ mice have marked steatosis.....36
4.1.2 Molecular characterization of *Sco1*$^{liv/liv}$ mice.....36
4.1.2.1 Livers from *Sco1*$^{liv/liv}$ mice have a severe isolated COX deficiency and increase in mitochondrial content.....36
4.1.2.2 *Sco1*$^{liv/liv}$ mice have a severe hepatic copper deficiency that is accompanied by an increase in the levels of hepatic iron stored in Kupffer cells.....38
4.1.2.3 Copper deficiency in livers of *Sco1*$^{liv/liv}$ mice is driven by a progressive decrease in the abundance of the high affinity copper transporter CTR1.....40
4.1.3 Investigating the mechanism of mitochondrial copper signalling.....42
4.1.3.1 Decreased CTR1 abundance is mirrored in *Cox10* but not *Lrpprc* null livers.....42
4.1.3.2 *Sco1* null MEFs are copper deficient owing to enhanced proteasomal degradation of CTR1.....44

4.2 The role of SCO1 in maintaining cellular copper homeostasis in the murine heart..... 47

4.2.1 Physiological characterization of *Sco1*$^{hrt/hrt}$ mice..... 47

4.2.1.1 Validation of heart-specific *Sco1* deletion..... 47

4.2.1.2 Heart-specific deletion of *Sco1* is lethal with mice exhibiting left ventricular dilation and cardiomyocyte vacuolization..... 47

4.2.2 Molecular characterization of *Sco1*$^{hrt/hrt}$ mice..... 49

4.2.2.1 *Sco1* knockout hearts exhibit both a severe, isolated COX deficiency..... 49

4.2.2.2 *Sco1* knockout hearts have a modest copper deficiency that is not caused by a change in CTR1 abundance..... 49

4.2.2.3 The livers of *Sco1*$^{hrt/hrt}$ mice have a significant copper deficiency and a decrease in CTR1 abundance..... 49

4.2.3 Physiological characterization of *Sco1*$^{stm/stm}$ mice..... 52

4.2.3.1 Validation of striated muscle-specific *Sco1* deletion..... 52

4.2.3.2 *Sco1*$^{stm/stm}$ mice develop severe cardiomyopathy with significant fibrosis and enlarged cardiomyocytes..... 52

4.2.2.3 Echo-cardiogram of *Sco1*$^{stm/stm}$ hearts shows dilation of left ventricle..... 54

4.2.4 Molecular characterization of *Sco1*$^{stm/stm}$ mice..... 55

4.2.4.1 *Sco1*$^{stm/stm}$ mice have isolated COX deficiency combined with a deficiency in SOD1 activity..... 55

4.2.4.2 *Sco1*$^{stm/stm}$ mice have a severe copper deficiency not caused by a change in the abundance of CTR1..... 55

4.2.4.3 The combined COX and copper deficiencies progressively worsen with age..... 57

4.2.4.4 Copper deficiency in *Sco1*$^{stm/stm}$ hearts is caused by the mislocalization of CTR1..... 59

4.2.5 Characterization of a *Sco1*$^{G115S/G115S}$ knock-in mouse..... 59

**5. DISCUSSION**..... 65

**6. CONCLUSIONS**..... 73

**7. FUTURE DIRECTIONS**..... 75

**6. REFERENCES**..... 77

**LIST OF TABLES** **PAGE**

**Table 1.1: COX structural subunits**.....13

**Table 1.2: COX assembly factors**.....16

**Table 3.1: PCR primer list**.....24

**Table 3.3: Common buffer solutions**.....27

**Table 3.4: Primary antibodies used**.....29

**LIST OF FIGURES** **PAGE**

**Figure 1.1: Free radical generation through the Harber-Weiss Reaction.....** 2

**Figure 1.2: Topology of human CTR1.....**3

**Figure 1.3: Pathways of mammalian mitochondrial copper acquisition and trafficking.....**9

**Figure 1.4: Electron flow through the catalytic core of cytochrome *c* oxidase.....**13

**Figure 1.5: COX assembly pathway.....** 14

**Figure 1.6: Relative roles of SCO1 and SCO2 in the metallation of the $Cu_A$ site.....**18

**Figure 1.7: Location of critical amino acids within SCO1.....** 20

**Figure 3.1: Cre-lox deletion scheme for *Sco1*.....** 23

**Figure 4.1: Deletion of *Sco1* in the liver is lethal and presents with a severe growth deficiency.....** 35

**Figure 4.2: Liver-specific knockout of *Sco1* results in severe steatosis.....** 37

**Figure 4.3: Deletion of *Sco1* in the liver causes an isolated COX deficiency.....** 38

**Figure 4.4: Deletion of *Sco1* in the liver causes a hepatic copper deficiency.....** 39

**Figure 4.5: Deletion of *Sco1* in the liver causes a change of localization and a decrease in the abundance of CTR1.....** 41

**Figure 4.6: Changes in CTR1 abundance are not correlated with a general energy deficiency.....** 43

**Figure 4.7: Deletion of *Sco1* in mouse embryonic fibroblasts results in a decrease of CTR1 abundance.....**45

**Figure 4.8: CTR1 abundance in MEFs is rescued by the proteosome inhibitor MG132.....** 46

**Figure 4.9: Deletion of *Sco1* in the heart is lethal and presents with dilated cardiomyopathy.** 48

**Figure 4.10: Deletion of *Sco1* in the heart causes an isolated COX deficiency.....** 50

**Figure 4.11: Deletion of *Sco1* in the heat causes a mild copper deficiency.....**51

**Figure 4.12: Deletion of *Sco1* in the striated muscle is lethal and presents with cardiomyopathy.....** 53

**Figure 4.13: Deletion of *Sco1* in the striated muscle causes dilated cardiomyopathy.....** 54

**Figure 4.14: Deletion of *Sco1* in the striated muscle causes an isolated COX deficiency.....** 56

**Figure 4.15: Copper and COX deficiencies in striated muscle-specific *Sco1* knockout mice get progressively worse over time.....** 58

**Figure 4.16: Deletion of *Sco1* in the striated muscle causes the mislocalization of CTR1 in cardiomyocytes.....** 60

**Figure 4.17: Mislocalized CTR1 in the hearts of striated muscle-specific mice co-localizes with Rab5**..... 61

**Figure 4.18: Mislocalized CTR1 does not co-localize with EEA1 or LAMP1**..... 62

**Figure 4.19: Mice harboring G115S homozygous mutation in *Sco1* phenocopy the striated muscle-specific *Sco1* knockout mice**..... 63

**Figure 4.20: CTR1 in G115S homozygous knock-in mice is mislocalized from plasma membrane**..... 64

**Figure 6.1: Deletion of *Sco1* causes changes in CTR1 localization and abundance**..... 74

**LIST OF ABBREVIATIONS**

| | |
|---|---|
| CCS | Copper chaperone for superoxide dismutase |
| Ch | Cholesterol |
| COA | Cytochrome *c* oxidase assembly |
| COX | Cytochrome *c* oxidase |
| CS | Citrate synthase |
| CTR1 | Copper transporter 1 |
| ES | Embryonic stem cell |
| ETC | Electron transport chain |
| FA | Fatty acid |
| GSH | Glutathione |
| H&E | Hematoxylin and Eosin |
| ICP-OES | Inductively couple plasma optical emission spectrometry |
| IF | Immunofluorescence |
| IHC | Immunohistochemistry |
| LC-MS | Liquid chromatography – mass spectrometry |
| MEF | Mouse embryonic fibroblast |
| OXPHOS | Oxidative phosphorylation |
| PAGE | Polyacrylamide gel electrophoresis |
| PBS | Phosphate buffered saline |
| PCR | Polymerase chain reaction |
| PFA | Paraformaldehyde |
| RIPA | Radioimmunoprecipitation assay buffer |
| SCO | Synthesis of cytochrome *c* oxidase |
| SDS | Sodium dodecyl sulphate |
| SOD | Superoxide dismutase |
| TBST | Tris buffered saline with 0.05% Tween 20 |
| TEM | Transmission electron microscope |
| TM | Transmembrane |

# 1.0 INTRODUCTION

## 1.1 Copper in the human body

### 1.1.1 Physiological roles of copper within the cell

Copper is an essential dietary micronutrient required by all five kingdoms of life. The essentiality of copper comes from its ability to rapidly switch between two redox states, from $Cu^{+1}$ to $Cu^{+2}$, which allows the metal ion to accept and donate electrons and therefore contribute to oxidation-reduction reactions. Cells exploit this ability, utilizing copper as a structural or catalytic cofactor in enzymes which catalyze a multitude of reactions involved in maintaining cellular homeostasis (Kim et al., 2008). In humans, multiple, well-characterized cuproenzymes exist including cytochrome *c* oxidase (electron transport chain complex) (Timón-Gómez et al., 2017), superoxide dismutase (removal of toxic free radicals) (Robinson and Winge, 2010), dopamine β-hydroylase (norepinephrine biosynthetic pathway) (Lutsenko et al., 2010), lysyl oxidase (collagen crosslinking) (Finney et al., 2014), tyrosinase (pigment formation) (Ramsden and Riley, 2014), as well as multiple enzymes involved in maintaining proper iron homeostasis (ceruloplasmin, hephaestin, zyklopen) (Vashchenko and MacGillivray, 2013). Copper also fulfills other, more direct roles within the cell and is crucial to innate immunity (Festa and Thiele, 2012), oncogenesis (Brady et al., 2014), and signal transduction (Krishnamoorthy et al., 2016), all of which are relatively new and prominent topics in the field.

Despite the fact copper is essential for proper cell growth and function, it is toxic in excess. Excess, or mishandled, copper can potentiate the production of dangerous oxidative molecules through Haber-Weiss and Fenton-like reactions (Figure 1.1). These oxidative molecules, which include superoxide or hydrogen peroxide, are highly reactive and can induce oxidative damage to nucleic acids, proteins and lipids thereby disrupting cellular functions (Stohs and Bagchi, 1995). Although elevated free radical generation is still a prevalent issue in copper overloaded cells (Jomova and Valko, 2011), recent studies suggest that the primary cause of copper toxicity reflects its ability to displace iron from iron-sulphur cluster containing proteins leading to their inactivation (Brancaccio et al., 2017; Macomber and Imlay, 2009). Iron-sulphur clusters are key catalytic co-factors for several proteins with critical roles in cellular homeostasis and their loss of function is extremely detrimental to cell viability (Lill, 2009). These two sides of copper, how it is essential for life but toxic in excess, make the homeostatic regulation of the metal ion important. The mechanisms involved in maintaining copper homeostasis are therefore discussed below.

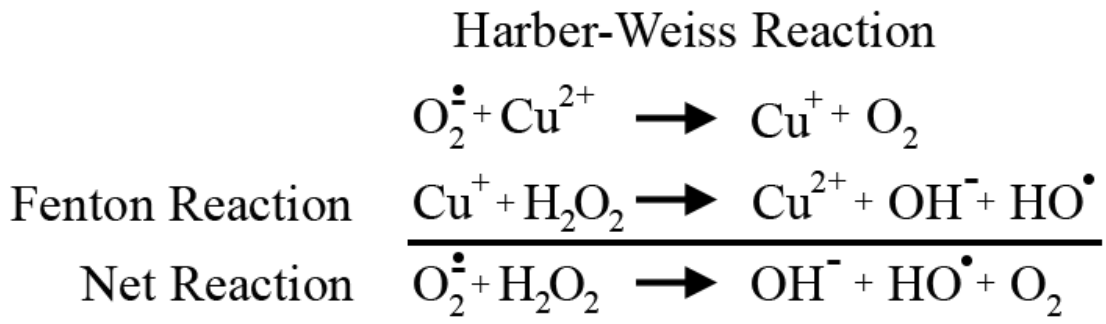


**Figure 1.1: Free radical generation through the Harber-Weiss Reaction**
By switching between two redox states ($Cu^{2+}$ and $Cu^{+}$) copper can catalyze the generation of free radicals, such as the hydroxyl radical shown here, through Fenton and Harber-Weiss reactions.

### 1.1.2 Import and export of copper across the plasma membrane

The most logical place to begin the discussion of copper homeostasis is import of the metal ion into the cell. Copper uptake into the eukaryotic cell is mediated predominantly by the evolutionarily conserved protein CTR1, the only known high affinity copper importer in mammals (Dancis et al., 1994; Zhou and Gitschier, 1997). Although other, low affinity mechanisms exist for copper import (Kidane et al., 2012; Lee et al., 2002), they are ill-defined and unable to fully compensate for loss of CTR1 function as *Ctr1* deletion in the mouse is embryonic lethal (Lee et al., 2001). CTR1 functions as a homotrimer, with each monomer consisting of a 190-amino acid protein with 3 transmembrane regions (Figure 1.2) (Lee et al., 2002). These monomers interact through their extracellular N-termini, effectively forming a pore to facilitate copper transport across the plasma membrane (Aller and Unger, 2006; De Feo et al., 2009; Klomp et al., 2003; Schushan et al., 2010). Functional characterization of CTR1 deletion mutants in yeast and mammalian cells identified a conserved $Mx_3M$ motif within the second transmembrane domain which is not involved in localizing the protein to the plasma membrane but is essential for copper transport (Guo et al., 2004; Puig et al., 2002). It is thought that this $Mx_3M$ motif functions as a copper-binding site, with the methionine residues acting as soft Lewis bases to facilitate copper transport across the membrane. Although not essential, other N-terminal extracellular motifs have also been shown to influence the kinetics of copper transport. Deletion of one of the two conserved MxxMxM motifs in CTR1 does not completely abolish copper transport but prevents it from rescuing the growth defect of a *Δctr1* yeast strain under copper-depleted conditions, suggesting this motif has a role in high affinity uptake (Puig et al., 2002).

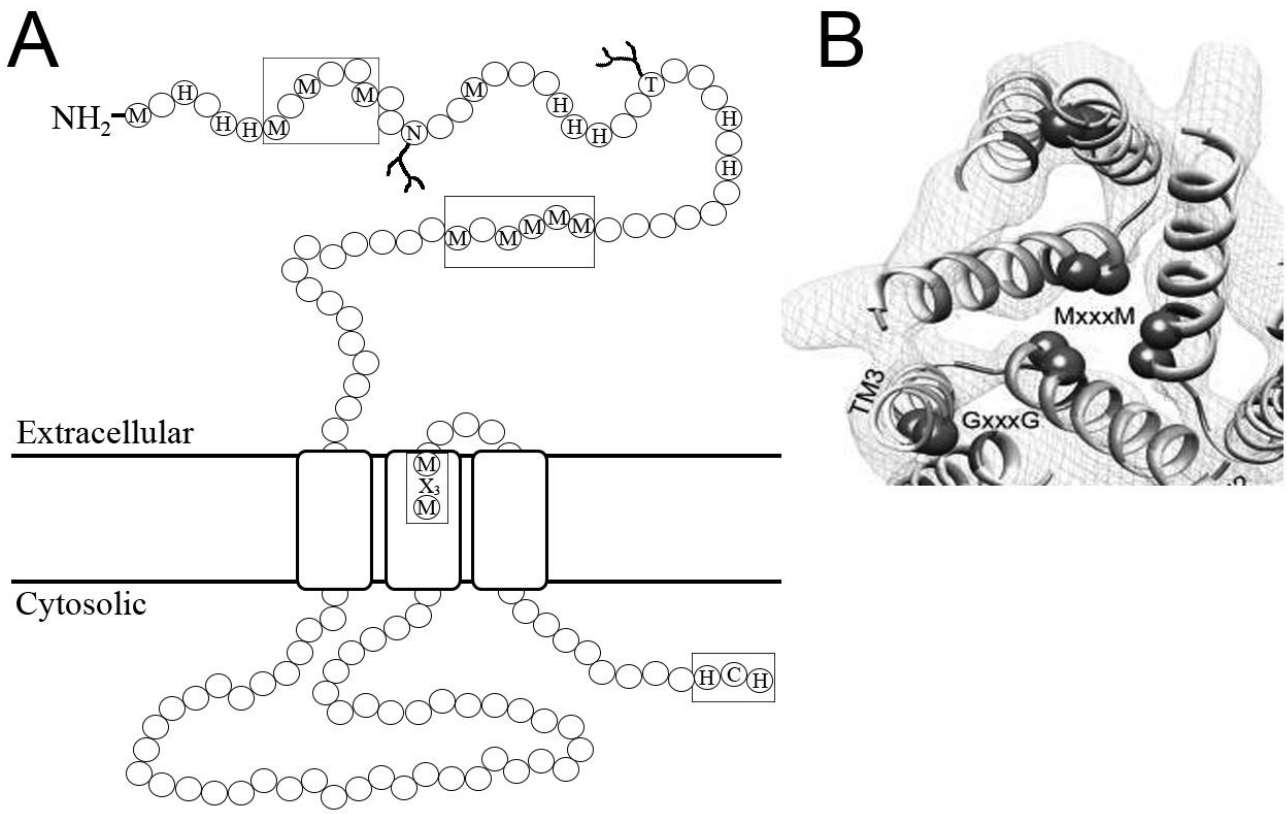


**Figure 1.2: Topology of human CTR1**
(A) Diagram of a topological model of human CTR1 (hCTR1). Critical motifs discussed in text are noted in boxes. hCTR1 has 3 transmembrane domains (TM1-3), the second of which contains the $Mx_3M$ motif which is critical for binding copper and allowing import across the membrane. The N-terminus of hCTR1 contains histidine (H) and methionine (M) rich regions, and the two MxMxxM motifs that are critical for binding copper and allowing for high-affinity import of the ion. The C-terminal HCH motif is involved in the regulation of copper import. There are two glycosylation events at the N-terminal region of the protein, at N15 and T27, noted with black branches. (B) A model of the pore formed by hCTR1 trimer that facilitates copper transport, as determined by cryo-electron microscopy. (Figure adapted from Schushan et al., 2010.)

Under conditions of copper excess, CTR1 is removed from the plasma membrane to limit a further increase in intracellular copper concentrations (Petris et al., 2003). This copper-mediated endocytosis of CTR1 is dependent on copper transport, as the $Mx_3M$ mutant is constitutively localized to the plasma membrane independent of the extracellular copper concentration (Guo et al., 2004). Similarly, the localization of the MxxMxM mutant is unresponsive to mild copper excess (Puig et al., 2002). These data collectively suggest that cellular copper sensing does not occur extracellularly and that the critical residues of CTR1 involved in stimulating copper-mediated endocytosis are localized on the cytosolic face of the plasma membrane. Consistent with this idea, deletion of the copper-binding intracellular HCH motif has been shown to abolish copper-mediated endocytosis while increasing copper transport activity (Maryon et al., 2013a). In fact, deletion and point mutants of this HCH motif are highly sensitive to increases in extracellular copper concentrations suggesting that these residues are critical for the regulation of copper homeostasis (Maryon et al., 2013a). Under prolonged conditions of copper excess, endocytosed CTR1 is degraded (Petris et al., 2003) or maintained within the cytosol on recycling endosomes to allow for its eventual return to the plasma membrane upon normalization of intracellular copper concentrations (Clifford et al., 2016; Molloy and Kaplan, 2009). Despite the fact copper driven endocytosis of CTR1 is a well-characterized phenomenon, little is known about the associated regulatory mechanisms or the cell-type specific differences in inputs that determine whether internalized CTR1 is degraded or trafficked within recycling endosomes.

Like many other plasma membrane transporters, CTR1 function is heavily influenced by several post-translational modifications (PTMs). The first PTM during its maturation is an N-linked glycosylation event at the Asn15 residue, which shifts the apparent molecular weight of CTR1 from 21 kDa to ~30 kDa. Although this glycosylation step is conserved in mammals, mutating the conserved asparagine does not affect the trafficking of the protein to the plasma membrane or high-affinity copper import (Klomp et al., 2002; Maryon et al., 2007). The second PTM is an O-linked glycosylation event at Thr27 which induces a more modest ~2 kDa shift in the apparent molecular weight of CTR1 (Maryon et al., 2007). Glycosylation at this residue has been shown to protect the N-terminal ectodomain of CTR1 from targeted proteolytic cleavage, which results in a truncated version of the protein of ~17 kDa (Maryon et al., 2007, 2009). The exact location of this cleavage site in human CTR1 was first reported to be between residues 29–33 (ASHSH), based primarily on the different in-gel migration pattern of relevant point mutants (Maryon et al., 2009). Recently, however, liquid chromatography-mass spectrometry (LC-MS) analysis of both the human and murine forms of

truncated CTR1 identified multiple cleavage events within the ectodomain at the methionine residues at positions 40, 41, 42, and 45 (Öhrvik et al., 2013). The truncated version of CTR1 traffics primarily to late endosomes with a lower rate of copper transport (Maryon et al., 2007) and its endosomal localization depends on the homologous CTR2 protein, which functions to recruit the full-length CTR1 protein to the protease cathepsin L to promote its cleavage (Öhrvik et al., 2013). Notably, copper accumulates in punctate structures within both the brains of mice lacking CTR2 and *Ctr2* knockout MEFs, both of which lack the truncated form of CTR1. This has led to the suggestion that the truncated form of CTR1 may play a role in releasing endosomal copper stores (Öhrvik et al., 2013; Öhrvik et al., 2016).

The P-type ATPases ATP7A and ATP7B are involved in both the metallation of secreted cuproproteins and copper export from the cell. Mutations in *ATP7A* and *ATP7B* disrupt protein function and cause Menkes and Wilson disease respectively, fatal clinical conditions in which patients experience marked tissue-specific perturbations in copper homeostasis (Chelly et al., 1993; Mercer et al., 1993; Petrukhin et al., 1994; Vulpe et al., 1993). ATP7A and ATP7B are integral membrane proteins of 180 and 160 kDa and share significant sequence identity, each having eight transmembrane domains and 6 cytosolic N-terminal, metal-binding domains containing conserved MxCxxC motifs (Lutsenko et al., 2007). Both P-type ATPases localize primarily to the *trans*-Golgi network (TGN), where they serve to transport copper across the lumen of the Golgi for the metallation of secreted cupro-proteins like ceruloplasmin (Schaefer et al., 1999; Yamaguchi et al., 1996). Their ability to transport copper involves initial binding of the metal ion by a CPC motif and active coupling of ATP hydrolysis within the ATP binding domain to create a phosphorylated intermediate. This phosphorylation event induces a conformational change in the protein that then enables the release of the copper ion on the obverse side of the membrane (Petris et al., 2002).

Despite their high degree of homology, ATP7A and ATP7B fulfill unique functions within mammals. Both proteins exhibit opposing localization patterns (apical vs. basolateral) during copper-stimulated trafficking in polarized epithelial cells (Braiterman et al., 2009; Greenough, 2004). ATP7B also exhibits a restricted expression profile relative to ATP7A, and is most readily detectable in the liver, kidney, brain, epithelial cells and eyes (Wang et al., 2011). One of the most widely recognized and well-characterized functions of ATP7B is the export of excess copper into the bile. Under conditions of hepatic copper excess, the localization of ATP7B in hepatocytes shifts from the TGN to the apical canalicular membrane (Yamaguchi et al., 1996), an event that requires a highly conserved stretch of 9 amino acids (Braiterman et al., 2009). Near the canalicular membrane, ATP7B interacts

with lysosomes, pumping excess copper into the lysosomal lumen (Polishchuk et al., 2014). These lysosomes then undergo exocytosis from the canalicular membrane thereby releasing copper into bile for its subsequent excretion from the body in the feces (Polishchuk et al., 2014).

ATP7A is more widely expressed across tissues than ATP7B, and is therefore responsible for metallating the majority of secreted proteins within the body (Wang et al., 2011). ATP7A also functions to pump copper across membranes to supply it to peripheral tissues. This is perhaps best illustrated by the intestinal enterocyte, which utilizes apically localized CTR1 to absorb dietary copper and basally localized ATP7A to promote its subsequent release into the portal circulation (Nevitt et al., 2012). However, ATP7A is also involved in copper transport across the blood-cerebrospinal fluid barrier into the cerebrospinal fluid and copper export from the kidneys. Therefore, mutations that affect ATP7A function cause severe changes in the physiological concentrations of copper in the brain and kidney (Yoshimura et al., 1995) as well as the intestinal enterocyte (Danks et al., 1973). To facilitate copper transport under both normal and excess copper conditions, a percentage of the total pool of ATP7A protein re-localizes from the TGN to the plasma membrane and cytoplasmic vesicles (Petris et al., 1996, 2002). Dynamic ATP7A trafficking depends on its ability to transport copper, and point mutations that compromise this property abolish its regulated redistribution to the cellular periphery (Petris et al., 2002; Voskoboinik et al., 2003). Additional structure-function studies established that at least one of the $5^{th}$ or $6^{th}$ N-terminal metal binding sites is required for ATP7A trafficking to the plasma membrane (Strausak et al., 1999), and a C-terminal di-leucine motif is essential for TGN recycling (Petris and Mercer, 1999). Although a change in ATP7A localization to the cellular periphery is required for copper export, whether export occurs via direct pumping of the metal ion across the plasma membrane or through copper loading of vesicles which are then exocytosed is unknown.

Patients suffering from Menkes disease exhibit copper overload within the intestine due to compromised export into the general circulation which in turn produces a severe copper deficiency in most peripheral tissues (Danks et al., 1973; Kaler, 2013). This peripheral copper deficiency results in loss of copper-dependent enzyme activities and leads to severe neurological defects. Currently there is no cure for Menkes disease; however, subcutaneous and intracardiac injections of copper into the blood stream can help delay the onset of neurological symptoms in some patient backgrounds (Kaler et al., 2008). As the predominant function of ATP7B is to pump excess copper into the bile, hepatic copper overload and eventual toxicosis is a primary symptom of Wilson disease patients (Kaler, 2013).

Treatment for Wilson disease involves chelation therapy, a strategy in which copper within the blood and tissues is bound to promote its subsequent excretion (Bandmann et al., 2015).

### 1.1.3 Copper trafficking and storage within the cell

The toxic properties of copper necessitate that the bioavailability of the metal ion be tightly controlled and it is estimated that on average there is less than one free copper atom per cell (Rae et al., 1999). To regulate the amount of free intracellular copper while allowing for its proper trafficking, the metal ion is typically bound to peptides or proteins including glutathione (GSH), metallothioneins or other dedicated chaperones (Prohaska and Gybina, 2004). The first of these, the tripeptide GSH, is the major determinant of redox balance within the cell, as in its reduced form GSH can act as an electron donor to neutralize dangerous oxidative molecules from the cellular environment (Valko et al., 2006). GSH also binds to and sequesters copper *in vivo* to prevent copper toxicity, and its cellular concentration actually increases under conditions of copper overload (Freedman et al., 1989). Fitting with a role in maintaining cellular copper homeostasis, GSH is required for copper import into the cell (Maryon et al., 2013b), and a *Drosophila melanogaster* model with genetically depleted GSH levels in neurons has a lethal phenotype, with flies exhibiting unexpanded wings and decreases in axon branching, characteristics reminiscent of a copper deficient phenotype (Mercer et al., 2016). Further, the lethal phenotype is partially rescued with copper supplementation and exasperated by the knockdown of *Ctr1* (Mercer et al., 2016). The second protein involved in the sequestration of cellular copper is the low molecular weight protein metallothionein. Mammals express multiple forms of metallothionein that vary in size; however, they all contain multiple, cysteine rich motifs which are used to bind copper and other heavy metals (Hamer, 1986). Like GSH, metallothionein expression is increased under conditions of copper excess (Freedman et al., 1989; Fürst et al., 1988) to buffer against copper toxicity, and mice lacking both metallothionein I and II have a much lower LD(50) for copper than wild-type littermates indicating an increase in copper sensitivity (Park et al., 2001).

The last and most important class of copper-binding proteins is comprised of dedicated chaperones, which bind copper and deliver it to specific proteins that require the metal ion for their function. The yeast protein ATX1 was the first of these proteins to be discovered (Klomp et al., 1997; Lin and Culotta, 1995; Lin et al., 1997). Both ATX1 and its human homolog ATOX1 have since been shown to play direct and important roles in oxidative defence (Hatori et al., 2012; Lin and Culotta, 1995). However, their primary function is to deliver copper to the P-type ATPases ATP7A and ATP7B for subsequent maturation of secreted cuproenzymes. Consistent with this idea, both *atx1Δ* yeast and

*Atox1* knockout mice display significant decreases in the activity of extracellular cuproenzymes (Hamza et al., 2001; Lin et al., 1997). Under high copper conditions ATOX1 can also form a dimer and re-localize to the nucleus (Itoh et al., 2008), where it binds to ATOX1-specific promoter elements and transactivates the expression of genes encoding factors involved in cell proliferation (*Cyclin D*) and the removal of free radicals (*Sod3)* (Itoh et al., 2008, 2009). Translocation of the ATOX1 dimer through the nuclear pore is conceivable given that its mass is 14.8kDa, and the pore can accommodate proteins of up to 60 kDa (Wang and Brattain, 2007).

The copper chaperone for superoxide dismutase (CCS) is another dedicated copper chaperone within the cell. CCS has two known functions; to deliver copper within the cytosol to the Cu/Zn form of superoxide dismutase, SOD1, and to catalyze the formation of a critical intramolecular disulphide bond within SOD1. Both SOD1 metallation and disulphide bond formation are not essential for protein stability (Bartnikas and Gitlin, 2003), but are needed for proper protein folding and catalytic competence (Culotta et al., 1997; Furukawa et al., 2004). CCS is also localized to the mitochondrial intermembrane space (IMS) where it similarly promotes the maturation of a small but physiologically significant fraction of SOD1 (Sturtz et al., 2001). Interestingly, the abundance of CCS depends on the bioavailability of copper, with CCS protein levels being inversely correlated with dietary copper levels (Bertinato et al., 2003; Prohaska et al., 2003). Copper-dependent regulation of CCS abundance is maintained in a fibroblast *CCS* overexpression model with changes in extracellular copper concentrations (Caruano-Yzermans et al., 2006), suggesting that the regulation of CCS abundance occurs post-translationally. Fitting with this model, treatment of cells with the proteasome inhibitor MG132 prevented the degradation of CCS even upon culture in high copper conditions (Caruano-Yzermans et al., 2006). With the abundance of CCS being so tightly correlated with cellular copper status, the protein is thought to be a reliable biomarker of copper availability (West and Prohaska, 2004), and CCS abundance within erythrocytes can be used as a sensitive measure of copper deficiency (Lassi and Prohaska, 2011, 2012).

The mitochondrial protein COX17 is at the head of a pathway of copper chaperones within the organelle that function collectively to deliver and insert copper into cytochrome *c* oxidase (COX), the terminal enzyme of the electron transport chain. How copper chaperones deliver copper to COX and how this pathway is tied to the regulation of copper homeostasis will be discussed below.

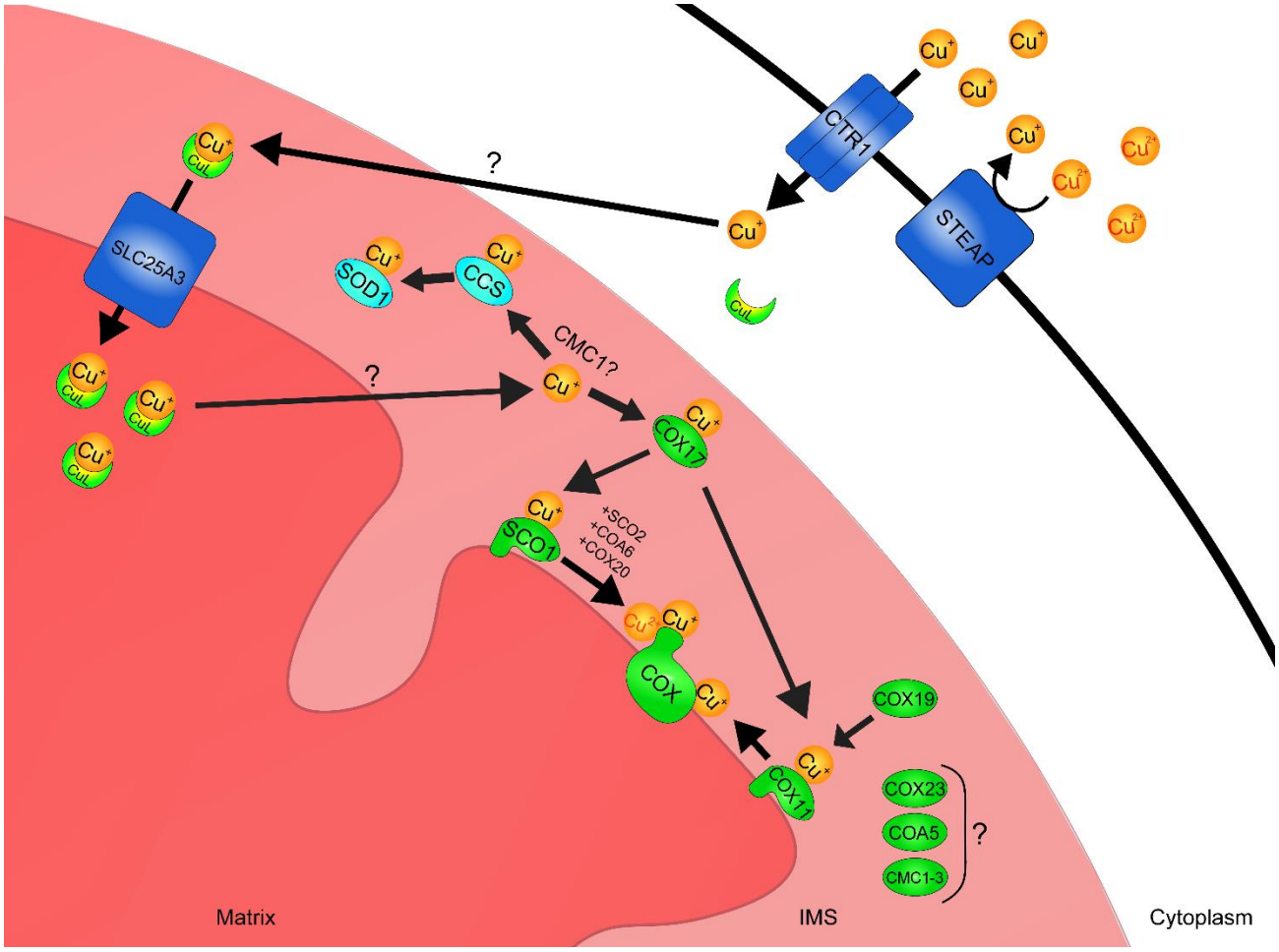


**Figure 1.3: Pathways of mammalian mitochondrial copper acquisition and trafficking**
Dietary copper ($Cu^{2+}$) is reduced extracellularly by a member of the STEAP family of oxidoreductase proteins. The high affinity copper transporter CTR1 can then transport the reduced cuprous ($Cu^{+}$) ion across the plasma membrane into the cytosol. Copper is targeted to the mitochondria via an unknown mechanism, however, the ion is bound to an unidentified organic ligand (CuL) within the cytosol which is thought to facilitate its transport across the inner-mitochondrial membrane into the matrix. This mitochondrial copper import is accomplished by SLC25A3, the mammalian homolog of the yeast phosphate transporter Pic2. Matrix copper is pumped back into the IMS and is used to metallate the cuproenzymes that reside there, COX and SOD1. This metallation occurs through protein specific chaperones such as CCS, COX17, SCO1, and COX11. Despite the characterization of these copper handling pathways there exist many other mitochondrial proteins known to be involved in COX assembly which have unknown functions but may involved in protein metallation, including COX23, COA5 and CMC1-3. (Figure from Baker et al., 2017)

### 1.1.4 Copper within the mitochondrion

In addition to copper trafficking pathways, the cell can store the metal ion in concentrated labile pools, one of which is localized to the mitochondrial matrix (Figure 1.3) (Cobine et al., 2004; Leary et al., 2009). Fitting with a role in sequestration of copper, the mitochondrial copper pool is dynamic in nature and can expand during cellular copper overload, presumably protecting the rest of the cell from copper toxicity (Bhattacharjee et al., 2016; Cobine et al., 2004). The storage capacity within the organelle is not limitless, however, as patients with Wilson disease who accumulate high amounts of hepatic mitochondrial copper exhibit severe perturbations in mitochondrial ultrastructure and function (Roberts et al., 2008; Sternlieb, 1968; Zischka and Lichtmannegger, 2014). Symptoms attributable to supranormal levels of mitochondrial copper are reversible upon treatment with methanobactin, a copper chelator capable of reducing the amount of copper contained within the organelle (Lichtmannegger et al., 2016). The mitochondrial matrix copper pool is used to metallate the two known cuproenzymes within the IMS, SOD1 and COX, and its targeted depletion greatly reduces the activity of both enzymes (Cobine et al., 2006a). These enzymes are critical for proper cellular function and, as such, the cell places a premium importance on maintaining adequate levels of mitochondrial copper under whole cell copper deficiency (Dodani et al., 2011; Hlynialuk et al., 2015), even at the expense of other organelles (Merchant and Bogorad, 1986; Merchant et al., 2006).

How copper is delivered to the mitochondrion is unknown. The COX assembly factor COX17 was previously hypothesized to perform this function, as it is known to partition between both the cytosol and IMS in yeast and humans (Glerum et al., 1996; Oswald et al., 2009); however, a *cox17Δ* yeast strain has normal mitochondrial copper levels and strains expressing a version of COX17 tethered to the inner mitochondrial membrane have wild-type levels of COX and IMS-SOD1 activity (Cobine et al., 2004; Maxfield et al., 2004). Independent of the mechanisms that deliver copper to the organelle, its storage within the matrix requires at least one transporter owing to the impermeability of the inner mitochondrial membrane. Recently, studies in yeast have implicated the mitochondrial carrier family proteins Pic2 and Mrs3 as copper transporters (Vest et al., 2013, 2016). Although Pic2 and Mrs3 are known phosphate and iron transporters respectively, each also exhibits copper transport activity *in vitro* (Vest et al., 2016). Furthermore, a double *pic2Δmrs3Δ* yeast strain has greatly reduced mitochondrial copper stores and a deficiency in COX and IMS-SOD1 activities (Vest et al., 2016). The closest human orthologue to yeast Pic2, SLC25A3, can rescue copper transport in *pic2Δ* yeast strains, suggesting that this mechanism for mitochondrial copper transport is evolutionarily conserved (Boulet et al., 2017). Fittingly, SLC25A3 knockdown or deletion in mouse

or human fibroblasts results in an isolated COX deficiency, which can be rescued with the addition of excess copper to the media (Boulet et al., 2017). Copper within the mitochondrial matrix is bound to an as of yet unidentified anionic ligand and it is thought that formation of the copper ligand complex promotes its translocation across the inner mitochondrial membrane (Cobine et al., 2004). How copper is exported back into the IMS, where it then interacts with specific chaperones required for copper delivery to SOD1 and COX is unknown.

## 1.2 Assembly of the COX $Cu_A$ site

### 1.2.1 COX and the electron transport chain

The conversion of nutrients to a usable form of energy is essential for all living organisms. Ultimately, the primary goal of this conversion process is to generate ATP, the energy currency within the cell. Hydrolysis of ATP to ADP releases substantial amounts of free energy that can then be coupled to unfavourable endergonic reactions. The bulk of ATP is generated within the mitochondrion where reducing equivalents generated through catabolism supply electrons that are subsequently transferred through the complexes of the electron transport chain (ETC). These redox reactions are in turn coupled to the transport of protons from the mitochondrial matrix to the IMS to generate the proton motive force that is ultimately harnessed by ATP synthase (Complex V) to convert ADP into ATP. The ETC consists of 4 enzymatic complexes: NADH dehydrogenase (Complex I), Succinate Dehydrogenase (Complex II), Ubiquinone:Cytochrome *c* oxidoreductase (Complex III) and Cytochrome *c* oxidase (COX/Complex IV).

COX is the final complex of the ETC and catalyzes the transfer of electrons from cytochrome *c* to molecular oxygen to produce water while simultaneously pumping protons across the mitochondrial inner membrane. COX is a multimeric protein complex and assembly of the holoenzyme is a complicated process. In mammals, COX contains 14 subunits that are encoded by both the mitochondrial and nuclear genomes (Table 1.1). Three of its subunits, COX1-3, are conserved from α-proteobacteria and are encoded by the mitochondrial genome. These proteins represent the catalytic core of the holoenzyme and contain the metal co-factors required for catalytic competence; two heme groups (heme *a* and $a_3$) and two copper sites ($Cu_A$ and $Cu_B$). The binuclear $Cu_A$ site is located within the IMS in a solvent exposed portion of COX2 and it is involved in the first step of catalysis, accepting electrons upon the oxidation of cytochrome *c* (Figure 1.4). Electrons are transferred sequentially to the heme *a* group within the transmembrane domain of the COX1 subunit, then to the binuclear $Cu_B$:heme $a_3$ centre, and finally to an oxygen molecule on the matrix side of the membrane. The 11

nuclear-encoded subunits represent the “structural” subunits of the holoenzyme. These proteins act as a protective structural scaffold to stabilize the catalytic core of the enzyme, offer regulatory sites for the allosteric modulation of COX activity (Acin-Perez et al., 2011) and provide physical interfaces for interactions with other ETC enzymes that allows for the formation of respiratory super-complexes (Ikeda et al., 2013). Many of these nuclear-encoded subunits also have tissue-specific isoforms and can undergo post-translational modifications which affect COX function and add further regulatory complexity to the system (Kadenbach and Hüttemann, 2015).

With so many variable components from different sources, the assembly of the COX holoenzyme is an increasingly complex process that is constantly being updated. Currently, COX assembly is believed to occur in a linear and modular hybrid model (Timón-Gómez et al., 2017). The catalytic subunits of the holoenzyme (COX1-3) are matured as individual modules, which requires their insertion into the membrane, the addition of their metal co-factors and in some cases the incorporation of a subset of additional, nuclear-encoded COX subunits. These subassembly modules are subsequently integrated into a linear pipeline in which the remaining structural subunits are added sequentially to yield the fully functional COX holoenzyme (Figure 1.5). The complex assembly of the COX holoenzyme is facilitated by a large number of proteins termed COX assembly factors.

**Table 1.1: COX structural subunits**

List of all known mammalian COX subunits. COX1-3 make up the catalytic core of the enzyme and are encoded within the mitochondrial genome. The other 11 subunits are structural subunits, encoded within the nuclear genome and imported into the mitochondria for assembly.

| CORE COX SUBUNITS |
|---|
| COX1 |
| COX2 |
| COX3 |
| STRUCTURAL SUBUNITS |
| COX4 |
| COX5A |
| COX5B |
| COX6A |
| COX6B |
| COX6C |
| COX7A |
| COX7B |
| COX7C |
| COX8 |
| NDUFA4 |

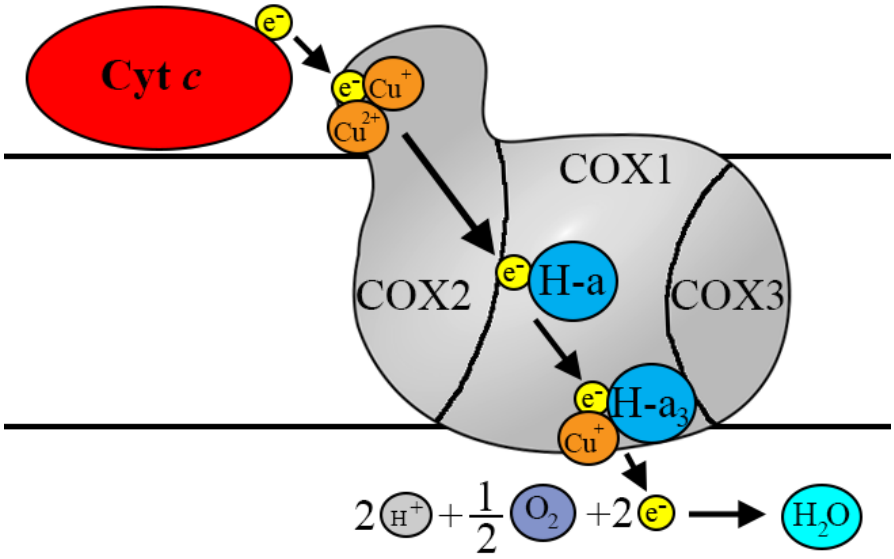


**Figure 1.4: Electron flow through the catalytic core of cytochrome *c* oxidase**
Cytochrome *c* oxidase (COX) collects an electron through the oxidation of cytochrome *c*. This electron is first received by the binuclear $Cu_A$ site in the IMS portion of the COX2 subunit. From here the electron is passed to the Heme a group, and then to the binuclear Heme-$a_3$: $Cu_B$ site both of which are located within the COX1 subunit. Finally, the electron is passed to reduce molecular oxygen and generate a molecule of water.

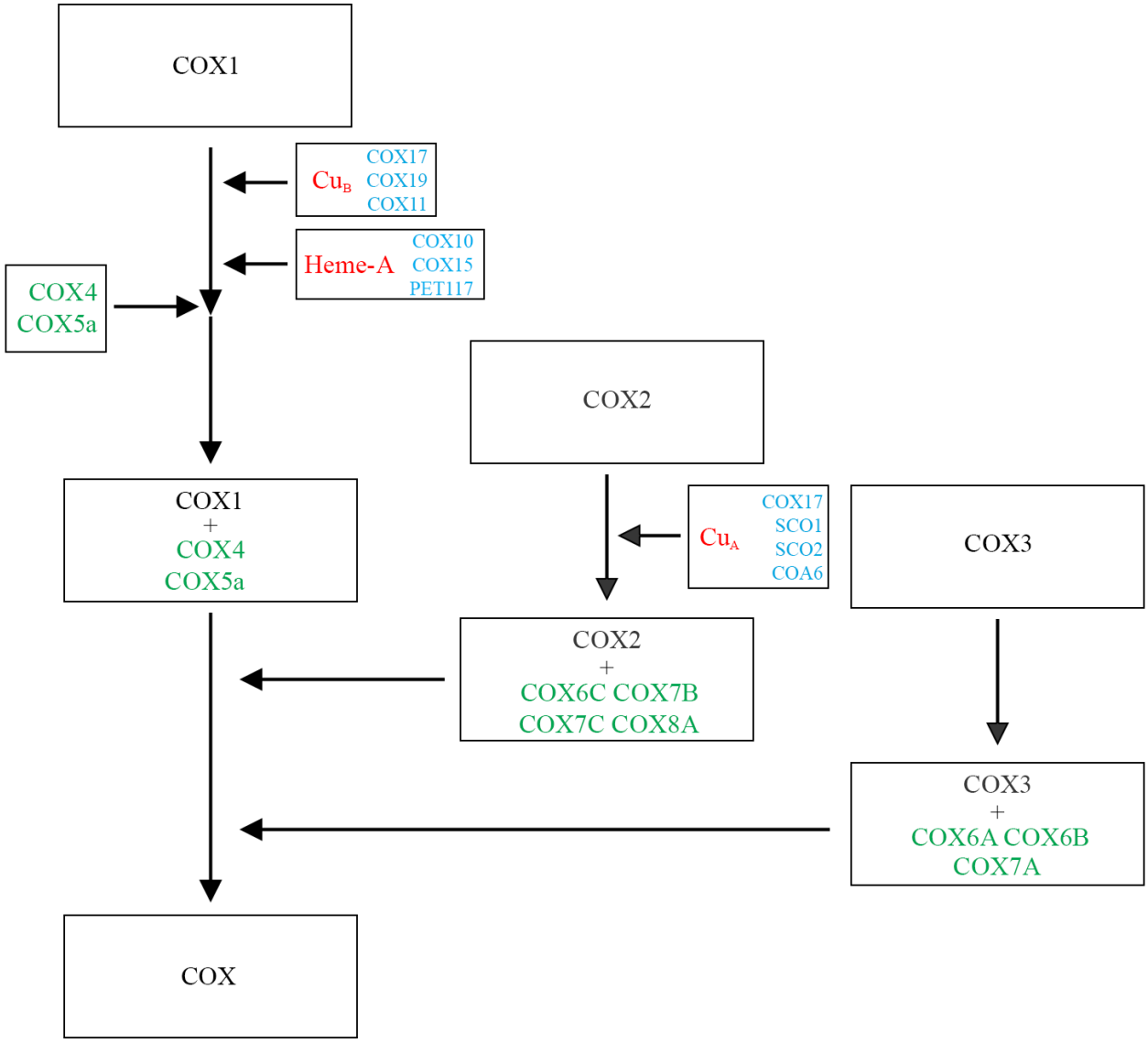


**Figure 1.5: COX assembly pathway**
COX is thought to be assembled in a hybrid between linear and modular models. COX core subunits (black) are first assembled into subassembly complexes featuring structural subunits (green), and metal cofactors (red). Following insertion into the membrane and addition of $Cu_B$, Heme A, and Heme $A_3$ groups, COX1 first forms a complex with COX4:COX5A. This complex then comes together with the other subassembly complexes containing COX2 and COX3 as well as other structural subunits to make the ultimate holoenzyme (COX). Many assembly factors are involved in all processes of this assembly. Those involved in the insertion of the metal cofactors are included here (blue).

### 1.2.2 COX assembly factors

At present there are more than 30 known COX assembly factors in mammals (Table 1.2) (reviewed in Timón-Gómez et al., 2017), although this number continues to expand with more research (Vidoni et al., 2017). These accessory proteins perform a variety of different functions important to RNA stability and translation, protein insertion into and stability within the inner mitochondrial membrane, and synthesis, delivery and insertion of the heme and copper co-factors. Almost all COX assembly factors were first discovered in *Saccharomyces cerevisiae* as petite mutants with an isolated COX deficiency (McEwen et al., 1986; Tzagoloff and Dieckmann, 1990), and their human orthologues identified by mapping disease genes in patients who presented with an isolated COX deficiency (Tiranti et al., 1998; Zhu et al., 1998). Other genes involved in COX assembly were identified using suppressor screens in yeast and cultured cells to identify genes or proteins which reverse the bioenergetic defect (Barros et al., 2004; Glerum et al., 1996). Identified assembly factors have allowed for significant advancement in the understanding of holoenzyme assembly through the study of stalled COX assembly intermediates that occur in their absence. Now, with the advent of next generation and exome sequencing, the rate of discovery of pathogenic mutations in human patients with mitochondrial diseases caused by an isolated COX deficiency or other genetic lesions has increased significantly, resulting in a significant growth in the characterization of proteins with previously unknown functions (Lyons et al., 2016; Wortmann et al., 2015). We will now restrict our focus to those proteins with known roles in the assembly of the $Cu_A$ site of COX.

**Table 1.2: COX assembly factors**
List contains all known COX assembly factors along with the function for those identified. Assembly factors which have been indicated to be involved in the metallation of the enzyme are coloured in blue and those with unknown functions are coloured in gold.

| COX ASSEMBLY FACTOR | FUNCTION |
|---|---|
| LRPPRC | mitochondrial mRNA stability |
| TACO1 | *COX1* mRNA translational activator |
| OXA1L | Membrane insertion of COX subunits |
| COX20 | COX2 chaperone |
| COX18 | Export of the COX2 C-terminus |
| COX17 | Cu chaperone involved in both $Cu_A$ and $Cu_B$ site formation |
| SCO1 | Transfer of copper to COX2 |
| SCO2 | Reduction of COX2 CX3C motif |
| COA6 | Involved in $Cu_A$ metallation |
| COX11 | Involved in $Cu_B$ metallation |
| COX19 | Involved in $Cu_B$ site formation |
| COX10 | Farnesylation of heme B |
| COX15 | Involved in heme O oxidation |
| FDX2 | Involved in heme O oxidation |
| ADR | Involved in heme O oxidation |
| SURF1 | Involved in heme A delivery |
| CMC1 | Stabilizes COX1 with COX14 and COA3 possibly involved in metallation |
| COX14 | Required for COX1 stability |
| COA3 | Required for COX1 stability |
| COA1 | Required for COX1 stability |
| HIGD1A | Stabilizes COX4:COX5A complex |
| MITRAC7 | Stabilizes COX1:COX4:COX5A complex |
| MR-S1 | Involved in the formation of late assembly intermediates |
| PER100 | Involved in the formation of late assembly intermediates |
| PET117 | Involved in the formation of late assembly intermediates |
| HIGD2A | Supercomplex formation |
| PET191 | Unknown function |
| CMC2 | Unknown function |
| COX23 | Unknown function |
| COX16 | Unknown function |

### 1.2.3 Assembly of the $Cu_A$ site within COX2

Copper used for the metallation of the $Cu_A$ site comes from the labile pool sequestered within the mitochondrial matrix. This copper crosses back into the IMS, through an unknown mechanism, and is bound by the copper chaperone COX17 (Beers et al., 1997; Glerum et al., 1996). Copper-loaded COX17 subsequently delivers the metal ion to at least three other cuproproteins within the IMS; COX11, which is involved in the metallation of the $Cu_B$ site, and SCO1 and SCO2, which are required for copper insertion into the $Cu_A$ site (Horng et al., 2004). SCO1 and SCO2 are paralogs that were first identified in a high copy suppressor screen of a *Cox17* point mutant (Glerum et al., 1996). Both proteins use an evolutionarily conserved CxxxC motif and a distal histidine residue to bind copper, which is essential for their function as point mutants within the copper binding site result in a non-functional COX (Nittis et al., 2001). COX17 donates copper to each SCO protein via transient ligand exchange, and in the case of SCO1, this reaction may be coupled with electron transfer to reduce the CxxxC motif to prime it for copper-loading (Banci et al., 2008; Horng et al., 2004).

Once copper bound, SCO1 and SCO2 form a ternary complex with a third protein, COA6, that physically associates with the COX2/COX20 complex within the inner membrane (Figure 1.6) (Bourens and Barrientos, 2017). The exact function of each protein within the SCO1/SCO2/COA6 complex is still an active area of research. SCO1 is known to directly bind COX2 using critical amino acids within loop 8 (Lode et al., 2000; Rigby et al., 2008), and *in vitro* experiments demonstrated that SCO1 is specifically involved in copper transfer to COX2 (Morgada et al., 2015). These *in vitro* analyses also identified SCO2 as a disulphide reductase that reduces the copper-binding cysteinyl sulphurs of COX2 (Morgada et al., 2015). COA6 is a small, soluble protein of unknown function which has been shown to be essential for the metallation of the $Cu_A$ site in both yeast and humans (Ghosh et al., 2014). COA6 binds SCO1, SCO2 and COX2 which points to a possible role in facilitating the formation or promoting the stabilization of the ternary complex required for $Cu_A$ site maturation (Ghosh et al., 2016; Pacheu-Grau et al., 2015; Stroud et al., 2015); however, COA6 has been hypothesized to bind copper and therefore may have a role in removing the $Cu^{2+}$ from SCO2 after the protein reduces COX2, thereby priming SCO2 for multiple rounds of copper binding (Ghosh et al., 2016). COX2 receives copper from SCO1 and binds the metal ion using two conserved cysteines, two histidines, a glutamate and a methionine residue, all of which reside within a cuproredoxin fold (Speno et al., 1995). Once the assembly of the $Cu_A$ site is complete the COX2 module is incorporated into the maturing holoenzyme.

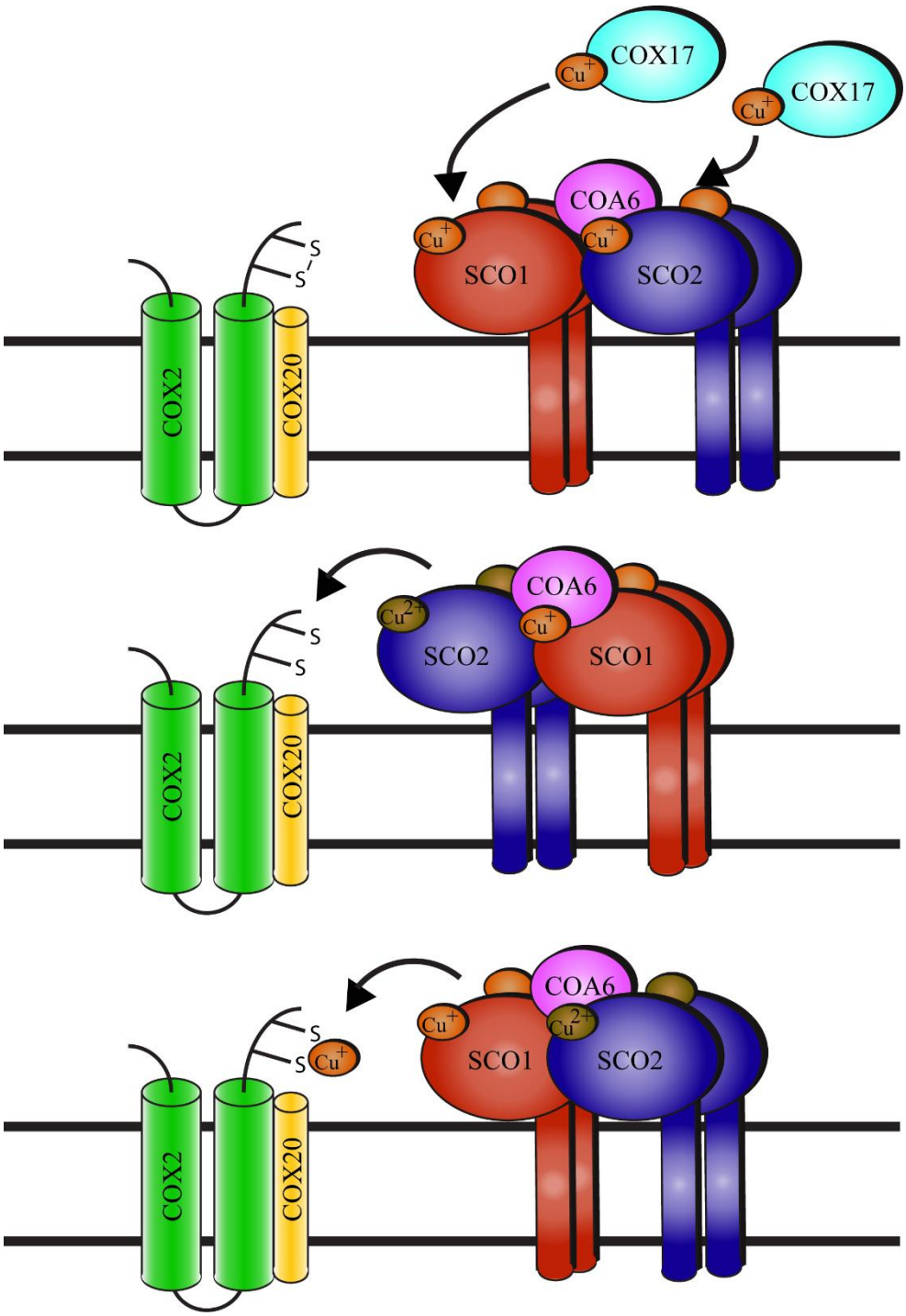


**Figure 1.6: Relative roles of SCO1 and SCO2 in the metallation of the $Cu_A$ site**
(Top) Both SCO1 and SCO2 function as homodimers functioning within a complex that includes the soluble IMS protein COA6. SCO1 and SCO2 receive copper from COX17 in the cupric ($Cu^{+}$) form. (Middle) *In vitro* studies have suggested that SCO2 then functions to reduce the cysteinyl sulphurs of COX2, while oxidizing its own copper ions to the cuprous ($Cu^{2+}$) form. (Bottom) COX2 is now able to accept cupric copper donated from SCO1.

### 1.2.4 The role of COX assembly factors in maintaining cellular copper homeostasis

Much of the work done to characterize assembly of the $Cu_A$ site has come from studying patients affected by pathogenic mutations in genes encoding factors crucial to this process. Human patients have been described for 3 different proteins involved in generating the $Cu_A$ site, SCO1 (Leary et al., 2013a; Stiburek et al., 2009; Valnot et al., 2000), SCO2 (Papadopoulou et al., 1999) and COA6 (Baertling et al., 2015). These patients all predictably presented with an isolated COX deficiency stemming from an inability to properly assemble the holoenzyme. Interestingly, however, affected tissues from patients with mutations in *SCO1* and *SCO2* not only exhibited a profound COX deficiency but also a deficiency in total cellular copper suggesting that these proteins may have an additional role in maintaining cellular copper homeostasis (Leary et al., 2007). So far more than 50 *SCO2* pedigrees have been discovered (Pronicka et al., 2013), with almost all containing at least one E140K allele and presenting with a fatal hypertrophic cardio-encephalopathy (Jaksch et al., 2000; Papadopoulou et al., 1999; Vesela et al., 2004). Patients homozygous for the E140K mutation have a less severe phenotype than their compound heterozygous counterparts (Jaksch et al., 2001), suggesting that the E140K variant is more functional than other pathogenic mutations. Consistent with this idea, overexpression of SCO2 E140K can rescue the COX deficiency in *SCO2* patient cells (Leary et al., 2007).

Contrary to the large number of discovered *SCO2* pedigrees, only three *SCO1* pedigrees have been identified to date and patients from each pedigree present with clinically heterogeneous, fatal forms of disease. The first pedigree, harbouring a nonsense mutation on one allele and a proline to leucine substitution at position 174 on the other allele, presented neonatally with lethal hepatopathy and encephalopathy (Valnot et al., 2000). The second *SCO1* pedigree was homozygous for a glycine to serine substitution at position 132. The patient died at 6 months of age and presented with hypertrophic cardio-encephalopathy as well as a very mild hepatopathy (Stiburek et al., 2009). The third, and most recently identified *SCO1* pedigree, harboured a nonsense mutation on one allele and a methionine to valine substitution on the other allele (Leary et al., 2013a). The patient died at 5 months of age from a severe encephalopathy and, interestingly, had an unaffected liver and heart (Leary et al., 2013a). The cause of the unique tissue-specific phenotypes in each of the *SCO1* pedigrees is unknown, although it may be that the individual missense mutations differentially impinge upon one or both functions of SCO1.

Since the P174L mutation is adjacent to the CxxxC copper-binding motif (Figure 1.7), it was originally hypothesized that the mutation may affect the ability of the protein to bind copper. This

hypothesis, however, is likely an oversimplification as even though the mutant protein binds copper normally *in vitro* (Cobine et al., 2006b) and the COX deficiency phenotype can be partially rescued in patient fibroblasts by supplementing the culture media with copper salts (Leary et al., 2004), the P174L changes the structure of the protein enough that it abolishes its interaction with COX17 and prevents ligand exchange reactions between the two proteins *in vivo* (Banci et al., 2007; Cobine et al., 2006b). The G132S mutation is near the transmembrane helix, within the portion of SCO1 involved in protein dimerization (Stiburek et al., 2009). The mutation disrupts SCO1 dimerization and the mutant protein appears to migrate only in its monomeric form under native conditions (Stiburek et al., 2009). Overexpression of the G132S mutant causes a dominate negative effect on COX activity when overexpressed in control or *SCO1* patient fibroblasts from other backgrounds, further suggesting that the inability of the mutant protein to dimerize disrupts its function (Leary et al., 2013a). While both the P174L and G132S substitutions alter specific properties of the protein crucial to its function thereby resulting in a severe, combined COX and copper deficiency, the M294V mutation appears to predominantly affect protein folding (Leary et al., 2013a). However, patient fibroblasts with this mutation have a milder COX deficiency and overexpression of the M294V SCO1 variant fully rescues the COX deficiency in two different *SCO1* patient backgrounds, arguing that the residual mutant protein that is able to properly fold is functional (Leary et al., 2013a).

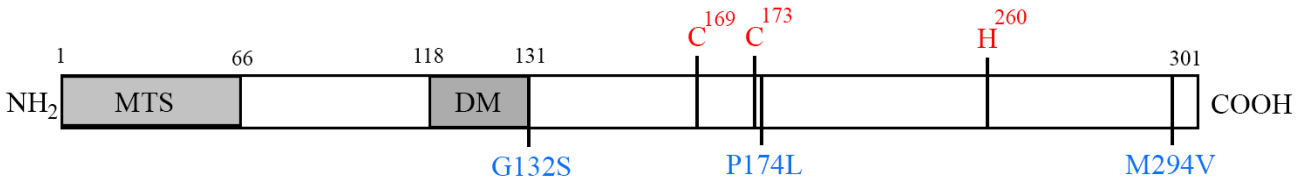


**Figure 1.7: Location of critical amino acids within SCO1**
Schematic drawing of the SCO1 protein with critical copper binding residues listed in red and identified pathogenic mutations in blue. The first 66 amino acids of SCO1 represent the mitochondrial targeting sequence of the protein and are cleaved upon translocation into the mitochondria. The region of 118-131 is critical for dimerization of SCO1 molecules, and the G132S mutation immediately following this region predictably affects homodimer formation. The $CX_3C$ motif at residues 169-173 is critical for copper binding, however, the P174L mutation immediately following this region does not affect copper binding but instead results in an inability for SCO1 to be properly metallated by COX17. The third critical residue involved in copper binding is the histidine at position 260, which functions as a molecular lid keeping the copper bound. Finally, the last identified pathogenic mutation is the M294V mutation that results in an unstable rapidly degraded protein.

## 2. RATIONALE AND OBJECTIVES

### 2.1 Rationale and hypothesis

Despite the importance of dysregulation of copper homeostasis to the etiology of several human diseases, little is known about how copper levels are sensed and regulated at the cellular and whole organ levels. It is clear, however, that mitochondria have an essential yet poorly understood role in this process. Existing literature argues that the mitochondrial inner membrane protein SCO1 is central to a copper sensing pathway whose signalling activity is critical to maintaining cellular copper levels. We hypothesize that the deletion of *Sco1* in mouse tissues will similarly affect copper homeostasis, thereby providing a model system that may shed light on the downstream mechanisms relevant to the maintenance of cellular copper levels that are specific to individual human tissues. Our focus on the liver and heart in these studies reflects the fact these are two of the most severely affected tissues in *SCO1* patients described to date.

As perturbations in SCO1 function are known to selectively affect distinct tissues for reasons that remain unclear, we require a model system amenable to the biochemical analysis of multiple tissues. Using transgenic mice therefore allows us to investigate how SCO1 protein function impinges upon copper homeostasis in the tissues *in situ* and examine whether the associated homeostatic mechanisms differ between organs where systemic influences remain intact. Other, simpler model organisms or cultured cells are not tractable in this context.

### 2.2 Specific objectives

1) To generate tissue-specific *Sco1* knockout mouse models in which the gene is specifically deleted in the liver or the heart.
2) To characterize these tissue-specific *Sco1* knockout mouse models on a biochemical, physiological, molecular, and elemental level.
3) To investigate the mechanisms by which ablation of *Sco1* expression in the liver and heart causes a cellular copper deficiency and determine if these mechanisms differ between the two tissues.
4) To generate and characterize a knock-in mouse model harbouring a *Sco1 G115S* missense mutation which in humans causes cardiac dysfunction and determine the extent to which it phenocopies the relevant *SCO1* pedigree and the heart-specific *Sco1* knockout models.

# 3. MATERIALS AND METHODS

## 3.1 Generation of model organisms

### 3.1.1 Generation and validation of tissue-specific *Sco1* knockout mice

Embryonic stem (ES) cells containing loxP sites flanking the second exon of *Sco1*, and *frt* sites flanking a Neomycin cassette with a *lacZ* gene, were purchased from the Knockout Mouse Project Repository (Figure 3.1). Deletion of the second exon in *Sco1* generates a premature stop codon resulting in the degradation of the *Sco1* transcript via that nonsense mediated decay pathway. These "floxed-Neo" ES cells were used to generate male chimera transmitter mice, through morula aggregation, by the Toronto Centre for Phenogenomics and germline transmission of the modified *Sco1* allele was verified. Following shipment to the University of Saskatchewan, verified male mice containing the "floxed-Neo" *Sco1* were crossed to C57BL/6N females, and subsequent progeny were intercrossed for multiple generations. Female $Sco1^{flox\text{-}Neo/flox\text{-}Neo}$ mice were next crossed to male C57BL/6N mice expressing the FlpE recombinase (Taconic), collapsing the *frt* sites to remove the Neomycin cassette and *lacZ* gene. Resultant heterozygous mice were intercrossed to generate homozygous mice containing a collapsed *frt* site and the floxed second exon of *Sco1* (herein referred to as $Sco1^{flox/flox}$ mice). To generate all tissue-specific knockout mice, female $Sco1^{flox/flox}$ mice were first crossed to male C57BL/6N mice expressing *Cre recombinase* under the expression of either the liver-specific albumin promoter (for $Sco1^{liv/liv}$ mice, Jackson Laboratories #003574), the heart-specific α-myosin heavy chain promotor (for $Sco1^{hrt/hrt}$ mice, Jackson Laboratories #018972), or the striated muscle-specific muscle creatine kinase promotor (for $Sco1^{stm/stm}$ mice, Jackson Laboratories #006475). F1 progeny from these crosses ($Cre^{+/-}$, $Sco1^{flox/wt}$), were next back-crossed to the $Sco1^{flox/flox}$ mice, generating the tissue-specifc *Sco1* knockout mice containing the collapsed second exon of *Sco1*. Genotyping of *Sco1* alleles and excision of both *frt* and *loxp* sites was confirmed using a common three primer PCR mix (Figure 3.1, Table 3.1). Existence of *Cre recombinase* gene was confirmed using a common 4 primer mix (Table 3.1).

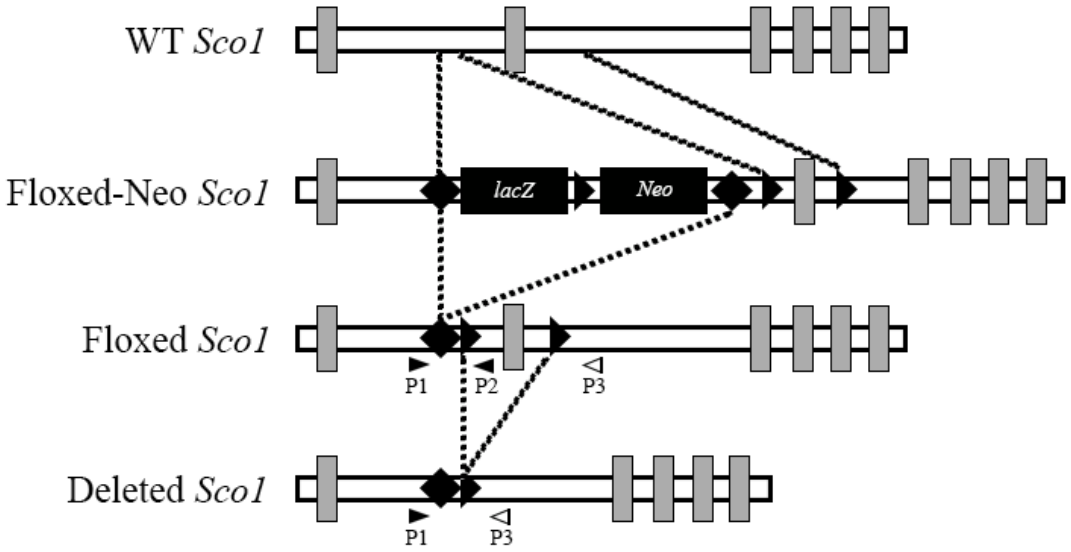


**Figure 3.1: Cre-lox deletion scheme for *Sco1***
Schematic depicting wild-type *Sco1* gene with exons and introns (top). Embryonic stem cells were first generated having loxP (triangles) sites flanking the second exon of *Sco1* and contained both a *lacZ* gene and a Neomycin resistance cassette flanked by *frt* (diamonds) sites (Floxed-Neo *Sco1*). ES cells were used to generate founder mice, which were then bred to remove the *frt* sites leaving the loxp sites (Floxed *Sco1*). Finally, to generate knockouts the Floxed *Sco1* mice were bred to mice expressing Cre recombinase, excising the region of DNA between the loxp sites (Deleted *Sco1*). Primers listed (P1-3) depict 3 primer PCR used to genotype wild-type, floxed, and deleted alleles.

**Table 3.1: PCR Primer List**

List contains details for all primers and probes used for PCR, including primer name, 5'-3' sequence, and the function of the reaction they were included in. + indicates a locked amino acid. Lower case letters in probes represent differences in sequence designed to recognise knock-in mutation in *Sco1*$^{G115S/G115S}$.

| Primer Name | Sequence (5'-3') | Used in |
|---|---|---|
| *Sco1-P1* | GTCACATCTCAGGAACTTCCTGG | Genotyping *Sco1 WT/flox* |
| *Sco1-P2* | CCACAACGGGTTCTTCTGTT | Genotyping *Sco1 WT/flox* |
| *Sco1-P3* | ACCTAAAAGTGGGGCTTCCTGAAAACTAA | Genotyping *Sco1 WT/flox* |
| *Cre-P1* | ATGACAGACAGATCCCTCCTATCTCC | Genotyping Cre animals |
| *Cre-P2* | CTCATCACTCGTTGCATCATCGAC | Genotyping Cre animals |
| *Cre-P3* | CAAATGTTGCTTGTCTGGTG | Genotyping Cre animals |
| *Cre-P4* | GTCAGTCGAGTGCACAGTTT | Genotyping Cre animals |
| G115S-F | TTAGAGCTGGAGAAACAACGG | Genotyping G115S mice |
| G115S-R | GGCTCTCCATTGTGAGTTGTA | Genotyping G115S mice |
| G115S-WT-Probe | CA+TT+g+G+gAA+GCC | Genotyping G115S mice |
| G115S-KI-Probe | CA+TT+a+G+cAA+G+CCT | Genotyping G115S mice |
| *Sco1* cDNA-F | AAAAAGCAGGCTACCATGGCAGCACTTGTACGCGCCGC | Overexpression of *Sco1* |
| *Sco1* cDNA-R | CTTCATGTGTGACCTCACGTGTGCAGCAATTGAG | Overexpression of *Sco1* |
| *Ctr1* cDNA-F | AAAAAGCAGGCTACCATGAACCATATGGGGATGAACC | Overexpression of *Ctr1* |
| *Ctr1* cDNA-R | AGAAAGCTGGGTTCAATGGCAGTGCTCTGTGATG | Overexpression of *Ctr1* |
| RT-*Ctr1*- F | GTCTTGTTGGCCCAGTGTTT | RT-PCR analysis of *Ctr1* |
| RT-*Ctr1-R* | GCACCTTAATGTTGGGCTGT | RT-PCR analysis of *Ctr1* |
| RT-*Slc41a2*- F | CTGGCATGGTTTTGGACA | RT-PCR analysis of *Slc41a2* |
| RT-*Slc41a2-R* | CCACTTCTCAATGGGTGAG | RT-PCR analysis of *Slc41a2* |
| RT-*Mt1*- F | GTCCTCTAAGCGTCACCAC | RT-PCR analysis of *Mt1* |
| RT-*Mt1*- R | GAGCAGTTGGGGTCCATTC | RT-PCR analysis of *Mt1* |
| RT-*Gapdh* - F | GCCGTGAGTGGAGTCATACT | RT-PCR analysis of *Gapdh* |
| RT-*Gapdh* - R | ATGGTGAAGGTCGGTGTGAA | RT-PCR analysis of *Gapdh* |
| RT-*Anp* - F | GCTTCCAGGCCATATTGGAG | RT-PCR analysis of *Anp* |
| RT-*Anp* - R | GGGGGCATGACCTCATCTT | RT-PCR analysis of *Anp* |
| RT-*Bnp* - F | GAGGTCACTCCTATCCTCTGG | RT-PCR analysis of *Bnp* |
| RT-B*np* - R | GCCATTTCCTCCGACTTTTCTC | RT-PCR analysis of *Bnp* |
| RT-*aSA* - F | CCCAAAGCTAACCGGGAGAAG | RT-PCR analysis of $\alpha$ *Sa* |
| RT-*aSA* - R | CCAGAATCCAACACGATGCC | RT-PCR analysis of $\alpha$ *Sa* |
| RT-*Serca2a* - F | TGGAACAACCCGGTAAAGAGT | RT-PCR analysis of *Serca2a* |
| RT-*Serca2a* - R | CACCAGGGGCATAATGAGCAG | RT-PCR analysis of *Serca2a* |

### 3.1.2 Generation and validation of *Sco1* G115S homozygous knock-in mice

*Sco1*$^{G115S/wt}$ mice were generated at the Toronto Centre for Phenogenomics. C57BL/6NCrl zygotes were co-injected with the guide RNA 5'-GCATTAGCAAGCCTTTACTA-3', Cas9 mRNA, and a single-stranded oligonucleotide repair template with both the desired substitution to induce the G115S mutation and a silent mutation to interrupt the protospacer adjacent sequence. Successful mutagenesis was then confirmed via the DNA sequencing of PCR amplicons. Mice were crossed to C57BL/6NCrl mice and screened for germline transmission, with the resultant mice further back-crossed for multiple generations. Heterozygous *Sco1*$^{G115S/wt}$ were shipped to the University of Saskatchewan and inter-crossed to generate homozygous *Sco1*$^{G115S/G115S}$ mice used for experimentation. Genotyping of knock-in animals was completed using real-time PCR. Tail DNA from both wild-type and knock-in was extracted using the KAPA Mouse Genotyping Kit (KAPA Biosystems). 2µL of a 1:1 dilution of tail DNA was used in a 10µL reaction, containing 500 nM primers and 250 nM probes (Integrated DNA, Table 3.1), in the PerfeCTa qPCR ToughMix (VWR) on an Applied Biosystems Step One Plus Real-Time Thermocycler.

### 3.1.3 Animal husbandry and tissue collection

Animals from all models were housed in a 12h light: 12h dark photoperiod and provided with food and water ad libitum. Equal numbers of male and female mice were used for all models and experimental analysis. Tissues from mature animals used in enzymology, molecular biology, elemental and genetic analysis were collected from mice following cervical dislocation and immediately flash frozen. Blood from mice was collected from either the superficial temporal vein or heart (*Sco1*$^{liv/liv}$ and *Sco1*$^{stm/stm}$), or the chest cavity (*Sco1*$^{hrt/hrt}$). Serum was collected using two sequential 5-minute spins at 1,000 x g at 4$^{o}$C.

## 3.2 Cell culture

### 3.2.1 Generation of *Sco1* null mouse embryonic fibroblasts

MEFs were isolated from pregnant *Sco1*$^{flox/flox}$ females at embryonic day 13-15 (Anand et al., 2014), cultured and subsequently immortalized using retroviral transduction with telomerase and the E7 gene of human papillomavirus (Lochmuller et al., 1999; Yao and Shoubridge, 1999). To generate *Sco1* knockouts, recombinant Cre recombinase was first purified from transformed *Escherichia coli* and added to *Sco1*$^{flox/flox}$ MEFs. *Sco1* knockout and wild-type cells were passaged to clonal density then expanded to ensure a homogeneous population. All cultured cells were maintained in high

glucose DMEM with 1.2 M pyruvate, 205 µM uridine and 10% fetal bovine serum at 37ºC and 5% $CO_2$.

### 3.2.2 Transfection and retroviral transduction for protein overexpression

For overexpression of *Sco1* and *Ctr1* in wild-type and *Sco1* knockout MEFs, cDNAs were first amplified from *Sco1*$^{flox/flox}$ isolated mRNA using sequence specific primers (Table 3.1). cDNAs were cloned into Gateway-modified retroviral expression vectors (Antonicka et al., 2003), and sequenced using Sanger sequencing. Retroviral particles were generated through transfection of retroviral expression particles, containing relevant cDNAs, into Phoenix Amphotrophic packaging cell line (Leary et al., 2013b) using the JetPrime transfection reagent. MEFs were subsequently stably transduced with retroviral particles and successful integration was selected for in fibroblasts using media containing 2µg/mL puromycin.

## 3.3 Immunoblot analysis

### 3.3.1 Blue Native Polyacrylamide Gel Electrophoresis

Blue native polyacrylamide gel electrophoresis (BN-PAGE) was performed as previously described elsewhere (McKenzie et al., 2007). Briefly, tissues were isolated from cervically dislocated mice and flash frozen on dry ice. Tissues were then resuspended and homogenized in extraction buffer (Table 3.3). Sample volume was adjusted to a protein concentration of 2 mg/ml, incubated on ice for 30 min, and finally centrifuged at 18,000 x g for 5 minutes at 4ºC. Equal protein loads (20 µg/lane) were resolved within a 6-16% acrylamide gradient gel and transferred to a nitrocellulose membrane using a semi-dry transfer system.

### 3.3.2 Denaturing Polyacrylamide Gel Electrophoresis

Sodium Dodecyl Sulphate Polyacrylamide Gel Electrophoresis (SDS-PAGE) was performed as previously described. Tissues were isolated as above, resuspended in RIPA extraction buffer (Table 3.2) and homogenized using a glass dounce homogenizer on ice. Sample volume was adjusted to a protein concentration of 5 mg/ml, incubated on ice for 30 minutes, and finally centrifuged at 12,000 x g for 10 minutes at 4ºC. Equal protein loads were resolved on a precast 4-20% SDS-PAGE gradient gel (BioRad) and transferred to a nitrocellulose membrane using a semi-dry transfer system.

**Table 3.3: Common buffer solutions**

List contains all common buffer solutions used in Methods

| Buffer Solution | Contents |
|---|---|
| 1X PBS | 2.7 mM KCl, 134 mM NaCl, 1.5 mM $KH_2PO_4$, 8 mM $K_2HPO_4$ |
| TBST | 25 mM Tris (pH 7.4), 137 mM NaCl, 2.5mM KCl and 0.05% Tween 20 |
| PCR reaction buffer | 1X NEB Phusion HF Buffer (50 mM KCl, 1.5 mM $MgCl_2$) 200 µM dNTPs, 0.5 µM primers, 1U DNA polymerase |
| RIPA Extraction Buffer | 50 mM Tris (pH 7.4), 150 mM NaCl, 1% Triton X-100, 0.5% sodium deoxycholate, 0.1% SDS, 1 mM EDTA and 1x Complete protease inhibitor cocktail |
| Blue Native Homogenization buffer | 20 mM bis-Tris (pH 7.4), 50 mM NaCl, 10% (v/v) glycerol and 0.2% (w/v) n-dodecyl -D-maltoside |
| ECL solution | 100 mM Tris-HCl (pH 8.5), 225 µM p-coumaric acid, 1.25 mM luminol, 2.94 mM $H_2O_2$ |
| Enzymology homogenization buffer | 25 mM $K_2HPO_4$ (pH 7.4), 5 mM $MgCl_2$, 0.6 mM DDM |
| COX assay buffer | 25 mM $K_2HPO_4$ (pH 7.4), 5 mM $MgCl_2$, 0.6 mM DDM, 2.5 mg/ml BSA, 50 µM Reduced cytochrome *c* |
| SOD1 assay buffer | 50 mM $K_2HPO_4$ (pH 7.8), 100 mM EDTA, 50 mM xanthine, 500 µM cytochrome *c*, 6 nM xanthine oxidase |
| CS assay buffer | 25 mM $K_2HPO_4$ (pH 7.4), 5 mM $MgCl_2$, 1.2 mM DDM, 10 mM DTNB, 10 mM Acetyl CoA |
| Tyrode's solution | 25 mM HEPES (pH 7.4), 119 mM NaCl, 5 mM KCl, 2 mM $CaCl_2$, 2 mM $MgCl_2$ and 33 mM glucose |
| Liver IF blocking solution | 1% BSA, 0.2% fat free milk, 5% v/v goat serum, and 0.2% Triton X-100 |
| Heart IF antibody buffer | 0.15 mM NaCl, 15 mM $Na_3C_6H_5O_7{*}2H_2O$, 2% goat serum, 1% BSA, 0.05% Triton X-100, 0.02% NaN3 |
| Heart IF blocking buffer | 2.7 mM KCl, 134 mM NaCl, 1.5 mM $KH_2PO_4$, 8 mM $K_2HPO_4$, 10% goat serum, and 6% bovine serum albumin |

### 3.3.3 Immunodetection of proteins

Membranes from Blue native and SDS-PAGE were first blocked for 2 hours in a Tris buffered saline solution with 5% milk and Tween 20 (Table 3.2) and incubated over night at 4ºC in primary antibody (list of primary antibodies is shown in Table 3.3). Membranes were next washed six times for 5 minutes in TBST (Table 3.2) and incubated for 60 minutes at room temperature in TBST with 5% Milk and the appropriate secondary antibody conjugated to horseradish peroxidase (1:2500, BioRad). Membranes were developed by incubation for 1 minute in a homemade enhanced chemiluminescence solution (ECL, Table 3.2) and visualized with X-ray film or a BioRad ChemiDocTM MP Imaging System.

## 3.4 Enzymatic Assays

Assays to determine enzymatic activities for cytochrome *c* oxidase (COX) and citrate synthase (CS) were performed as described elsewhere (Leary et al., 2004). For determining total superoxide dismutase activity, a modified xanthine oxidase assay was used (McCord and Fridovich, 1969). Briefly, small 3 $mm^3$ sections of frozen tissues were resuspended in 100 µL of homogenization buffer (Table 3.2) and homogenized using a plastic pestle. Following the determination of protein concentration, sample volume was adjusted to 2.5 mg/mL. Volumes of sample in linear increments (1, 2, and 4 µL) were incubated in 250 µL of the appropriate reaction mixture (Table 3.2), mixed using a pipette, and the change of absorbance was measured at either 550 nm (COX and SOD) and 412 (CS) for 3 minutes using a SPECTRA max 340PC 96 well plate reader (Molecular Devices). Changes in absorbance were used to calculate specific activities.

## 3.5 Elemental Analysis

Samples were isolated, and placed in metal-free, acid washed tubes. Samples were then incubated in 40% nitric acid for 1 hour at boiling temperature for digestion, diluted in ultra pure, metal-free water and analyzed by ICP-OES (Agilent, 7500ce). Concentrations were determined by the comparison to both a standard curve generated using two separate mixed metal standards (Optima) and nitric acid “blank” samples. All metal concentrations were normalized to the concentration of sulphur to allow for varying protein concentrations. For *Sco1*$^{hrt/hrt}$ mice, samples were normalized to the concentration of zinc to allow for the comparison of samples across different time points.

**Table 3.3: Primary antibodies used**

List contains all primary antibodies used for immunological techniques.

| Protein Name | Source | Type |
|---|---|---|
| WGA | Molecular Probes | 594-conjugated Mouse IgG |
| Porin | Calbiochem | Mouse IgG |
| Tubulin | Sigma | Mouse IgG |
| GAPDH | Invitrogen | Rabbit IgG |
| Com-1 39 kD subunit | Invitrogen | Mouse IgG |
| Com-2 70 kD subunit | Invitrogen | Mouse IgG |
| Com-3 Core 1 subunit | Invitrogen | Mouse IgG |
| COX1 | Invitrogen | Mouse IgG |
| COXIV | Invitrogen | Mouse IgG |
| ATPase α-subunit | Invitrogen | Mouse IgG |
| SOD1 | Enzo | Rabbit IgG |
| CTR1 | Gift from Dr. Jack Kaplan | Rabbit IgG |
| CCS | Gift from Dr. Joe Prohaska | Rabbit IgG |
| ATP7A | Gift from Dr. Micheal Petris | Rabbit IgG |
| ATP7B | Gift from Dr. Micheal Petris | Rabbit IgG |
| SCO1 | Made in House | Rabbit IgG |
| Na/K ATPase | Millipore | Mouse IgG |
| Rab5 | Abcam | Mouse IgG |
| EEA1 | BD Biosciences | Rabbit IgG |
| LAMP1 | Santa Cruz | Rat IgG |

### 3.6 Lipid Analysis

Livers were isolated from *Sco1*$^{liv/liv}$ mice as described above. Lipids were then extracted and resolved using thin-layer chromatography on Silica Gel G-60 TLC plates as described elsewhere (Stone et al., 2004). Lipids were visualized by dipping the plate into a solution of 10% cupric sulfate and 8% phosphoric acid and heating to 180°C. Triacylglycerol and cholesterol esters were quantified by scanning densitometry.

### 3.7 Immunohistochemical, Immunofluorescent, and TEM imaging

#### 3.7.1 Tissue perfusion, fixation, and preparation

To isolate livers from wild-type and liver-specific *Sco1* knockout mice, mice were anaesthetized with 3% isofluorane and oxygen and perfused with 10-15 mL of PBS at 5 mL/minute kept on ice. For TEM analysis, mice were subsequently perfused with 10-15 mL of ice-cold PBS with 2.5% glutaraldehyde and 2% freshly made paraformaldehyde (PFA). Livers were removed and minced into 1 $mm^3$ pieces and stored in the PFA solution at 4$^o$C. Further processing and analysis for TEM was performed as described elsewhere (Neuspiel et al., 2005). For immunohistochemistry, mice were subsequently perfused with 10-15 mL of ice-cold PBS with 4% PFA and stored in PFA solution overnight at 4$^o$C. Fixed livers were then dehydrated and embedded in paraffin blocks. For immunofluorescence analysis, livers were fixed in a similar manner as for IHC and placed in a protective sucrose solution at 15%, then 20% (w/v) until samples sunk to bottom of the container. Samples were then frozen in optical cutting temperature compound within cryomolds, using isopentane chilled to -80$^o$C with dry ice.

To isolate hearts from wild-type and *Sco1*$^{hrt/hrt}$ mice, mice were first euthanized and chest cavities were dissected out. Chest cavities were incubated in 10% formalin for 48 hours to allow for fixation. Hearts were dissected out of chest cavities, dehydrated, and embedded in paraffin. To isolate hearts from wild-type, *Sco1*$^{stm/stm}$, and *Sco1*$^{G115S/G115}$ mice, mice were first anaesthetized with 3% isofluorane and oxygen, and hearts were dissected out of chest cavity. Hearts were cannulated through the aorta and perfused with HEPES buffered Tyrode's solution (Table 3.2) using a modified Langendorff setup. For IHC analysis, hearts were incubated in 10% formalin for 48 hours, dehydrated, and embedded in paraffin. For IF analysis hearts were rapidly frozen in optical cutting temperature compound using isobutane chilled to -80$^o$C using dry ice.

### 3.7.2 Immunohistochemistry staining and imaging procedure

For IHC analysis, after preparation, hearts and livers from all mouse models were cut to either 10- (liver) or 6- (heart) micron sections and these sections were mounted on a Superfrost Plus coated slides (Fisher Scientific). Slides were next deparaffinized using xylene, dehydrated with varying concentrations of alcohol and then rehydrated. For H&E staining, slides were placed in Mayer's hematoxylin for 10 minutes, differentiated in 70% alcohol and stained with 0.01% Eosin Y for 1 minute. Slides were then rinsed, dehydrated in alcohol, incubated in xylene for 15 minutes, and finally cover slipped. For Perls staining, slides were first incubated in Perls Prussian blue until sufficiently stained and then counterstained with Nuclear Fast Red. For Masson's trichrome staining, slides were stained first in hematoxylin for 10 minutes, washed, stained in Scarlet-acid Fuchsin for 10 minutes, washed again, stained in Aniline Blue for 5 minutes, and finally differentiated in 1% acetic acid. Slides were then washed with alcohol, cleared using xylene and cover slips were placed on. All IHC slides were visualized using a light microscope and digital pictures were taken using Virtual Microscopy.

### 3.7.3 Immunofluorescent protocol and imaging procedure

Optical cutting temperature frozen tissues from all models were cut to 6-micron sections and mounted on Superfrost Plus coated slides (Fisher Scientific) for staining. For liver sections, slides were first blocked with Tris buffered saline solution containing BSA, milk, goat serum, and Triton X-100 (Table 3.2) for 1 hour, washed with PBS, and incubated overnight at 4$^{o}$C in blocking buffer with primary antibodies (Table 3.3). Following primary incubation, slides were washed in PBS and incubated in blocking buffer with the appropriate fluorescently conjugated secondary antibody. Finally, slides were washed in PBS and mounted with Prolong Gold Antifade Mountant containing DAPI (Life Technologies).

For heart samples, slides were fixed post-sectioning in acetone at -20$^{o}$C for 10 minutes, washed twice in PBS for 5 minutes, and washed once in 25 mM glycine for 10 minutes. For CTR1 and Rab5 antibody analysis, an additional permeabilization step containing 0.1% Triton X-100 in PBS was added. Slides were next blocked in heart-specific blocking buffer containing goat serum and BSA (Table 3.2) for 1 hour at room temperature and then incubated overnight in heart-specific antibody dilution buffer (Table 3.2) containing primary antibody (Table 3.3) in a humidified chamber kept at 4$^{o}$C. Following incubation with the primary antibody, slides were washed twice in PBS for 5 minutes and incubated for 1 hour in a humidified chamber at room temperature containing in antibody dilution

buffer and appropriate secondary antibodies (Table 3.3). Slides were washed twice in PBS for 5 minutes before imaging.

Imaging of stained slides was performed using a ZEISS LSM-700 laser-scanning confocal microscope. Fluorescent imaged were obtained concurrently with all image acquisition and calculation of correlation coefficient of co-staining (OCC) performed using ZEISS Zen Black imaging software.

### 3.8 Echocardiography

Echocardiography on *Sco1*$^{stm/stm}$ mice was performed as described elsewhere (56). Briefly, wild-type and *Sco1*$^{stm/stm}$ mice (n=4) at P60 and P90 were anaesthetized with 3% isoflurane for 1–2 minutes, and then maintained at 1.5–2% isoflurane after losing the righting reflex. Cardiac function was measured with mice laid supine on a heated platform using a high resolution Vevo 2100 ultrasound system (VisualSonics, Toronto, ON, Canada) equipped with an MS550 transducer. Left ventricle internal diameter end systole (LVIDs) and diastole (LVIDd), fractional shortening and ejection fraction were determined from the LV short-axis M-mode view. The heart rate, electrocardiogram (ECG), respiratory rate and body temperature of the mouse were monitored throughout the experiment.

### 3.9 Microarray and RT-PCR analysis

Tissues used for RNA extraction were isolated as described above. Total RNA was extracted and purified using RNeasy Mini Kit (Qiagen), with DNase digestion step. Following RNA quantification using NanoDrop Spectrophotometer ND-1000 (NanoDrop Technologies, Inc.), cDNA was synthesized from 250 ng of total RNA using either the Ambion WT Expression Kit (Microarray analysis, Life Technologies) or ProtoScript First Strand cDNA Synthesis Kit (RT-PCR, New England Biolabs). For microarray analysis, cDNA was fragmented, labeled with Affymetrix GeneChip® WT Terminal Labeling Kit (Affymetrix), and hybridized on Mouse Gene 2.0 ST (Affymetrix) in the Genechip® Hybridization oven 640 (Affymetrix) for 17 hours at 45$^{o}$C and 60 rpm. Genechips were washed with Affymetrix Hybridization Wash and Stain kit in a GeneChip® Fluidics Station 450 (Affymetrix). Genechips were scanned on a GeneChip® scanner 3000 (Affymetrix), and raw intensities were read, background corrected, normalized, $\log_2$ transformed and summarized at the transcript cluster level. Cut-off p-values for dysregulated genes were set at $\leq 0.05$ and successful

results were subjected to Ingenuity® Pathway Analysis (Qiagen), with Z-scores being used to rank predictions.

For RT-PCR, equal amounts of reverse-transcribed cDNA were used as the template in PCR amplification of transcripts of interest. PCR cycle number and conditions were optimized to ensure that amplification was optimal and in the log phase. Primers used for PCR reaction are included in Table 3.1.

### 3.10 Statistical Analysis

All error bars represent standard error of the mean. For those values depicted as ratios, the standard error of the mean was calculated using a previously validated set of statistical equations (Homes and Buhr, 2007). Where indicated, significant differences between experimental groups were detected using a two-sample Student's t-test assuming unequal variance. * - $P<0.05$, ** - $P<0.01$, *** - $P<0.001$, and NS - not significant.

# 4. Results

## 4.1 The role of SCO1 in maintaining cellular copper homeostasis in the murine liver

### 4.1.1 Physiological characterization of liver-specific *Sco1* (*Sco1*$^{liv/liv}$) knockout mice

#### 4.1.1.1 Validation of liver-specific *Sco1* deletion

As the first human *SCO1* patient to be identified presented with an acute, fatal hepatopathy, we decided to use the Cre-lox system to generate a liver-specific *Sco1* knockout mouse and examine the role of SCO1 in this tissue. Briefly, C57BL6/N mice expressing *Cre recombinase* under the control of the liver-specific albumin promoter (*Cre*$^{+/+}$, *Sco1*$^{wt/wt}$) were crossed to *Sco1* transgenic mice in which the second exon was flanked by loxP sites (*Cre*$^{-/-}$, *Sco1*$^{flox/flox}$). The resultant animals (*Cre*$^{+/-}$, *Sco1*$^{liv/wt}$) were then backcrossed to the homozygous *Sco1* floxed model to generate liver-specific *Sco1* knockout mice, herein referred to as *Sco1*$^{liv/liv}$ mice (for full details on breeding see Materials and Methods). Animals of all possible genotypes were born at the expected Mendelian frequencies and specific deletion of the *Sco1* exon in the liver was confirmed using a three primer PCR strategy (Figure 4.1A). SCO1 protein was not immunologically detectable in *Sco1* knockout livers (Figure 4.1B), while its abundance was unaltered in all other somatic tissues analyzed (Figure 4.1C).

#### 4.1.1.2 Liver-specific deletion of *Sco1* is lethal with mice having a pronounced growth deficiency

While *Sco1*$^{liv/liv}$ mice gained weight normally up to approximately postnatal day 28 (P28), they exhibited a severe growth deficiency thereafter and by P57 were runted compared to their wild-type littermates (Figure 4.1D,E). The growth deficiency preceded lethality, which was observed as early as P45, and *Sco1*$^{liv/liv}$ mice had a median lifespan of 70 days (Figure 4.1F). Lethality was likely caused by liver failure as the *Sco1*$^{liv/liv}$ mice exhibited hepatomegaly compared to their wild-type littermates (Figure 4.1G) and had increased alanine aminotransferase activity in their serum, a biomarker of severe hepatopathy (Figure 4.1H).

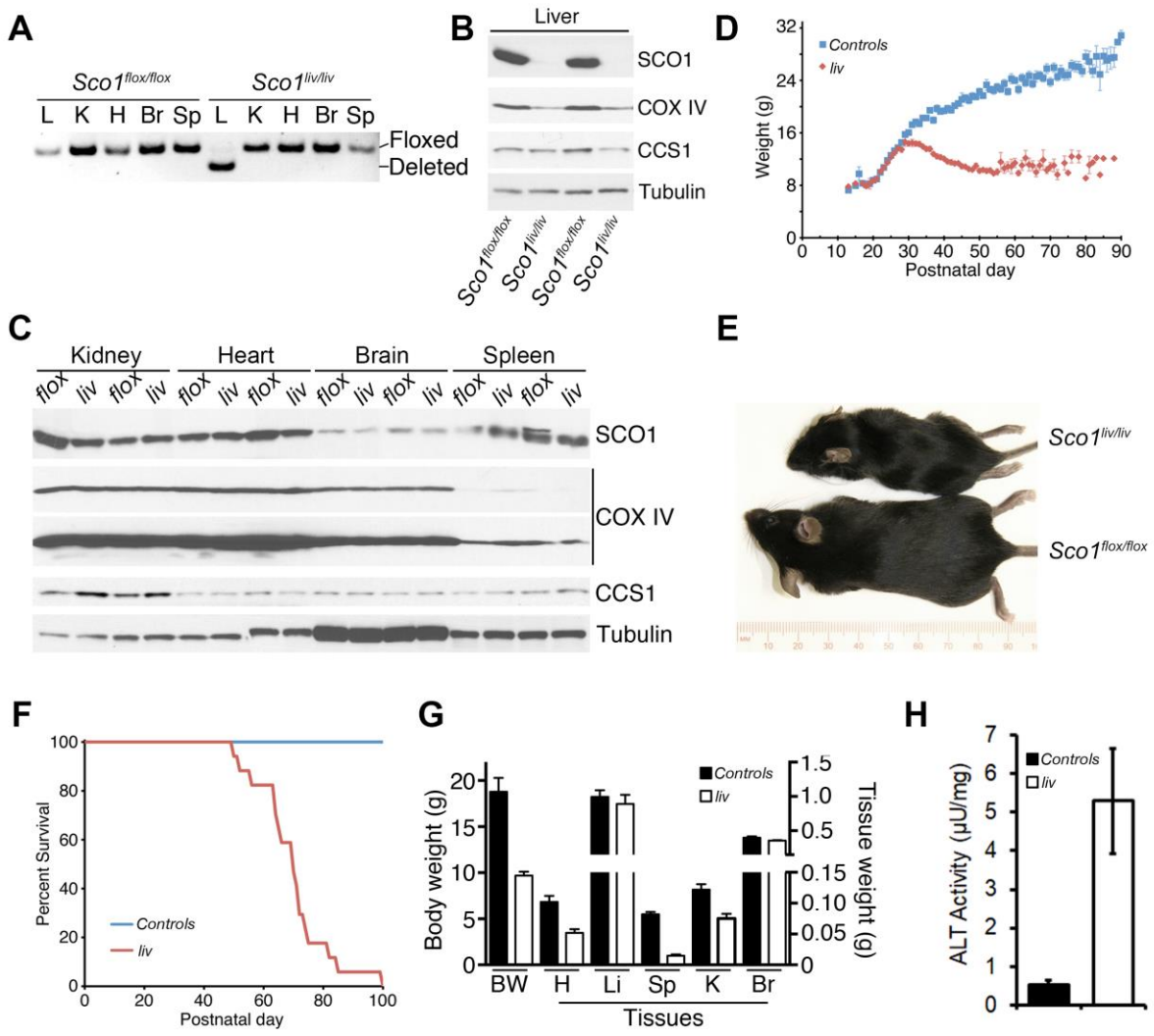


**Figure 4.1: Deletion of *Sco1* in the liver is lethal and presents with a severe growth deficiency**
(A) PCR analysis of the *Sco1* gene determining presence of a floxed (top) or deleted (bottom) second exon in various tissues (L= Liver, K= Kidney, H= Heart, Br= Brain, Sp= Spleen) in both wild-type (*Sco1*$^{flox/flox}$) and liver-specific knockout mice (*Sco1*$^{liv/liv}$) at P47. (B) Western blot analysis of SCO1, COX IV, and CCS abundance in the livers of both wild-type (*Sco1*$^{flox/flox}$) and liver-specific *Sco1* knockout mice (*Sco1*$^{liv/liv}$) at P47. Tubulin was used as a loading control. (C) Western blot analysis of SCO1, COX IV, and CCS abundance in various tissues in P47 wild-type (*flox*) and liver-specific *Sco1* knockout mice (*liv*). Tubulin was used as a loading control. Multiple images for SCO1 represent a long and short exposure times (D) Body weight (g) over time for both wild-type (*Controls*, n=184) and liver-specific *Sco1* knockout mice (*liv*, n=38). (E) Wild-type (bottom, *Sco1*$^{flox/flox}$) and liver-specific *Sco1* knockout mice (top, *Sco1*$^{liv/liv}$) at P57 with ruler for reference. (F) Kaplan-Meier survival curve of wildtype (blue, *Controls*, n=96) and liver-specific *Sco1* knockout mice (red, *liv*, n=17). (G) Total body weight (right y-axis, g) and tissue weight (left y-axis, g) in both wild-type (*Controls*, n=5) and liver-specific *Sco1* knockout mice (*liv*, n=5), (BW= Body Weight, H= Heart, Li=Liver, Sp= Spleen, K= Kidney, Br= Brain). (H) Total Alanine Transaminase (ALT) activity (µU/mg) in the serum of both wild-type (*Controls*) and liver-specific *Sco1* knockout mice (*liv*) at P57.

#### 4.1.1.3 Livers from *Sco1*$^{liv/liv}$ mice exhibit marked steatosis

Livers from *Sco1*$^{liv/liv}$ mice exhibited significant discolouration compared to wild-type livers, a phenotype that was manifest upon the onset of the growth deficiency (Figure 4.2A). Using transmission electron microscopy (TEM) we determined that this discolouration was caused at least in part by an increased number of lipid droplets (Figure 4.2B). This conclusion was confirmed by thin-layer chromatography, which showed an increase in hepatic cholesterol esters and triglycerides (Figure 4.2C,D). Finally, the analysis of microarray data obtained from the livers of both *Sco1*$^{liv/liv}$ and wild-type mice identified remodelling of the hepatic transcriptome and the upregulation of genes in pathways crucial to the induction of hepatic steatosis (Figure 4.2E).

### 4.1.2 Molecular characterization of *Sco1*$^{liv/liv}$ mice

#### 4.1.2.1 *Sco1* knockout livers exhibit a severe isolated COX deficiency and increased mitochondrial content

To determine the cause of the hepatopathy in *Sco1*$^{liv/liv}$ mice, we began to characterize their livers on a biochemical, molecular and ultrastructural level. Livers from *Sco1*$^{liv/liv}$ mice had a severe, isolated COX deficiency both with respect to enzymatic activity (Figure 4.3A) and holoenzyme abundance (Figure 4.3B). The COX deficiency was already severe by P18 and progressively worsened over time. Mirroring the decrease in COX activity was a corresponding increase in the activity of citrate synthase (CS) (Figure 4.3A), as well as an increase in the abundance of multiple other mitochondrial markers such as TOM40, ATPase α, and SOD2 (Figure 4.3B). Consistent with a compensatory increase in the mitochondrial content of *Sco1* knockout livers, TEM images also showed that the number of mitochondria was higher in livers lacking *Sco1* expression (Figure 4.2B).

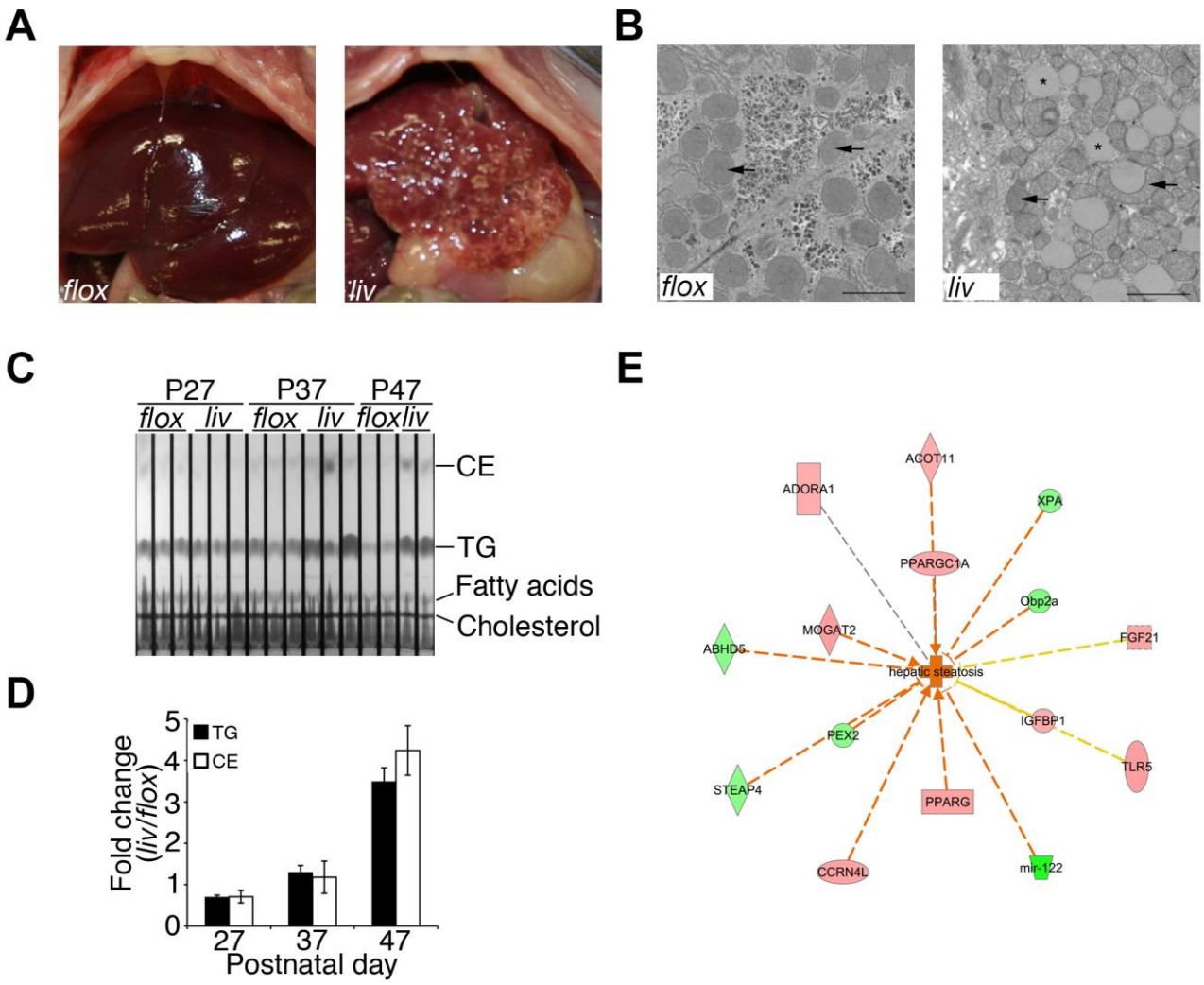


**Figure 4.2: Liver-specific knockout of *Sco1* results in severe steatosis**

(A) Livers from both wild-type (left, *flox*) and liver-specific *Sco1* knockout mice (*liv*) at P57. (B) TEM image at 3,330X magnification of P57 livers from both wild-type (*flox*) and liver-specific *Sco1* knockout mice (*liv*). Scale bar represents 2 μm. Arrows represent mitochondria. Asterisks represent lipid droplets (C) Thin-layer chromotographic analysis of lipid content (CE= cholesterol ester, Tg= Triglyceride, FA= Fatty acid, Ch = Cholesterol) in livers from both wild-type (*flox*) and liver-specific *Sco1* knockout mice (*liv*) at P27, P37, and P47. (D) Quantification of triglycerides (TG) and cholesterol esters (CE) at P27, P37, and P47 in livers of liver-specific *Sco1* knockout mice. (n=6 for each at all time points). (E) Ingenuity pathway analysis of microarray data showing both upregulated genes (red), and down regulated genes (green) involved in hepatic steatosis in the livers of liver-specific *Sco1* knockout mice. Orange lines represent the activation of specific pathways. Yellow lines represent gene expression profiles inconsistent with global pathway prediction.

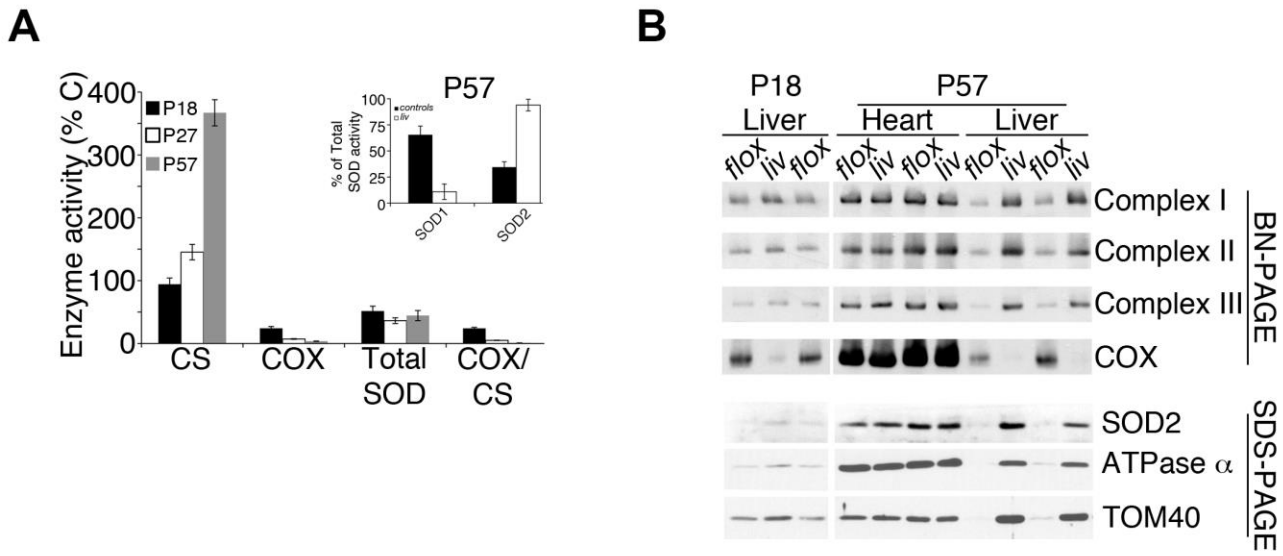


**Figure 4.3: Deletion of *Sco1* in the liver causes an isolated COX deficiency**
(A) Specific actives of citrate synthase (CS), cytochrome *c* oxidase (COX), and total super oxide dismutase (SOD) in the livers from P18 (black), P27 (white), and P57 (grey) liver-specific *Sco1* knockout mice (n= 4-5) expressed as a percentage of wild-type controls (n=5-7). (Inset) Percentage of total SOD activity from Cu,Zn-SOD1 (left), and Mn-SOD2 (right) in wild-type (black, *Controls*, n=5) and liver-specific *Sco1* knockout mice (white, *liv*, n= 4) at P57. (B) Blue Native PAGE (top) analysis of the electron transport chain complexes I, II, III, and IV and SDS-PAGE (bottom) analysis of the mitochondrial markers SOD2, ATPase α, and TOM40 in wild-type (*flox*) and liver-specific *Sco1* knockout mice (*liv*) at P18 and P57

### 4.1.2.2 *Sco1*$^{liv/liv}$ mice have a severe hepatic copper deficiency that is accompanied by an increase in the levels of iron stored in Kupffer cells

One of the hallmarks of patients with pathogenic mutations in *SCO1* is that affected tissues exhibit a combined isolated COX and whole cell copper deficiency. Given that *Sco1* knockout livers phenocopied affected patient tissues with respect to the COX deficiency, we next looked at their cellular copper levels. Livers from P47 *Sco1*$^{liv/liv}$ mice had significantly lower levels of copper than their wild-type littermates, without an appreciable copper deficiency in any of the other peripheral tissues that were examined (Figure 4.4A). A similar decrease was observed in the activity of the cuproenzyme SOD1 (Figure 4.3A), a common observation under copper-deficient conditions. This copper deficiency was observed at P18 and, like the COX deficiency, progressively worsened over time (Figure 4.4B). Metal concentrations in other tissues examined remained unchanged at all time points (Figure 4.4C). Despite the decrease in cellular copper levels within the *Sco1* null livers, the total amount of mitochondrial copper was preserved in these cells (Figure 4.4D). Interestingly, we also observed a sharp increase in the concentration of iron and a concomitant decrease in the

concentration of zinc (Figure 4.4A); however, these changes only occurred in the livers of end stage mice, long after the onset of the copper deficiency (Figure 4.4B). Furthermore, upon histological analysis we determined that this increase in iron levels was isolated to the Kupffer macrophages resident to the liver and not manifest in the *Sco1* null hepatocytes themselves (Figure 4.4E).

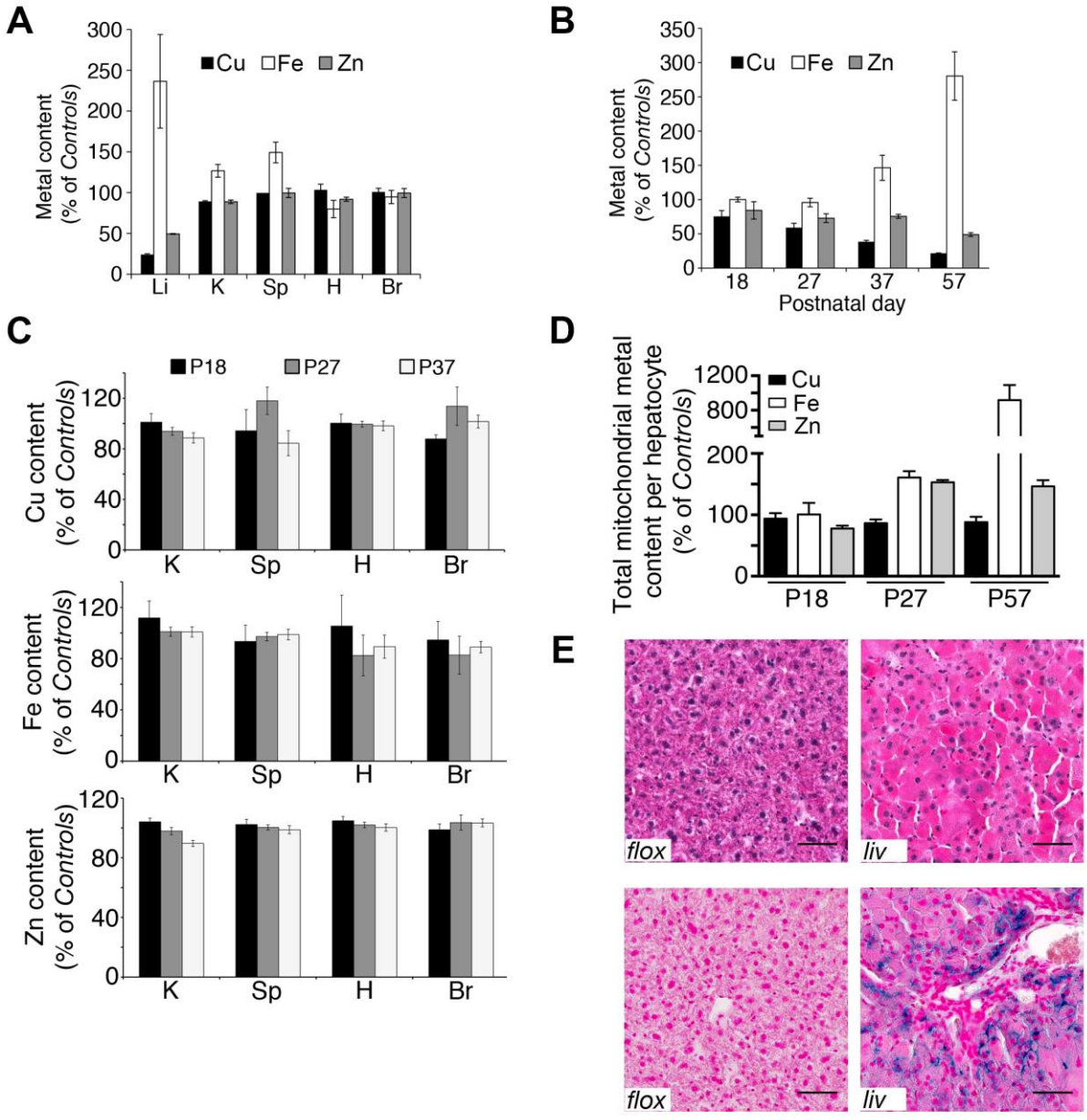


**Figure 4.4: Deletion of *Sco1* in the liver causes a hepatic copper deficiency**
(A) Total levels of copper (black), iron (white) and zinc (grey) in various tissues (Li= Liver, K= Kidney, Sp= Spleen, H= Heart, Br= Brain) from P47 liver-specific *Sco1* knockout mice (n=5 for all tissues and metals) expressed as a percentage of wild-type controls (n=8 for all tissues and metals). (B) Total levels of copper (black), iron (white) and zinc (grey) in livers of liver-specific *Sco1* knockout mice at P18, P27, P37, and P57 (n=4-5 for all metals at all time points) expressed as a percentage of

wild-type controls (n= 4-11 for all metals at all time points). (C) Total levels of copper (Cu, top), iron (Fe, middle), and zinc (Zn, bottom) in various tissues (K= Kidney, Sp= Spleen, H= Heart, Br= Brain) in P18 (black), P27 (grey), and P37 (white) liver-specific *Sco1* knockout mice (n= 4-5) expressed as a percentage of age matched wild-type controls (n= 4-11). (D) Total levels of mitochondrial copper (black), iron (white), and zinc (grey) in livers of liver-specific *Sco1* knockout mice at P18, P27, and P57 expressed as a percentage of wild-type controls. Data from panel C was multiplied by citrate synthase activity to account for increase in mitochondrial content within hepatocytes. (E) 20X magnification of Hematoxylin and Eosin (top) and Perls (bottom) stained sections of livers from both wild-type (left, *flox*) and liver-specific *Sco1* knockout (right, *liv*) mice at P57. Scale bar represents 50 μm.

#### 4.1.2.3 The copper deficiency in *Sco1* knockout livers is driven by a progressive decrease in the abundance of the high affinity copper transporter CTR1

The severe copper deficiency observed in *Sco1* knockout livers may be caused by either a defect in high affinity copper import or an increase in copper export. To distinguish between these two possibilities, we examined the abundance of known copper transporters. The abundance of ATP7B was unchanged upon hepatic deletion of *Sco1* (Figure 4.5A). In contrast, the levels of ATP7A, another protein involved in copper export, were increased in the livers of end stage $Sco1^{liv/liv}$ mice (Figure 4.5B). Although this may indicate an increase in copper export, the increase in ATP7A abundance occurs long after the establishment of the copper deficiency (Figure 4.4A), suggesting that elevated export is not driving the initial copper deficiency within the *Sco1* knockout liver. We therefore turned our attention to the high affinity copper importer, CTR1. The abundance of CTR1 was significantly decreased in the livers of $Sco1^{liv/liv}$ mice compared to their wild-type littermates at P27 (Figure 4.5A,B). CTR1 levels further decreased with little to no immunologically detectable protein being observed by P57 (Figure 4.5A). Importantly, although the abundance of CTR1 was unchanged in the copper-deficient P18 $Sco1^{liv/liv}$ mice, a high percentage of the protein was mislocalized from the plasma membrane at P22, demonstrated by reduced co-localization with the plasma membrane marker $Na^+/K^+$ ATPase (Figure 4.5C,D). These data collectively point to a significant perturbation in copper import within the *Sco1* knockout liver.

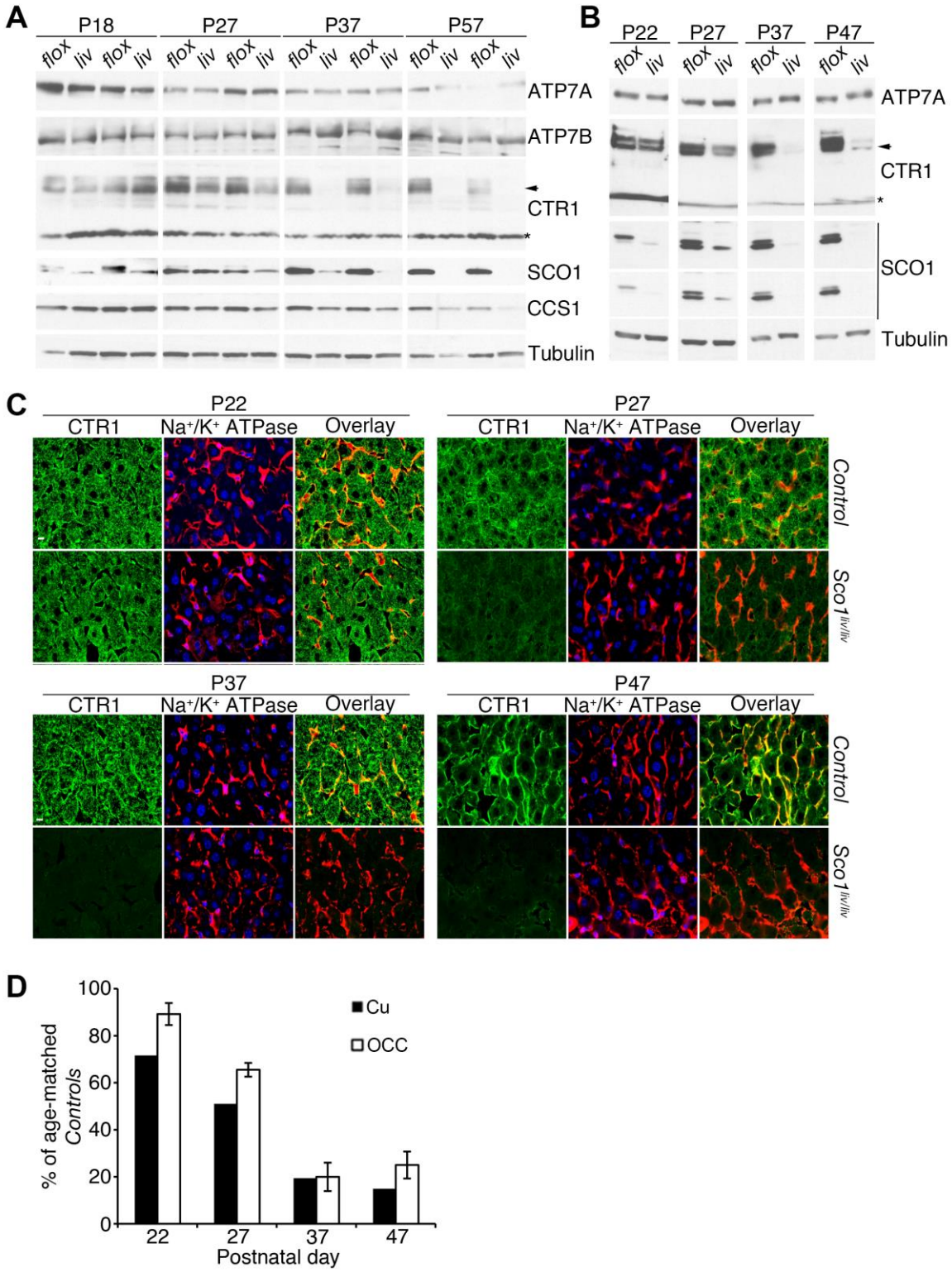


**Figure 4.5: Deletion of *Sco1* in the liver causes a change of localization and a decrease in the abundance of CTR1**

(A) Western blot analysis of ATP7A, ATP7B, CTR1, SCO1, and CCS abundance from the livers of wild-type (*flox*) and liver-specific *Sco1* knockout (*liv*) mice at P18, P27, P37, and P57. Tubulin was

used as a loading control. For SCO1, upper band represents true SCO1, lower band represents unknown, non-specific, immunoreactive band. (B) Western blot analysis of ATP7A, CTR1, SCO1, and CCS abundance from the livers of wild-type (*flox*) and liver-specific *Sco1* knockout (*liv*) mice at P22, P27, P37, and P47. (For A and B) Arrow represents the mature glycosylated form of CTR1, while the asterisk represents the truncated form of the protein. Tubulin was used as a loading control. Multiple images for SCO1 represent a long and short exposure times. For SCO1, upper band represents true SCO1, lower band represents unknown, non-specific, immunoreactive band. (C) Immunofluorescence analysis of CTR1 (green) localization in livers of wild-type (*Control*, top) and liver-specific *Sco1* knockout ($Sco1^{liv/liv}$, bottom) mice from panel B. $Na^+/K^+$ ATPase (red) was used as a marker for plasma membrane. Images were taken at 40X and scale bar represents 10 μm. Co-stained signal in overlay is shown in yellow. (D) Total copper content (Cu, black) and quantification of immunofluorescence correlation coefficient of co-staining between CTR1 and $Na^+/K^+$ ATPase (OCC, white, n= 7 for all time points) in livers of liver-specific *Sco1* knockout mice at P22, P27, P37, and P47 expressed as a percentage of wild-type littermates.

### 4.1.3 Investigating the mechanism of mitochondrial copper signalling

#### 4.1.3.1 Decreased CTR1 abundance is mirrored in *Cox10* but not *Lrpprc* knockout livers

The decrease in CTR1 abundance in the livers of $Sco1^{liv/liv}$ mice may be attributable to the lack of SCO1 or the isolated COX deficiency. To address this issue, we examined liver-specific knockout mice with deletions in two other genes known to be involved in COX assembly, *Cox10* and *Lrpprc*. Livers from both knockout mouse models were less affected than their $Sco1^{liv/liv}$ counterparts and had an increase in the abundance of SCO1 (Figure 4.6A,B). Although both *Cox10* and *Lrpprc* knockout livers exhibited comparable decreases in COX activity and copper levels (Figure 4.6A), only the *Cox10* knockout livers displayed a decrease in CTR1 abundance (Figure 4.6B). CTR1 levels were comparable in *Lrpprc* knockout and wild-type livers, although loss of LRPPRC function resulted in a significant increase in the abundance of ATP7A (Figure 4.6A). To further confirm that the abundance of CTR1 was not correlated with COX activity, we looked at its steady-state levels in $rho^0$ cells, which lack mitochondrial DNA. $Rho^0$ cells had only a modest reduction in CTR1 abundance (Figure 4.6C), further suggesting that the signalling mechanism that leads to a reduction in CTR1 levels is not the direct result of lower residual COX activity.

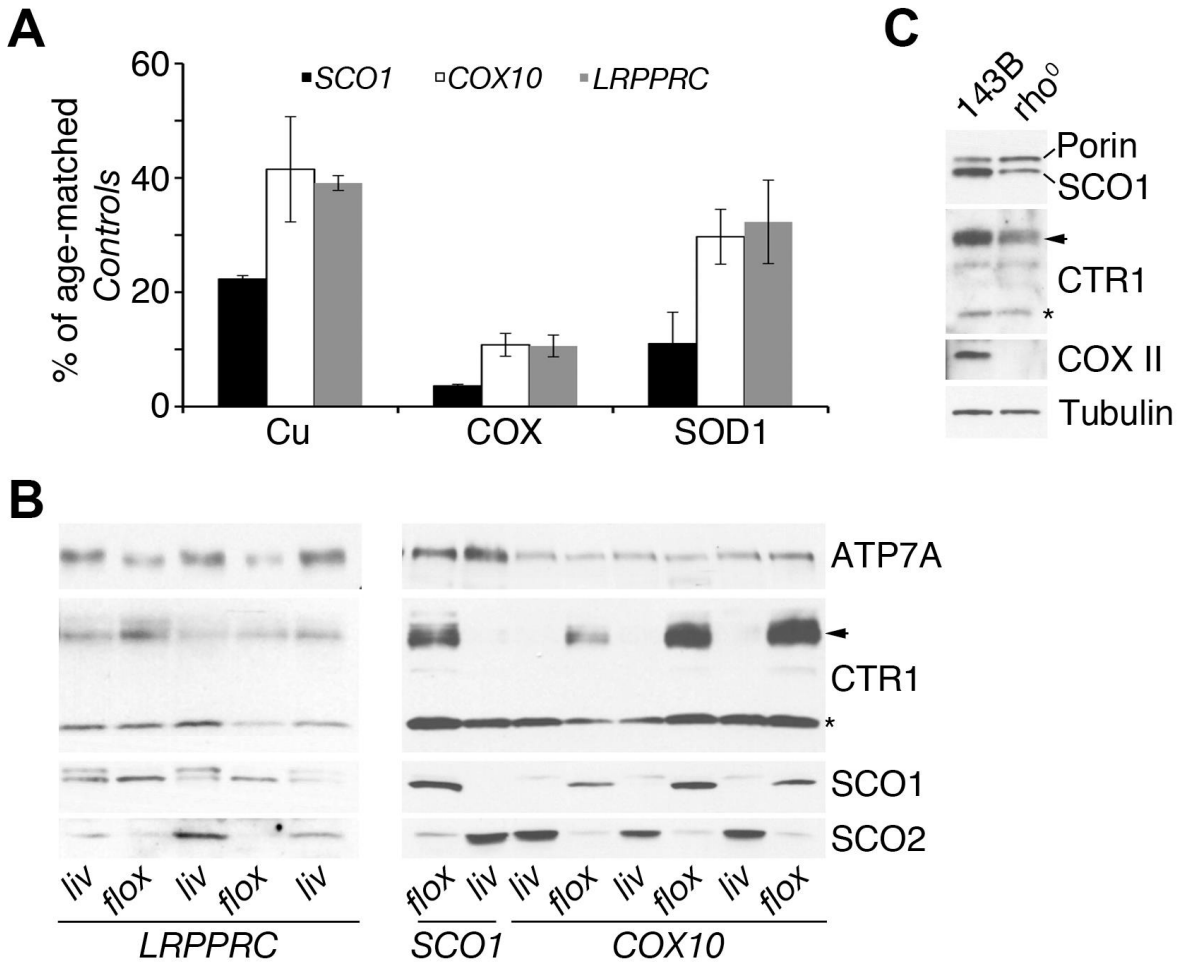


**Figure 4.6: Changes in CTR1 abundance are not correlated with a general energy deficiency** (A) Levels of total copper (Cu), cytochrome *c* oxidase activity (COX), and total superoxide dismutase activity (SOD) in livers of liver-specific knockouts of *Sco1* (black), *Cox10* (white, n= 8 for each measurement), and *Lrpprc* (grey, n= 3 for each measurement) at P57 expressed as a percentage of wild-type controls (n= 6 for *Cox10*, n= 3 for *Lrpprc*). *Sco1* data is included from Figure 3A and 4C for reference. (B) Western blot analysis of ATP7A, CTR1, SCO1 and SCO2 abundance from livers of wild-type (*flox*) and liver-specific *Lrpprc* (left), *Sco1* (middle), and *Cox10* (right) knockout (*liv*) mice at P70 (*Lrpprc*), and P47-67 (*Sco1* and *Lrpprc*). (C) Western blot analysis of SCO1, CTR1, and COX II abundance in control (143B) and rho$^0$ cells. Porin and Tubulin were used as loading controls for mitochondrial content and total protein respectively. (For B and C) Arrow represents the mature glycosylated form of CTR1, while the asterisk represents the truncated form of the protein.

#### 4.1.3.2 *Sco1* null MEFs are copper deficient owing to enhanced proteasomal degradation of CTR1

We next wanted to determine whether the observed change in CTR1 abundance was caused by a decrease in protein synthesis or an increase in the rate of protein degradation. *Ctr1* mRNA transcript levels in the liver of the $Sco1^{livliv}$ mice were unchanged in our genome-wide microarray RNA expression analysis (data not shown) and in our semi-quantitative, reverse-transcriptase PCR experiments (Figure 4.7A), suggesting that adequate mRNA existed to support protein synthesis. The lack of change in *Ctr1* transcript levels was in marked contrast to the increase and decrease, respectively, in the mRNA levels of metallothionein 1 (*Mt1*) and the solute carrier family protein *Slc41a2* (Figure 4.7A), which mirrored the changes in gene expression we observed in our microarray analysis. To consider the potential contribution of active CTR1 degradation, we first generated *Sco1* knockout mouse embryonic fibroblasts (MEFs). Successful excision at the *Sco1* locus and absence of SCO1 protein was confirmed by PCR genotyping (Figure 4.7B) and Western blot analysis (Figure 4.7C), respectively. Phenocopying the *Sco1* knockout livers, *Sco1* knockout MEFs had a reduction in the abundance of COX IV (Figure 4.7C), a severe copper deficiency (Figure 4.7F) and a decrease in the abundance of CTR1 (Figure 4.7D). CTR1 levels were rescued by overexpressing a *Sco1* cDNA, while CTR1 overexpression only led to the accumulation of the truncated form of the protein (Figure 4.7E). Consistent with these observations, the combined copper and COX deficiency was complemented by SCO1 but not CTR1 overexpression (Figure 4.7F). To further confirm that CTR1 is preferentially degraded in the absence of *Sco1* expression, we treated cells with the proteasomal inhibitor MG132 and found that it fully restored CTR1 levels in *Sco1* knockout MEFs (Figure 4.8A,B).

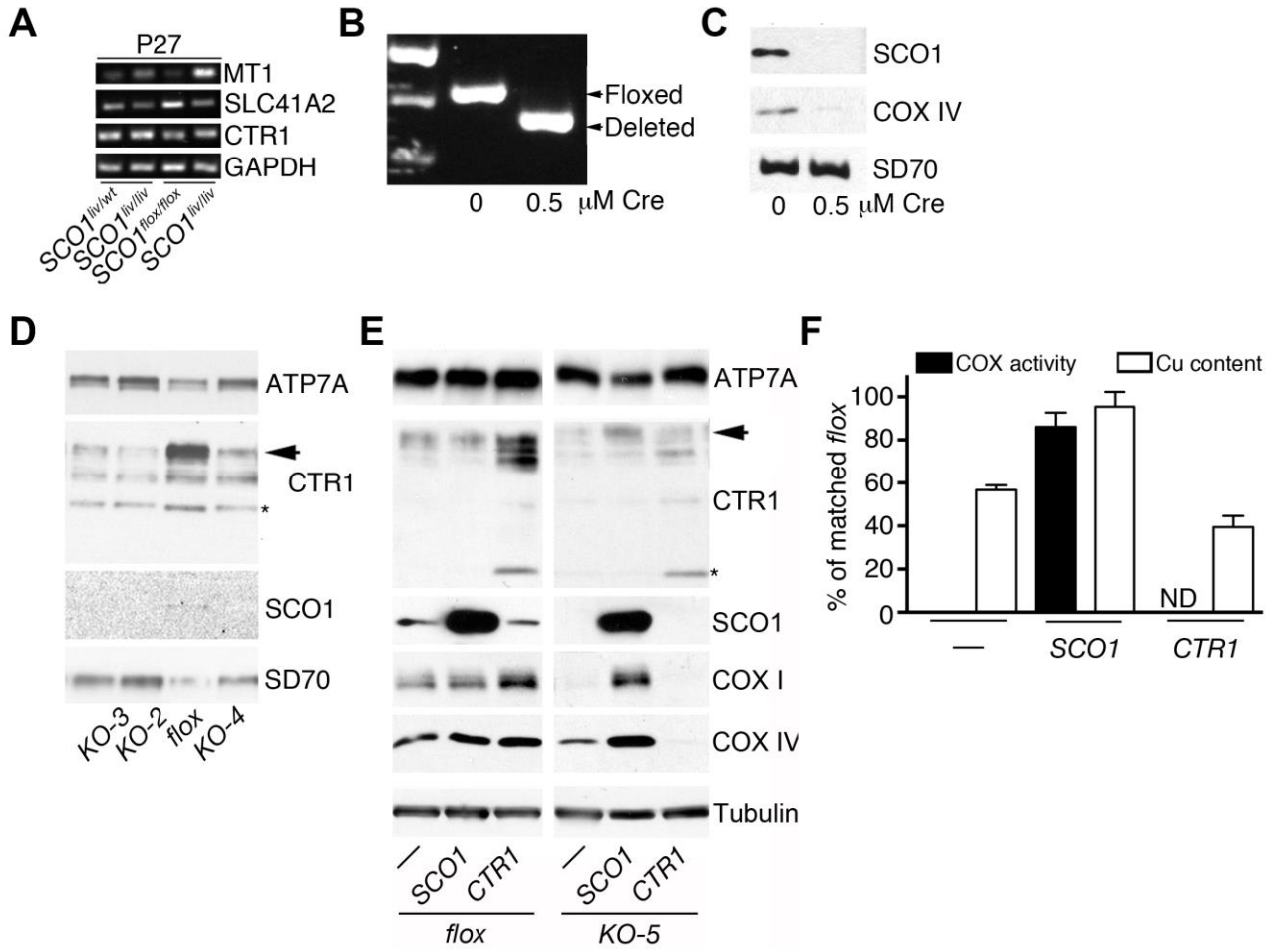


**Figure 4.7: Deletion of *Sco1* in mouse embryonic fibroblasts results in a decrease of CTR1 abundance**

(A) Semi-quantitative RT-PCR analysis of metallothionein 1 (MT1), solute carrier family 41 member A2 (SLC41A2), and CTR1 mRNA transcript levels from livers of wild-type (*Control*) and liver-specific *Sco1* knockout ($Sco1^{liv/liv}$) mice at P27. GAPDH was used as a loading control. (B) PCR genotyping of *Sco1* gene in both control (untreated) or *Sco1* knockout (treated with 0.5 μM purified CRE recombinase) MEFs determining presence of floxed (top) or deleted (bottom) second exon. (C) Western blot analysis of SCO1 and COX IV abundance in control (left) and *Sco1* knockout (right) MEFs. SD70 was used as a loading control. (D) Western blot analysis of ATP7A, CTR1, and SCO1 in both control (*flox*) and *Sco1* knockout (*KO-1-4*) MEFs. SD70 is used as a loading control. (E) Western blot analysis of ATP7A, CTR1, SCO1, COX I, and COX IV in control (*flox*) and *Sco1* knockout (*KO-5*) MEFs either untreated, or overexpressing SCO1 or CTR1. Tubulin was used as a loading control. (For D and E) Arrow represents the mature glycosylated form of CTR1, while the asterisk represents the truncated form of the protein. (F) Total cytochrome *c* oxidase activity (black) and copper levels (white) in *Sco1* knockout MEFs either untreated or overexpressing SCO1 or CTR1. Data are expressed as percentage of control MEFs. (n=4 for each measurement). ND = Not determined.

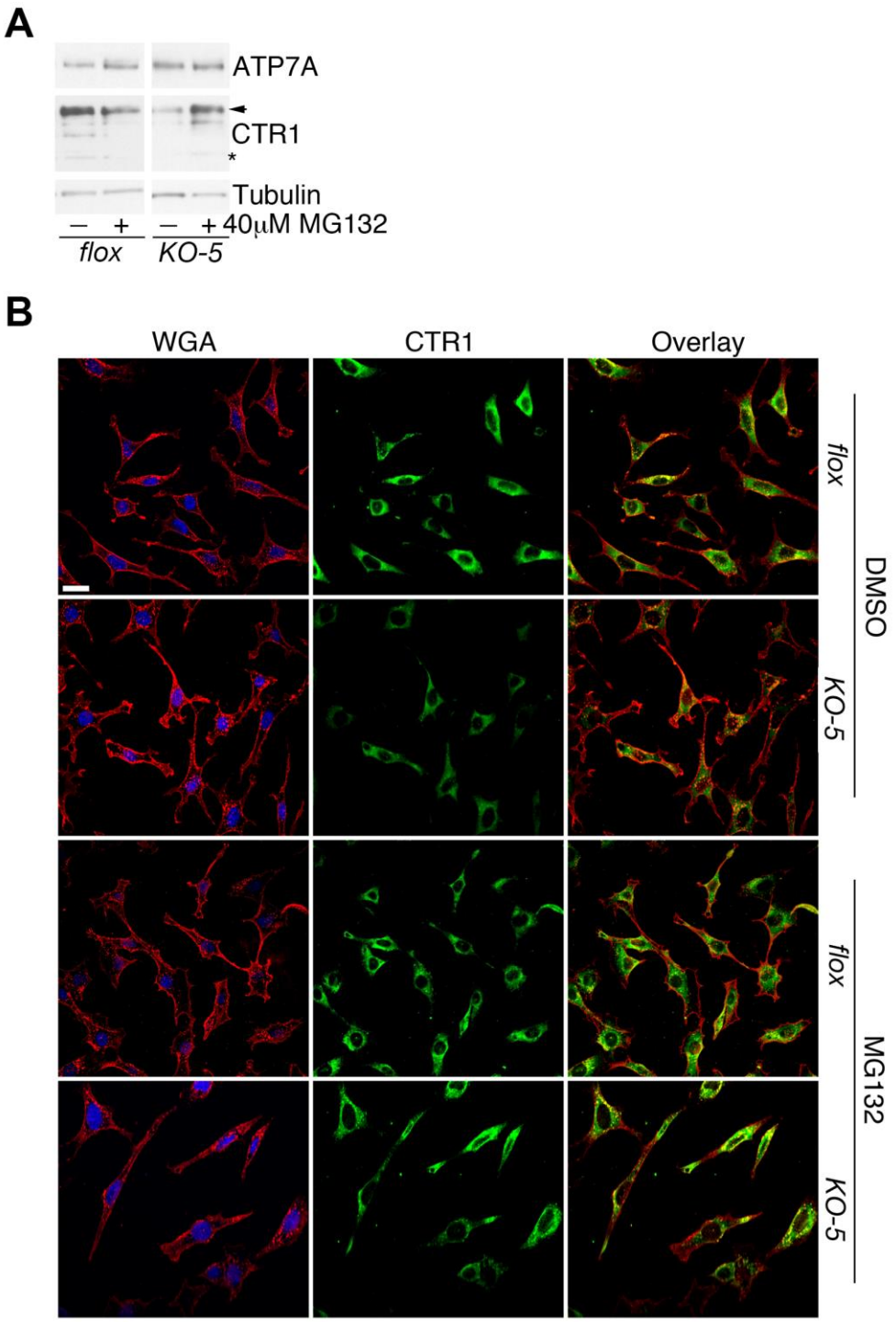


**Figure 4.8: CTR1 abundance in MEFs is rescued by the proteosome inhibitor MG132**
(A) Western blot analysis of ATP7A and CTR1 abundance in control (*flox*) and *Sco1* knockout MEFs both untreated and treated with 40 μM MG132. Arrow represents the mature glycosylated form of CTR1, while the asterisks represents the truncated form of the protein. Tubulin is used as a loading control. (B) Immunofluorescence analysis of CTR1 (green) expression and localization in control (*flox*) and *Sco1* knockout (*KO-5*) treated with DMSO or MG132. Wheat germ agglutinin (red) is used as a plasma membrane marker. Co-staining signal in overlay is shown in yellow.

## 4.2 The role of SCO1 in maintaining cellular copper homeostasis in the murine heart

### 4.2.1 Physiological characterization of *Sco1*$^{hrt/hrt}$ mice

#### 4.2.1.1 Validation of heart-specific *Sco1* deletion

Following the characterization of *Sco1*$^{liv/liv}$ mice, we next turned our attention to examining the role of SCO1 in the murine heart. We began by using an identical breeding strategy to that described in Section 4.1.1.1 and a transgenic line in which *Cre recombinase* expression is under the control of the α-myosin heavy chain promotor (αMHC) to generate a heart-specific *Sco1* knockout mouse, herein referred to as *Sco1*$^{hrt/hrt}$ mice. *Sco1*$^{hrt/hrt}$ mice were viable and observed at the expected Mendelian frequencies (data not shown). Successful heart-specific deletion of the second exon of *Sco1* was verified using a three-primer PCR method (Figure 4.9A), and reduced SCO1 protein expression in the heart was confirmed as early as embryonic day 15 (E15) by Western blot analysis (Figure 4.9B).

#### 4.2.1.2 Heart-specific deletion of *Sco1* is lethal with mice exhibiting left ventricular dilation and cardiomyocyte vacuolization

Excision of the *Sco1* alleles in the developing heart of *Sco1*$^{hrt/hrt}$ mice proved to be extremely severe. None of the *Sco1*$^{hrt/hrt}$ mice survived beyond P2 (Figure 4.9C), despite having the same body weight as their wild-type littermates (Figure 4.9D). To determine the cause of the observed perinatal lethality, we examined the heart of *Sco1*$^{hrt/hrt}$ mice histologically. *Sco1* knockout hearts were misshapen and exhibited an enlarged left ventricle, characteristic of a dilated cardiomyopathy (Figure 4.9E). Further characteristics of pathological cardiomyocyte dysfunction were observed upon hematoxylin and eosin (H&E) staining, including the enlargement of the cardiomyocytes as well as a distinct vacuolization (Figure 4.9F) in the absence any significant fibrosis (data not shown).

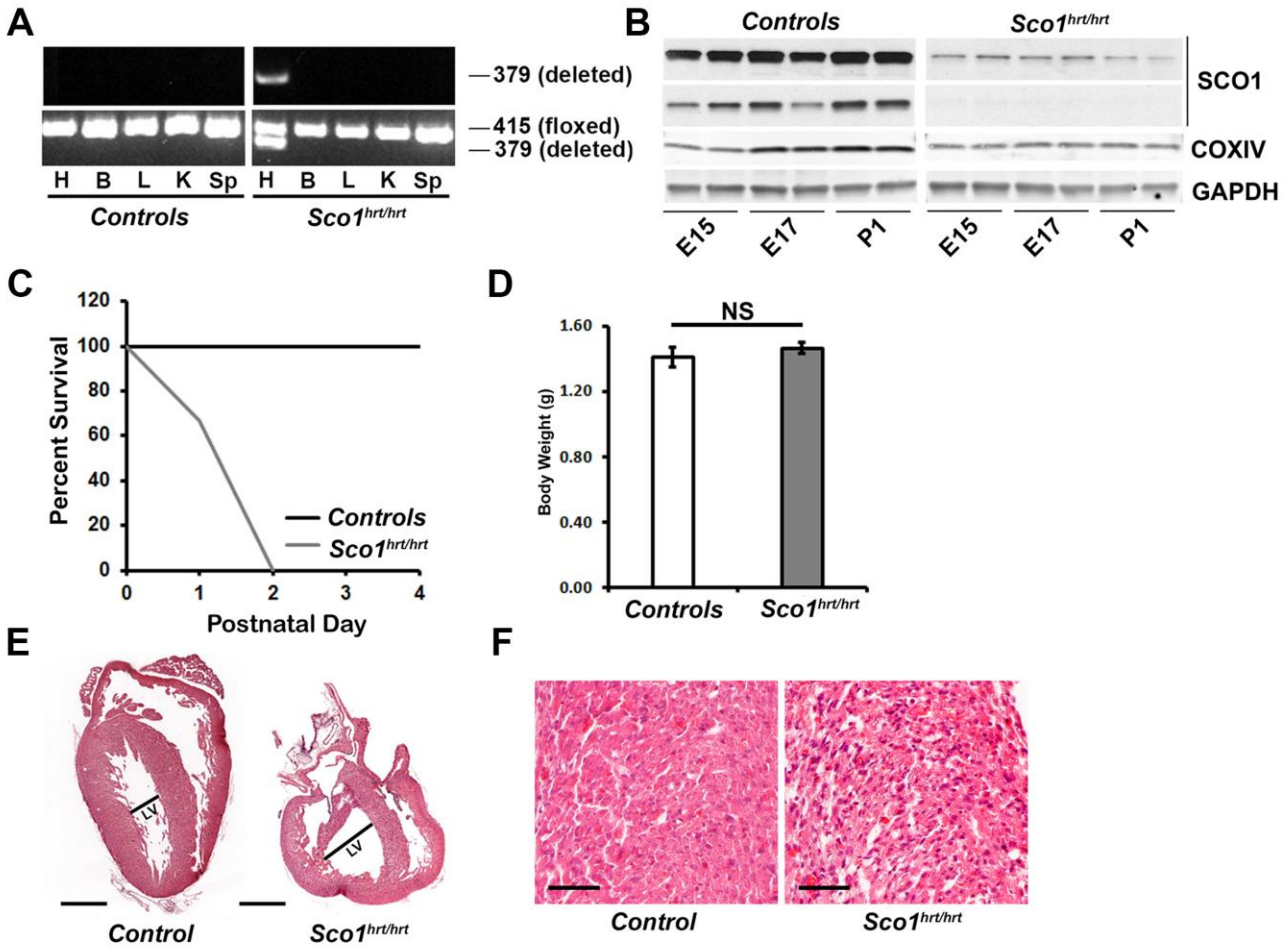


**Figure 4.9: Deletion of *Sco1* in the heart is lethal and presents with dilated cardiomyopathy**
(A) PCR analysis of the *Sco1* gene determining presence of a floxed (415 bp) or deleted (379 bp) second exon in various tissues (H= Heart, B= Brain, L= Liver, K= Kidney, Sp= Spleen) in both wild-type (*Controls*) and heart-specific knockout mice ($Sco1^{liv/liv}$) at P1. Top represents two primer PCR conditions to individually amplify the deleted allele. Bottom represents three primer PCR conditions to amplify both floxed and deleted alleles. (B) Western blot analysis of SCO1 and COX IV abundance in wild-type (*Controls*) and heart-specific *Sco1* knockout ($Sco1^{hrt/hrt}$) mice at E15, E17, and P1. GAPDH is used as a loading control. Multiple images for SCO1 represent a long and short exposure times. (C) Kaplan-Meier survival curve of wildtype (black, *Controls*, n=40) and heart-specific *Sco1* knockout mice (grey, $Sco1^{hrt/hrt}$, n=15). (D) Body weight (g) of wild-type (*Controls*) and heart-specific *Sco1* knockout ($Sco1^{hrt/hrt}$) mice at P1. (n= 6 for each genotype). (E) Hematoxylin and Eosin stained sections of hearts from wild-type (*Control*, left) and heart-specific *Sco1* knockout ($Sco1^{hrt/hrt}$, left) mice at P1. LV stands for left ventricle. Scale bar represents 500 µm. (F) 20X magnification of H&E stained sections of hearts from wild-type (*Control*, left) and heart-specific *Sco1* knockout ($Sco1^{hrt/hrt}$, right) mice from panel D. Scale bar represents 50 µm.

### 4.2.2 Molecular characterization of *Sco1*$^{hrt/hrt}$ mice

#### 4.2.2.1 *Sco1* knockout hearts exhibit a severe, isolated COX deficiency

To determine the cause of the cardiomyopathy observed in the *Sco1*$^{hrt/hrt}$ mice we further examined the molecular phenotype of these hearts. Hearts from *Sco1*$^{hrt/hrt}$ mice had a severe COX deficiency at the level of enzymatic activity (Figure 4.10A), abundance of the structural subunit COXIV (Figure 4.10B) and the amount of fully assembled holoenzyme (Figure 4.10C). Unlike the *Sco1* knockout liver, the hearts from *Sco1*$^{hrt/hrt}$ mice did not have an increase in mitochondrial content, as the activity of CS remained unchanged from wild-type littermates (Figure 4.10A).

#### 4.2.2.2 *Sco1* knockout hearts have a modest copper deficiency that is not caused by a change in CTR1 abundance

In addition to the COX deficiency, *Sco1* knockout hearts had a significant decrease in total superoxide dismutase activity (Figure 4.10A) that was specific to the copper-dependent SOD1 form of the enzyme, as the levels of cyanide resistant Mn-SOD2 remained unaffected (Figure 4.10D). The deficiency in SOD1 suggested that deletion of *Sco1* in the heart may result in a global copper deficiency. While *Sco1* knockout hearts exhibited a statistically significant decrease in total copper levels (Figure 4.11A), it was modest with respect to the fold change. Similar to the *Sco1*$^{liv/liv}$ mice, the abundance of the copper exporter ATP7A was unchanged in *Sco1* knockout hearts (Figure 4.11B). In contrast, however, CTR1 abundance was unaffected by lack of *Sco1* expression in cardiomyocytes (Figure 4.11B), and the abundance of CCS was unchanged (Figure 4.11B). This suggests that loss of SCO1 function affected the copper sensing and import machinery in a tissue-specific manner.

#### 4.2.2.3 The livers of *Sco1*$^{hrt/hrt}$ mice have a significant copper deficiency and a decrease in CTR1 abundance

Interestingly, the livers of *Sco1*$^{hrt/hrt}$ mice had a comparable copper deficiency to the hearts lacking *Sco1* expression (Figure 4.11A), and a decrease in the abundance of CTR1 (Figure 4.11C). Even though this finding is reminiscent of the copper deficiency phenotype observed in the *Sco1* knockout liver, the decrease in the copper content of the livers of *Sco1*$^{hrt/hrt}$ mice did affect the activity of COX or SOD1 (Figure 4.11D) or the abundance of COX IV (Figure 4.11E). Copper levels in all other somatic tissues and plasma of *Sco1*$^{hrt/hrt}$ mice were unchanged when compared to wild-type littermates (Figure 4.11F).

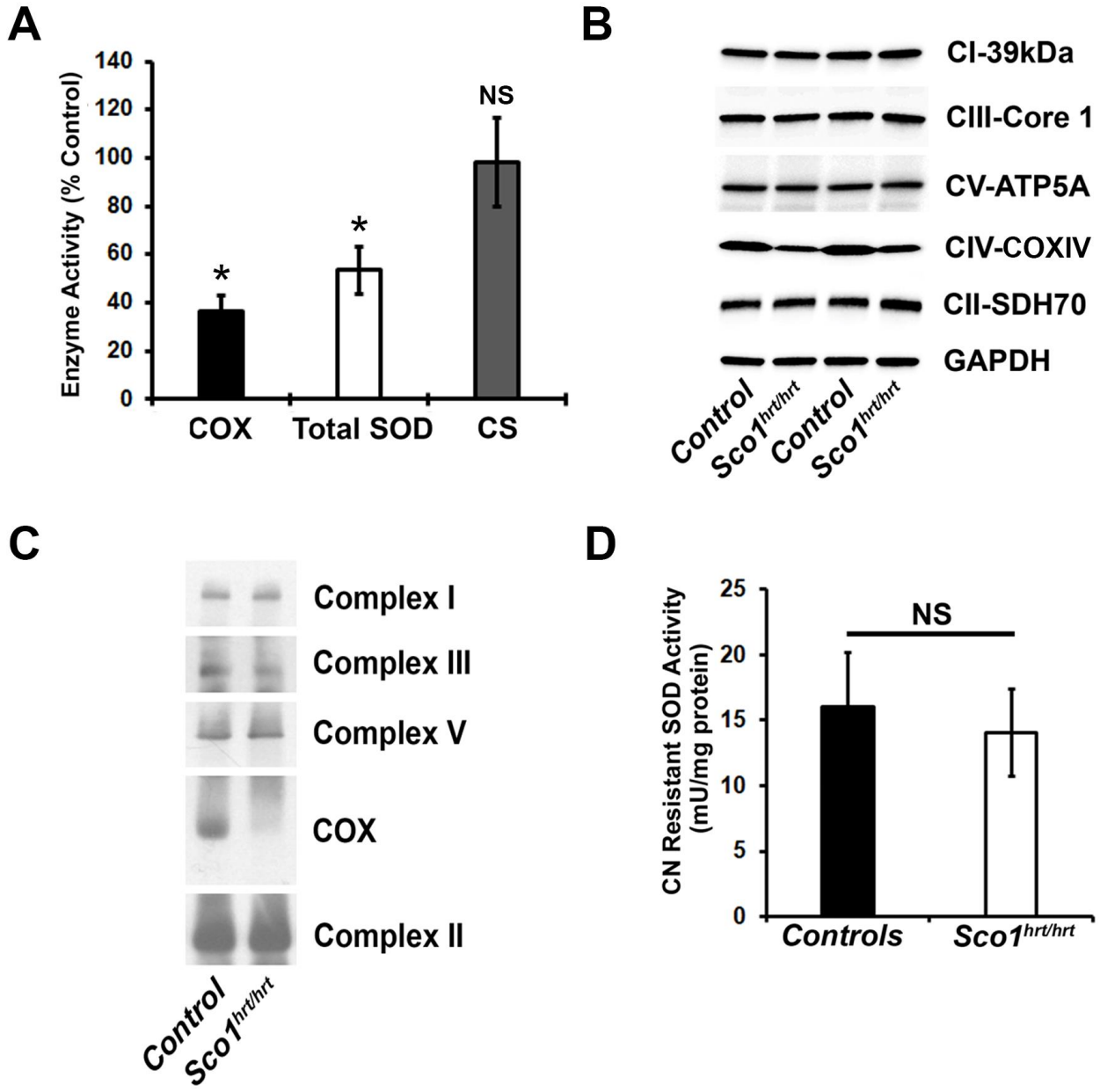


**Figure 4.10: Deletion of *Sco1* in the heart causes an isolated COX deficiency**
(A) Specific activities of cytochrome *c* oxidase (COX, black, n= 3), total super oxide dismutase (SOD, white, n= 6), and citrate synthase (CS, grey, n= 3) in the hearts from P1 heart-specific *Sco1* knockout (*Sco1*$^{hrt/hrt}$) mice expressed as a percentage of wild-type litter mates. (B) Western blot analysis of the abundance of representative subunits from complexes I-V of electron transport chain in hearts from wild-type (*Control*) and heart-specific *Sco1* knockout (*Sco1*$^{hrt/hrt}$) mice at P1. GAPDH is used as a loading control. (C) Blue Native PAGE analysis of the abundance of complexes I-V of electron transport chain in wild-type (*Control*) and heart-specific *Sco1* knockout (*Sco1*$^{hrt/hrt}$) mice at P1. (D) Specific activity of the cyanide-resistant Mn-SOD2 (mU/mg protein) in wild-type (*Control*, black) and heart-specific *Sco1* knockout (*Sco1*$^{hrt/hrt}$, white) mice at P1. (n= 3 for both genotypes).

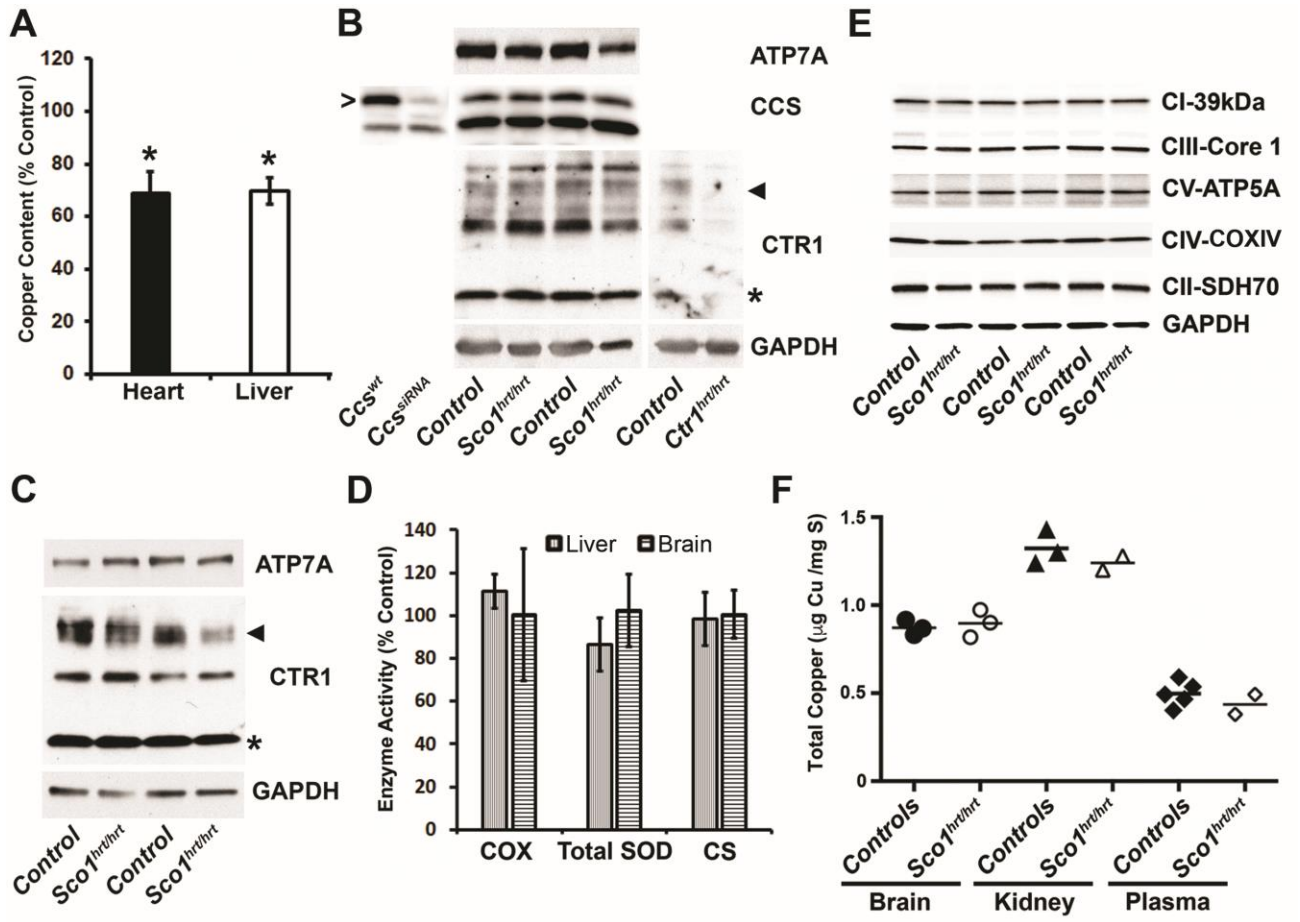


**Figure 4.11: Deletion of *Sco1* in the heart causes a mild copper deficiency**

(A) Total copper levels in the hearts and livers from heart-specific *Sco1* knockout (*Sco1*$^{hrt/hrt}$) mice at P1 expressed as a percentage of wild-type littermates. (n= 3 for each tissue). (B) Western blot analysis of ATP7A, CCS, and CTR1 abundance in hearts from wild-type (*Control*) and heart-specific *Sco1* knockout (*Sco1*$^{hrt/hrt}$) mice at P1. Hearts from P7 wild-type (*Control*) and heart-specific *Ctr1* knockout (*Ctr1*$^{hrt/hrt}$) mice were used as a control to identify specific CTR1 signal. MEFs treated with scrambled (*Ccs*$^{wt}$) and siRNA targeting *CCS* (*Ccs*$^{siRNA}$) were used as controls for confirming specific CCS signal represented by unfilled arrow. GAPDH is used as a loading control. (C) Western blot analysis of ATP7A, and CTR1 abundance in livers from wild-type (*Control*) and heart-specific *Sco1* knockout (*Sco1*$^{hrt/hrt}$) mice at P1. GAPDH is used as a loading control. (For B and C) Arrow represents the mature glycosylated form of CTR1, while the asterisk represents the truncated form of the protein. (D) Specific activities of cytochrome *c* oxidase (COX, left), total super oxide dismutase (SOD, middle), and citrate synthase (CS, right) in the livers (grey) and brains (hatched) from P1 heart-specific *Sco1* knockout (*Sco1*$^{hrt/hrt}$) mice expressed as a percentage of wild-type littermates. (n= 4 for each enzyme and tissue). (E) Western blot analysis of the abundance of representative subunits from complexes I-V of electron transport chain in livers from wild-type (*Control*) and heart-specific *Sco1* knockout (*Sco1*$^{hrt/hrt}$) mice at P1. GAPDH is used as a loading control. (F) Total copper levels (μg Cu/mg Sulphur [S]) in brain (left), kidney (middle), and plasma (right) from wild-type (*Control*) and heart-specific *Sco1* knockout (*Sco1*$^{hrt/hrt}$) mice at P1.

### 4.2.3 Physiological characterization of *Sco1*$^{stm/stm}$ mice

#### 4.2.3.1 Validation of striated muscle-specific *Sco1* deletion

As the perinatal lethality in the *Sco1*$^{hrt/hrt}$ mice precluded more meaningful investigation of the mechanisms underling the copper deficiency in the *Sco1* knockout heart, we generated a second mouse model in which *Sco1* was deleted in all striated muscle. Striated muscle-specific knockout mice, hereafter referred to as *Sco1*$^{stm/stm}$ mice, were generated by crossing *Sco1*$^{flox/flox}$ mice with a transgenic mouse expressing Cre recombinase under the control of the muscle-specific creatine kinase (MM-CK) promoter (see 4.1.1.1 and 4.2.1.1). *Sco1*$^{stm/stm}$ mice were viable and observed at the expected Mendelian frequencies (data not shown). *Sco1*$^{stm/stm}$ mice had a longer lifespan than the *Sco1*$^{hrt/hrt}$ mice; however, the deletion of *Sco1* was ultimately lethal and *Sco1*$^{stm/stm}$ mice had a median lifespan of 99 days (Figure 4.12A). Hearts of *Sco1*$^{stm/stm}$ mice exhibited expression of *Sco1* for significantly longer than the hearts of *Sco1*$^{hrt/hrt}$ mice as we were able to detect small amounts of the protein within the linear range of exposure up until P6 (Figure 4.12B). Deletion of the *Sco1* locus was restricted to the striated muscle as determined by PCR amplification of the genomic DNA from a number of peripheral tissues (Figure 4.12C).

#### 4.2.3.2 *Sco1*$^{stm/stm}$ mice develop severe cardiomyopathy with significant fibrosis and enlarged cardiomyocytes

The increased lifespan of the *Sco1*$^{stm/stm}$ mice allowed us to investigate the effect of *Sco1* ablation on cardiac function in the adult mouse. Although there was no difference between the body weight of the *Sco1*$^{stm/stm}$ mice and their wild-type littermates at P90 (Figure 4.12D), the hearts of *Sco1*$^{stm/stm}$ mice were significantly larger and weighed roughly 2 fold more (Figure 4.12E,F). Histological analysis of the hearts of *Sco1*$^{stm/stm}$ mice showed common signs of cardiac hypertrophy such as enlargement and vacuolization of the cardiomyocytes, as well as the presence of significant fibrosis within the cardiac tissue (Figure 4.12G). Consistent with the idea that the hearts of *Sco1*$^{stm/stm}$ mice develop a cardiomyopathy, we observed the upregulation of genes known to be biomarkers of fetal cardiac remodeling such as atrial natriuretic peptide (ANP), brain natriuretic peptide (BNP) and α-skeletal actin (α-SA), and the downregulation of the calcium pump SERCA2a (Figure 4.12H).

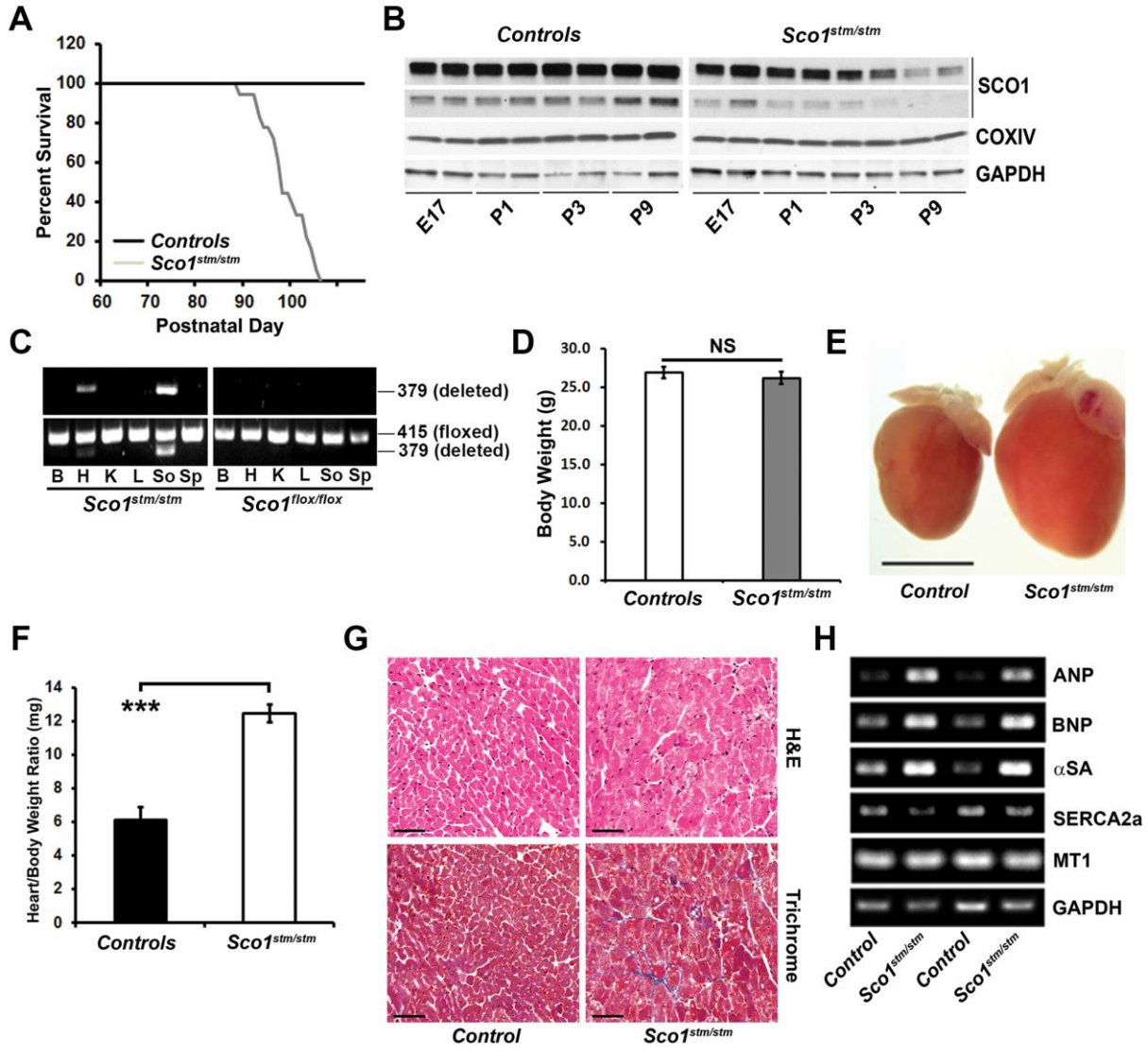


**Figure 4.12: Deletion of *Sco1* in the striated muscle is lethal and presents with cardiomyopathy**
(A) Kaplan-Meier survival curve of wild-type (black, *Controls*, n=22) and striated muscle-specific *Sco1* knockout (grey, *Sco1*$^{stm/stm}$, n=18) mice. (B) Western blot analysis of SCO1 and COX IV abundance in wild-type (*Controls*) and striated muscle-specific *Sco1* knockout (*Sco1*$^{stm/stm}$) mice at E17, P1, P3, and P9. GAPDH is used as a loading control. Multiple images for SCO1 represent a long and short exposure times. (C) PCR analysis of the *Sco1* gene determining presence of a floxed (415 bp) or deleted (379 bp) second exon in various tissues (B= Brain, H= Heart, K= Kidney, L= Liver, So= Soleus, Sp= Spleen) from both wild-type (*Controls*) and striated muscle-specific *Sco1* knockout (*Sco1*$^{stm/stm}$) mice at P1. Top represents two primer PCR conditions to individually amplify the deleted allele. Bottom represents three primer PCR conditions to amplify both floxed and deleted alleles. (D) Body weight (g) of wild-type (*Controls*) and striated muscle-specific *Sco1* knockout (*Sco1*$^{stm/stm}$) mice at P90. (n= 6 for each genotype). (E) Hearts from wild-type (*Control*, left) and striated muscle-specific *Sco1* knockout (*Sco1*$^{stm/stm}$, right) mice at P90. (F) Ratio of heart weight (mg) to body weight (g) for wild-type (*Controls*) and striated muscle-specific *Sco1* knockout (*Sco1*$^{stm/stm}$) mice at P90. (n= 7 for each genotype). (G) 20X magnification of Hematoxylin and Eosin (top) and Masson's trichrome (bottom) stained sections of hearts from both wild-type (*Control*, left) and striated muscle-specific

*Sco1* knockout (*Sco1*$^{stm/stm}$, right) mice at P90. Scale bar represents 50 μm. (H) Semi-quantitative RT-PCR analysis of atrial natriuretic peptide (ANP), brain natriuretic peptide (BNP), α-skeletal actin (αSA), sarco/endoplasmic reticulum $Ca^{2+}$-ATPase 2a (SERCA2a), and metallothionein 1 (MT1) mRNA transcript levels in livers from wild-type (*Controls*) and striated muscle-specific *Sco1* knockout (*Sco1*$^{stm/stm}$) mice at P90. GAPDH was used as a loading control.

#### 4.2.3.3 Echocardiogram of *Sco1*$^{stm/stm}$ hearts shows dilation of the left ventricle

To further investigate the observed cardiomyopathy, we performed echocardiography on the hearts of *Sco1*$^{stm/stm}$ and wild-type mice at P60 and P90. P60 *Sco1*$^{stm/stm}$ mice did not have any significant differences in heart function or ventricular size (data not shown); however, by P90 *Sco1*$^{stm/stm}$ mice displayed signs of a dilated cardiomyopathy including a dilated left ventricle which significantly impaired contraction (Figure 4.13A). Quantification of the echocardiographic data further revealed that the *Sco1* knockout hearts had significantly lower fractional shortening and ejection fractions, confirming that ventricular dilation adversely affected cardiac dysfunction (Figure 4.13B).

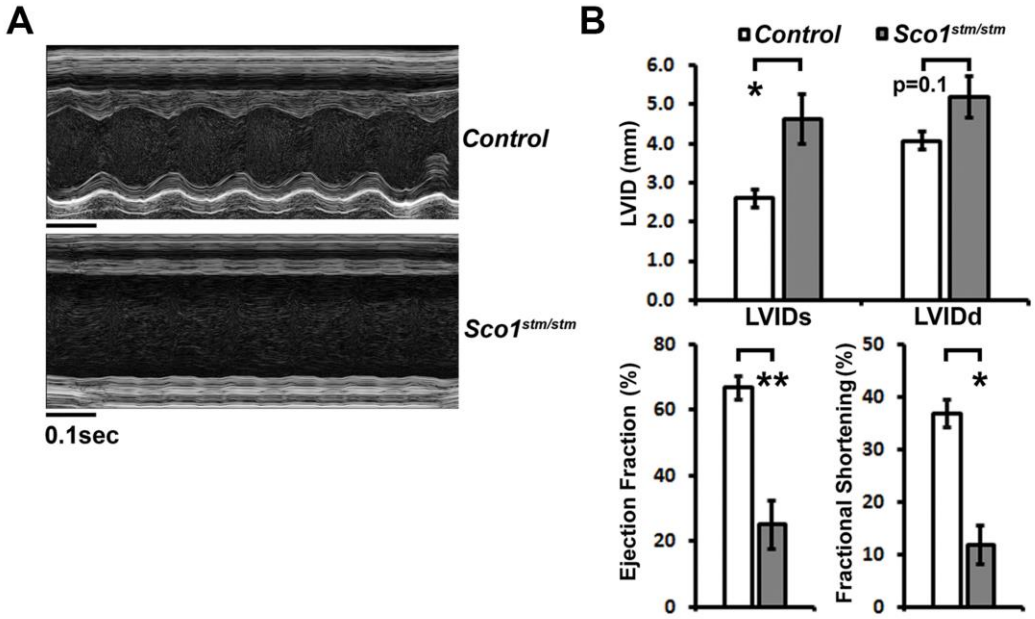


**Figure 4.13: Deletion of *Sco1* in the striated muscle causes dilated cardiomyopathy**
(A) Echocardiogram image of left ventricle from wild-type (*Control*) and striated muscle-specific *Sco1* knockout (*Sco1*$^{stm/stm}$) mice at P90. Scale bar represents 0.1 sec. (B) Quantification of cardiac output parameters: left ventricular internal diameter from systole (LVIDs) (top left) and diastole (LVIDd) (top right), ejection fraction (bottom left), and fractional shortening (bottom right) in wild-type (*Control*, white) and striated muscle-specific *Sco1* knockout (*Sco1*$^{stm/stm}$, grey) mice at P90 determined by echocardiogram. (n= 4 for each genotype and measurement).

### 4.2.4 Molecular characterization of *Sco1*$^{stm/stm}$ mice

#### 4.2.4.1 *Sco1*$^{stm/stm}$ mice have an isolated COX deficiency combined with a deficiency in SOD1 activity

Like the other tissue-specific *Sco1* knockout mouse models we characterized, the hearts of *Sco1*$^{stm/stm}$ mice exhibited a severe deficiency in the enzymatic activity of COX and the copper-dependent form of SOD1 (Figure 4.14A,B). Native and denaturing polyacrylamide gel electrophoresis analyses confirmed that the abundance of all the other complexes of OXPHOS was unaffected and that the deletion of *Sco1* in the heart resulted in an isolated COX deficiency (Figure 4.14C,D). The activity of CS was also unchanged in the hearts of *Sco1*$^{stm/stm}$ mice (Figure 4.14A) which, when combined with the lack of a change in other OXPHOS complexes, suggests that mitochondrial content remained constant.

#### 4.2.4.2 *Sco1*$^{stm/stm}$ mice have a severe copper deficiency that is not the result of reduced CTR1 abundance

The severe, combined COX and SOD1 deficiency suggested that the *Sco1* knockout heart was severely copper deficient. Consistent with this idea, we found that copper levels in the hearts of *Sco1*$^{stm/stm}$ mice were significantly lower relative to the hearts of their wild-type counterparts (Figure 4.14E). This copper deficiency occurred without changes in iron or zinc levels (Figure 4.14E) and was specific to the heart as the copper levels in the liver and brain were unaltered (Figure 4.14F). Interestingly, copper-deficient hearts of P90 *Sco1*$^{stm/stm}$ mice had normal levels of the copper importer CTR1 and a modest increase in ATP7A abundance (Figure 4.14G). These data corroborate the observations made in the *Sco1*$^{hrt/hrt}$ mice and further suggest that the underlying mechanisms responsible for the copper deficiency in the absence of SCO1 are different in the heart and liver.

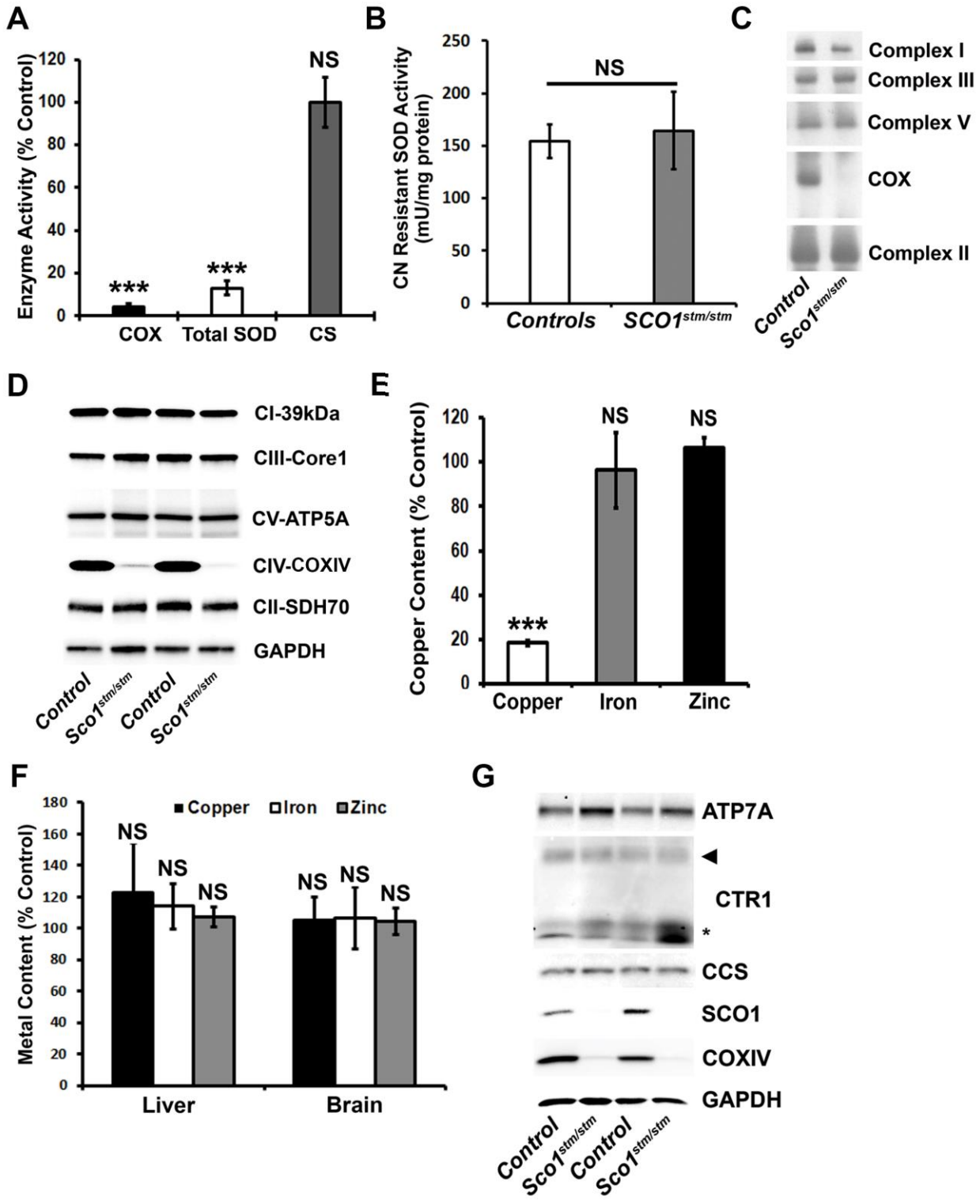


**Figure 4.14: Deletion of *Sco1* in the striated muscle causes an isolated COX deficiency**
(A) Specific activities of cytochrome *c* oxidase (COX, black), total super oxide dismutase (SOD, white), and citrate synthase (CS, grey) in the hearts from P90 striated muscle-specific *Sco1* knockout (*Sco1*$^{stm/stm}$) mice expressed as a percentage of wild-type litter mates. (n= 6 for all genotypes and enzymes). (B) Specific activity of the cyanide-resistant Mn-SOD2 (mU/mg protein) in wild-type (*Control*, white) and striated muscle-specific *Sco1* knockout (*Sco1*$^{stm/stm}$, grey) mice at P90. (n= 3 for

both genotypes). (C) Blue Native PAGE analysis of the abundance of complexes I-V of electron transport chain in wild-type (*Control*) and striated muscle-specific *Sco1* knockout (*Sco1*$^{stm/stm}$) mice at P90. (D) Western blot analysis of the abundance of representative subunits from complexes I-V of electron transport chain in hearts from wild-type (*Control*) and striated muscle-specific *Sco1* knockout (*Sco1*$^{stm/stm}$) mice at P90. GAPDH is used as a loading control. (E) Total levels of copper (white), iron (grey), and zinc (black) in hearts from striated muscle-specific *Sco1* knockout mice at P90 expressed as a percentage of wild-type littermates. (n= 3 for each genotype and measurement). (F) Total levels of copper (black), iron (white), and zinc (grey) in livers and brains from striated muscle-specific *Sco1* knockout mice at P90 expressed as a percentage of wild-type littermates. (n= 3 for each genotype, tissue, and measurement). (G) Western blot analysis of ATP7A, CTR1, CCS, SCO1, and COX IV abundance in hearts from wild-type (*Control*) and striated muscle-specific *Sco1* knockout (*Sco1*$^{stm/stm}$) mice at P90. GAPDH is used as a loading control. Arrow represents the mature glycosylated form of CTR1, while the asterisk represents the truncated form of the protein.

#### 4.2.4.3 The combined COX and copper deficiencies progressively worsen with age

Given that the hearts of P90 *Sco1*$^{stm/stm}$ mice are severely affected and the animals are in an advanced disease state, we characterized the effect of deleting *Sco1* in the heart of this mouse model on COX assembly and copper homeostasis at earlier time points. The hearts of *Sco1*$^{stm/stm}$ mice exhibited a mild COX deficiency at P18 in absence of any changes in total cellular copper levels (Figure 4.15A,B). However, both COX activity and total copper content progressively declined with time and a severe, combined deficiency was observed by P60 (Figure 4.15A,B). Despite a marked copper deficiency at P30 and P60, ATP7A levels were unchanged (Figure 4.15C) suggesting that the increase in its abundance at P90 occurs well after the onset of the copper deficiency. Remarkably and in marked contrast to the *Sco1*$^{liv/liv}$ phenotype (Figure 4.5A), CTR1 abundance was higher in the copper-deficient hearts of *Sco1*$^{stm/stm}$ mice at P30 and P60 (Figure 4.15C). The abundance of the cellular copper biomarker CCS was also unchanged in the hearts of these mice (Figure 4.15C).

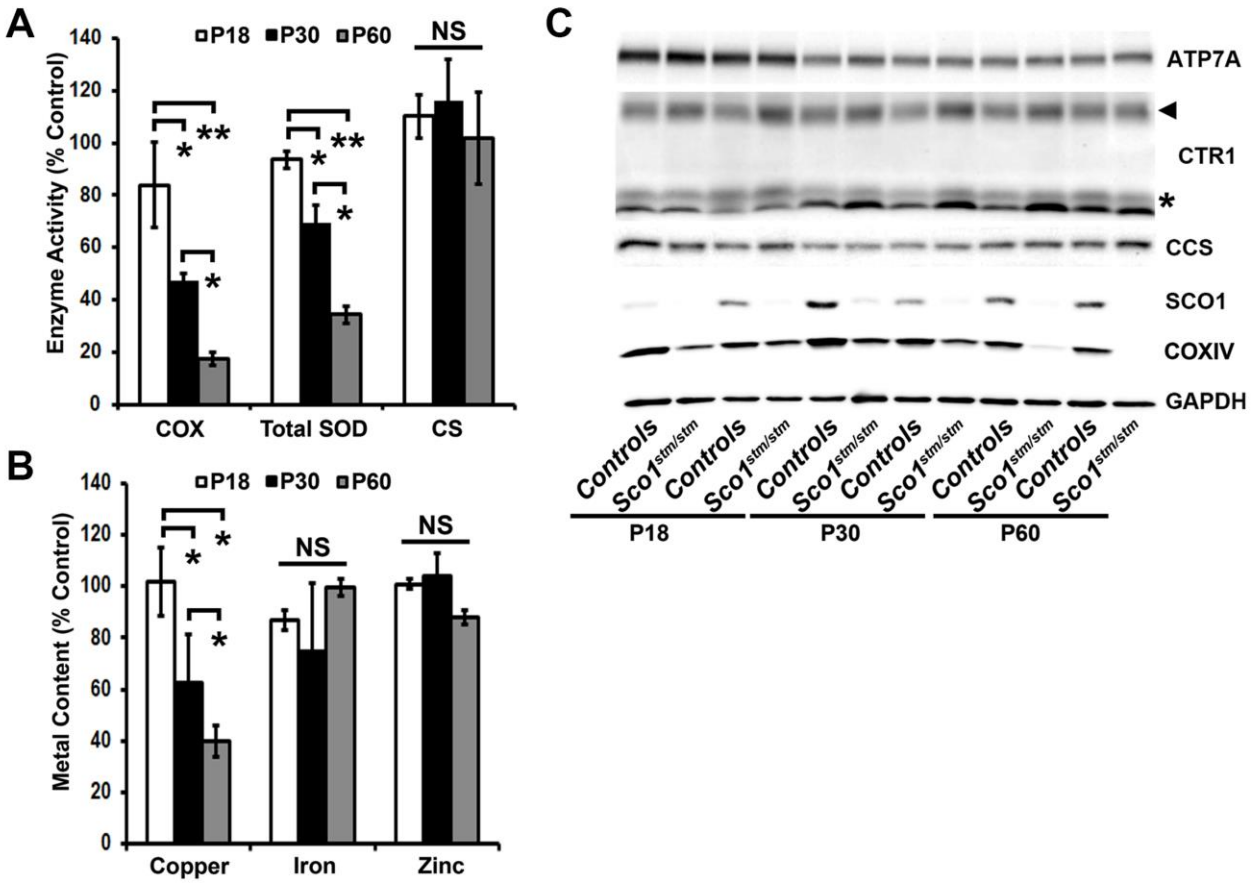


**Figure 4.15: Copper and COX deficiencies in striated muscle-specific *Sco1* knockout mice get progressively worse over time**

(A) Specific activities of cytochrome *c* oxidase (COX), total super oxide dismutase (Total SOD), and citrate synthase (CS) in the hearts from P18 (white), P30 (black), and P60 (grey) striated muscle-specific *Sco1* knockout (*Sco1*$^{stm/stm}$) mice expressed as a percentage of wild-type littermates. (n= 3 for all genotypes, timepoints and enzymes). (B) Total levels of copper, iron, and zinc in hearts from P18 (white), P30 (black), and P60 (grey) striated muscle-specific *Sco1* knockout (*Sco1*$^{stm/stm}$) mice expressed as a percentage of wild-type littermates. (n= 3 for all genotypes, timepoints and metals). (C) Western blot analysis of ATP7A, CTR1, CCS, SCO1, and COX IV abundance in hearts from P18, P30, and P60 wild-type (*Controls)* and striated muscle-specific *Sco1* knockout (*Sco1*$^{stm/stm}$) mice. GAPDH is used as a loading control. Arrow represents the mature glycosylated form of CTR1, while the asterisk represents the truncated form of the protein.

#### 4.2.4.4 The copper deficiency in *Sco1*$^{stm/stm}$ hearts is caused by the mislocalization of CTR1

The absence of changes in the abundance of CTR1 led us to consider whether deletion of *Sco1* in the heart leads to its mislocalization. We chose to examine the hearts of *Sco1*$^{stm/stm}$ mice at P60, because the copper deficiency is significant but cardiac function remains normal. Mirroring a prior study (Kuo et al., 2006), the hearts of wild-type mice had positive staining for CTR1 within the intercalated discs of the cardiomyocytes, with the most intense staining co-localizing with the plasma membrane marker $Na^+/K^+$ ATPase. (Figure 4.16A,B). In contrast, the hearts of *Sco1*$^{stm/stm}$ mice had intense intracellular CTR1 staining (Figure 4.16A,B). To determine whether the intracellular CTR1 in the *Sco1* knockout heart reflected its internalization from the plasma membrane or altered trafficking, we examined its co-localization with several intracellular markers. We found that the internalized CTR1 signal significantly overlaid with the endosomal marker Rab5, suggesting that intracellular CTR1 was located in endosomes (Figure 4.17A,B). However, intracellular CTR1 did not co-localize with either the early endosomal marker EEA1 or the late endosomal/lysosomal marker LAMP1 (Figure 4.18,AB).

### 4.2.5 Characterization of a *Sco1*$^{G115S/G115S}$ knock-in mouse

To further investigate how altered SCO1 function effects changes in CTR1 localization in the heart, we decided to generate *Sco1* knock-in mice harbouring the homologous glycine to serine substitution that causes a fatal hypertrophic cardiomyopathy in humans (Stiburek et al., 2009). The codon substitution causing this mutation (GGG-AGC) was successfully confirmed by real-time qPCR using probes specific to the wild-type or mutated region within the 3$^{rd}$ exon of *Sco1* (data not shown). Like the phenotypes observed in the *Sco1* knockout hearts, the hearts of *Sco1*$^{G115S/G115S}$ mice had both a severe COX and copper deficiency (Figure 4.19A,B), and the copper deficiency was not caused by changes in the abundance of the copper transporters ATP7A or CTR1 (Figure 4.19A). Finally, CTR1 was similarly mislocalized in the cardiomyocytes of the *Sco1*$^{G115S/G115S}$ mice, with focal intracellular staining rather than localization to the intercalated discs (Figure 4.20A,B).

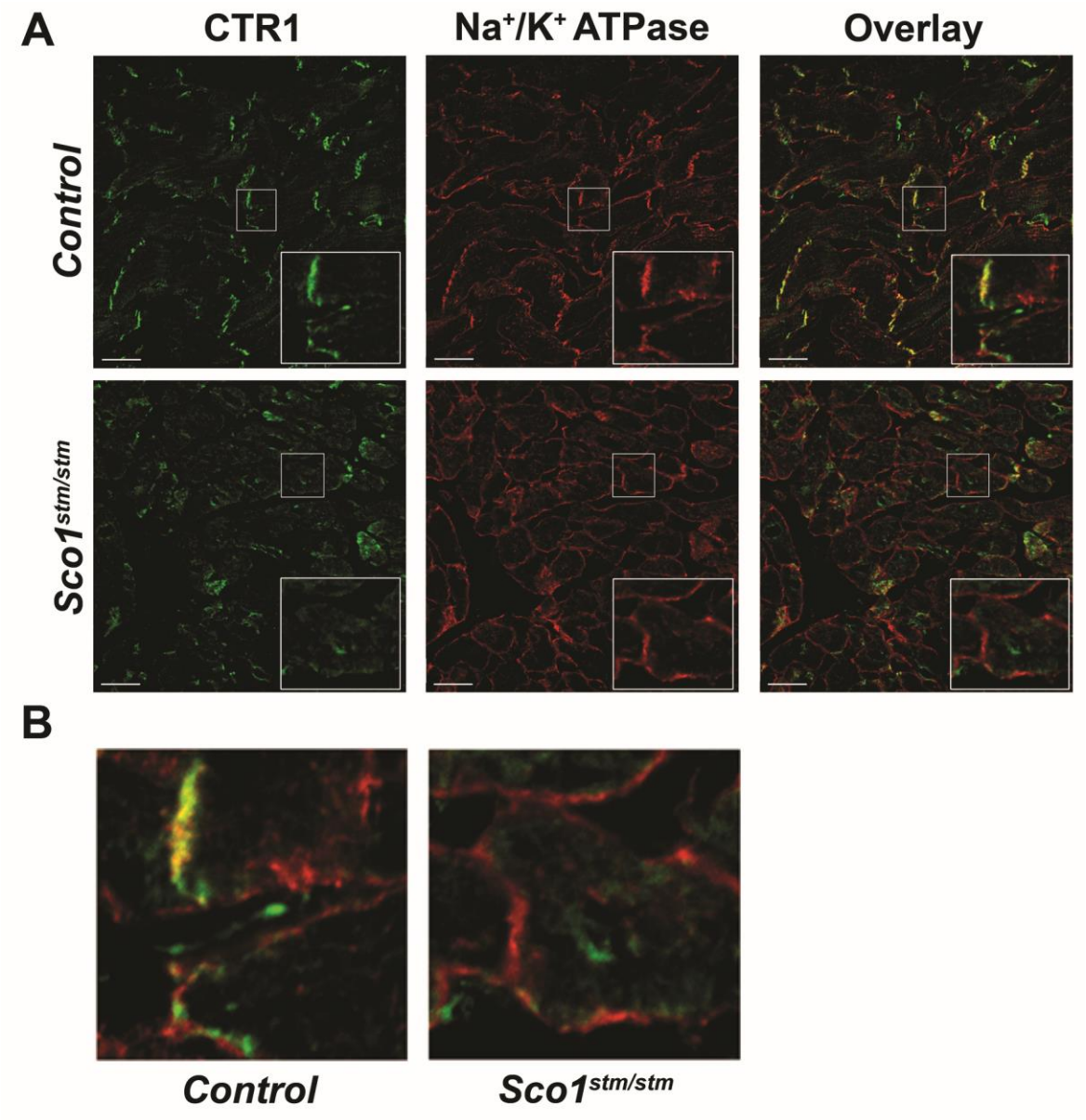


**Figure 4.16: Deletion of *Sco1* in the striated muscle causes the mislocalization of CTR1 in cardiomyocytes**

(A) Immunofluorescence analysis of CTR1 (green) localization in hearts of wild-type (*Control*, top) and striated muscle-specific *Sco1* knockout (*Sco1*$^{stm/stm}$, bottom) mice at P60. $Na^+/K^+$ ATPase (red) was used as a positive control for plasma membrane. Images were taken at 40X and scale bar represents 20 μm. Co-stained signal in overlay is shown in yellow. Inset represents magnified image of region of interest (white box). (B) Enlarged image of region of interest from overlay in A.

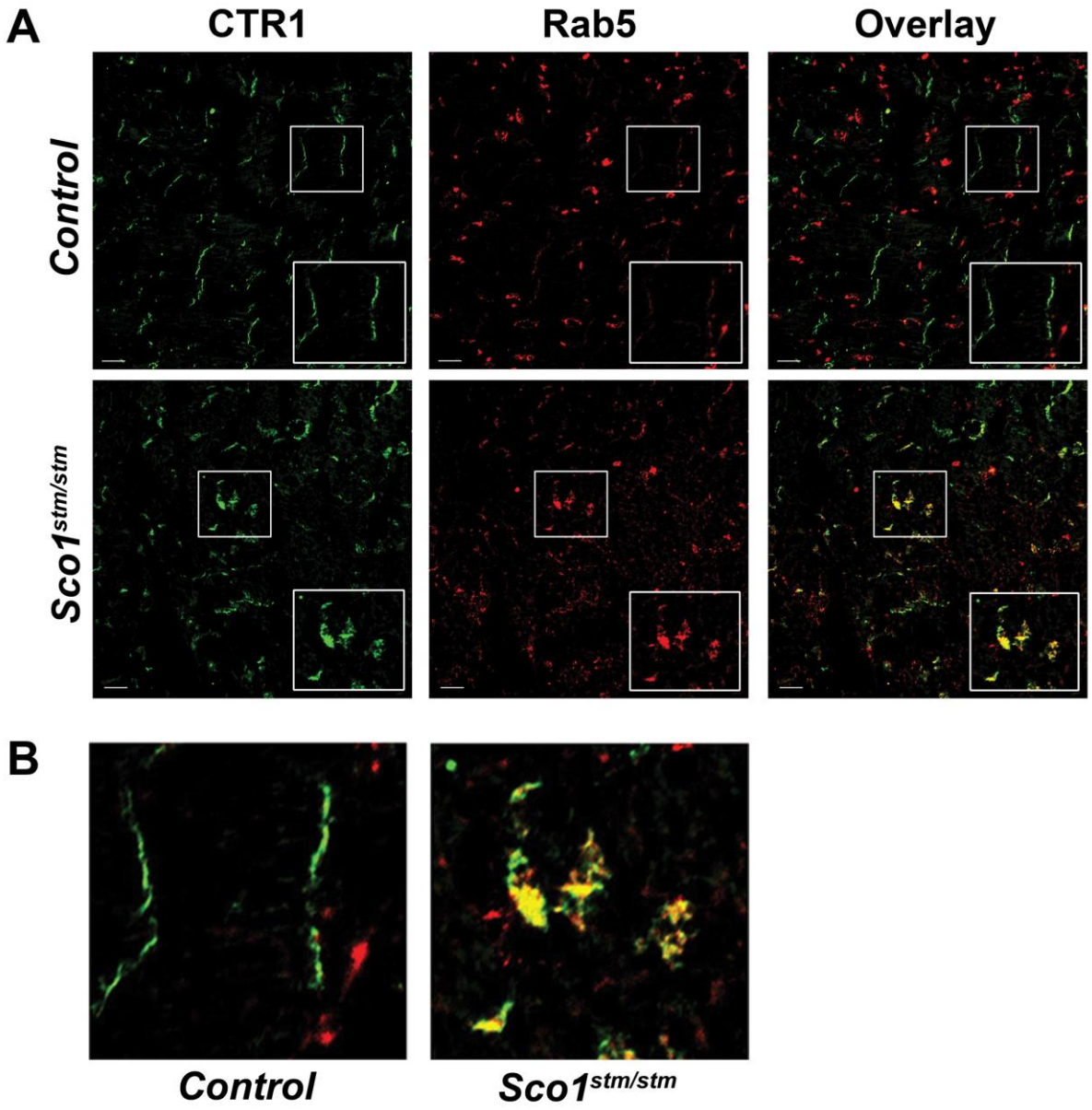


**Figure 4.17: Mislocalized CTR1 in the hearts of striated muscle-specific mice co-localizes with Rab5**

(A) Immunofluorescence analysis of co-localization between CTR1 (green) and endosomal marker Rab5 (red) in hearts of wild-type (*Control*, top) and striated muscle-specific *Sco1* knockout (*Sco1*$^{stm/stm}$, bottom) mice at P60. Images were taken at 40X and scale bar represents 20 μm. Co-stained signal in overlay is shown in yellow. Inset represents magnified image of region of interest (white box). Images were taken at 40X and scale bar represents 20 μm. Co-stained signals in overlay is shown in pink, yellow, and white. Inset represents magnified image of region of interest (white box). (B) Enlarged image of region of interest from overlay in A.

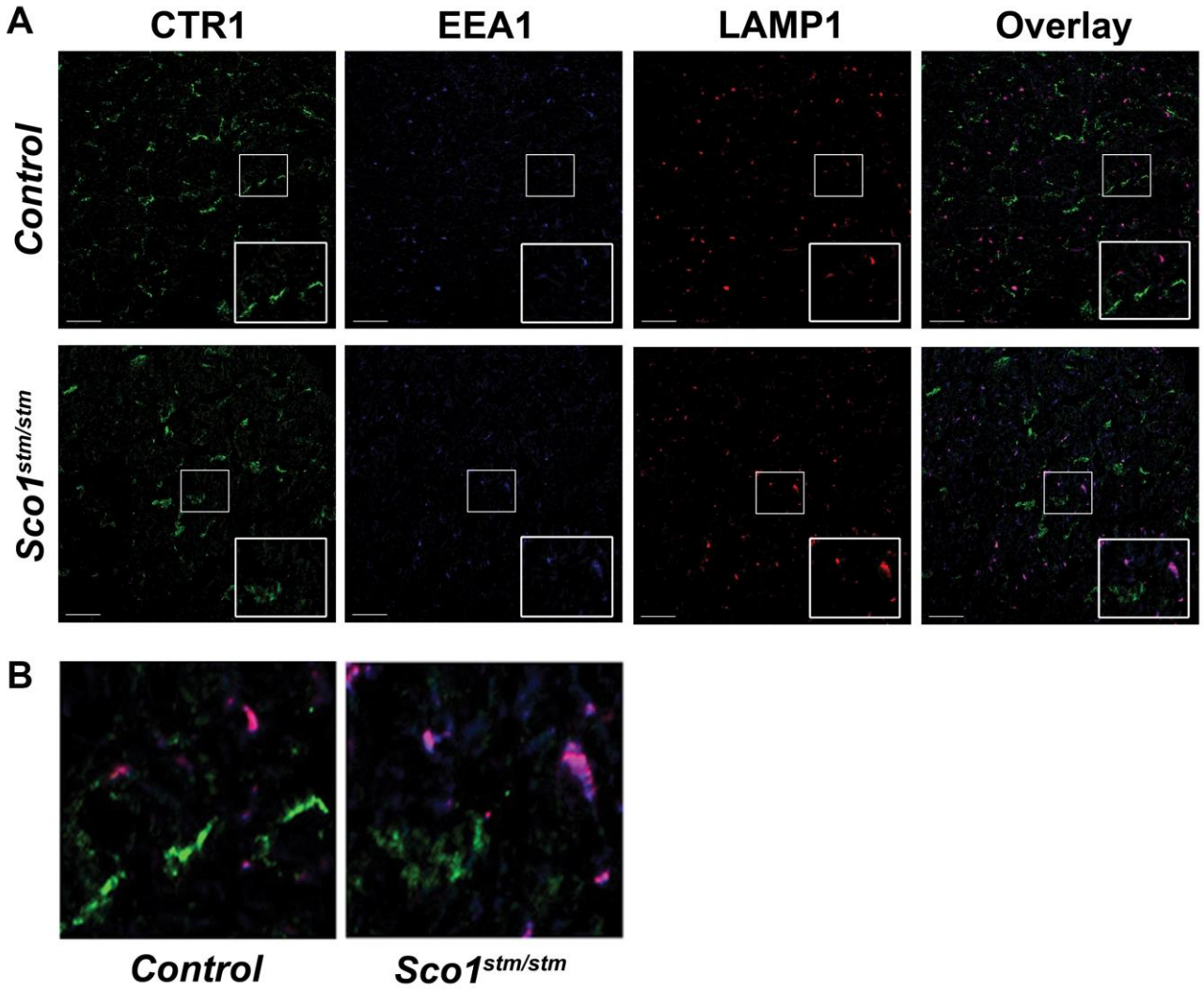


**Figure 4.18: Mislocalized CTR1 does not co-localize with EEA1 or LAMP1**

(A) Immunofluorescence analysis of co-localization between CTR1 (green), early endosomal marker EEA1 (blue), and late endosomal/lysosomal marker LAMP1 (red) in hearts of wild-type (*Control*, top) and striated muscle-specific *Sco1* knockout (*Sco1*$^{stm/stm}$, bottom) mice at P60. Images were taken at 40X and scale bar represents 20 μm. Co-stained signals in overlay is shown in pink, yellow, and white. Inset represents magnified image of region of interest (white box). (B) Enlarged image of region of interest from overlay in A.

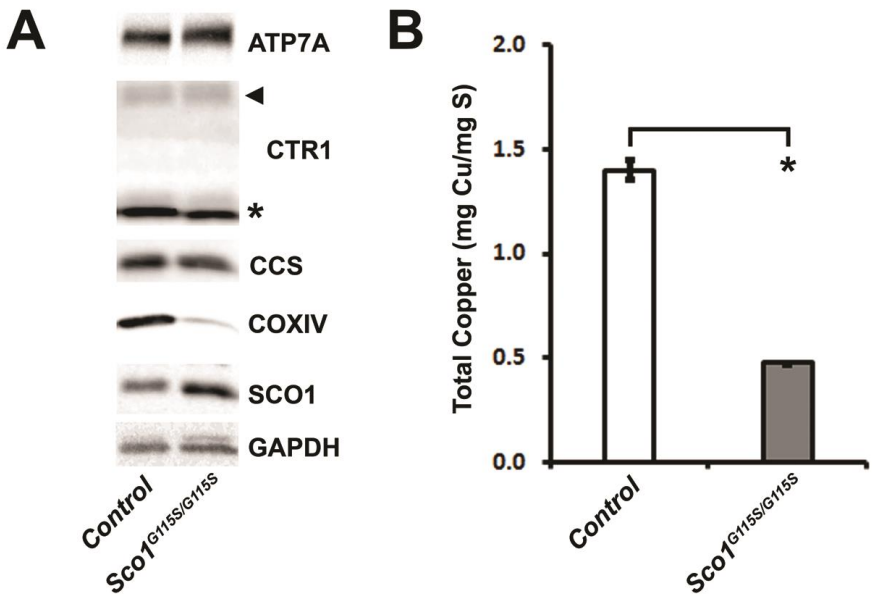


**Figure 4.19: Mice harboring G115S homozygous mutation in *Sco1* phenocopy the striated muscle-specific *Sco1* knockout mice**

(A) Western blot analysis of ATP7A, CTR1, CCS, SCO1, and COX IV abundance in hearts from wild-type (*Control)* and G115S *Sco1* knock-in (*Sco1*$^{G11S/G115S}$) mice at P120. GAPDH is used as a loading control. Arrow represents the mature glycosylated form of CTR1, while the asterisk represents the truncated form of the protein. (B) Total copper levels (µg/mg Sulphur [S]) in hearts from wild-type (*Control*, white) and G115S *Sco1* knock-in (*Sco1*$^{G11S/G115S}$, grey) mice at P120. (n= 3 for each genotype).

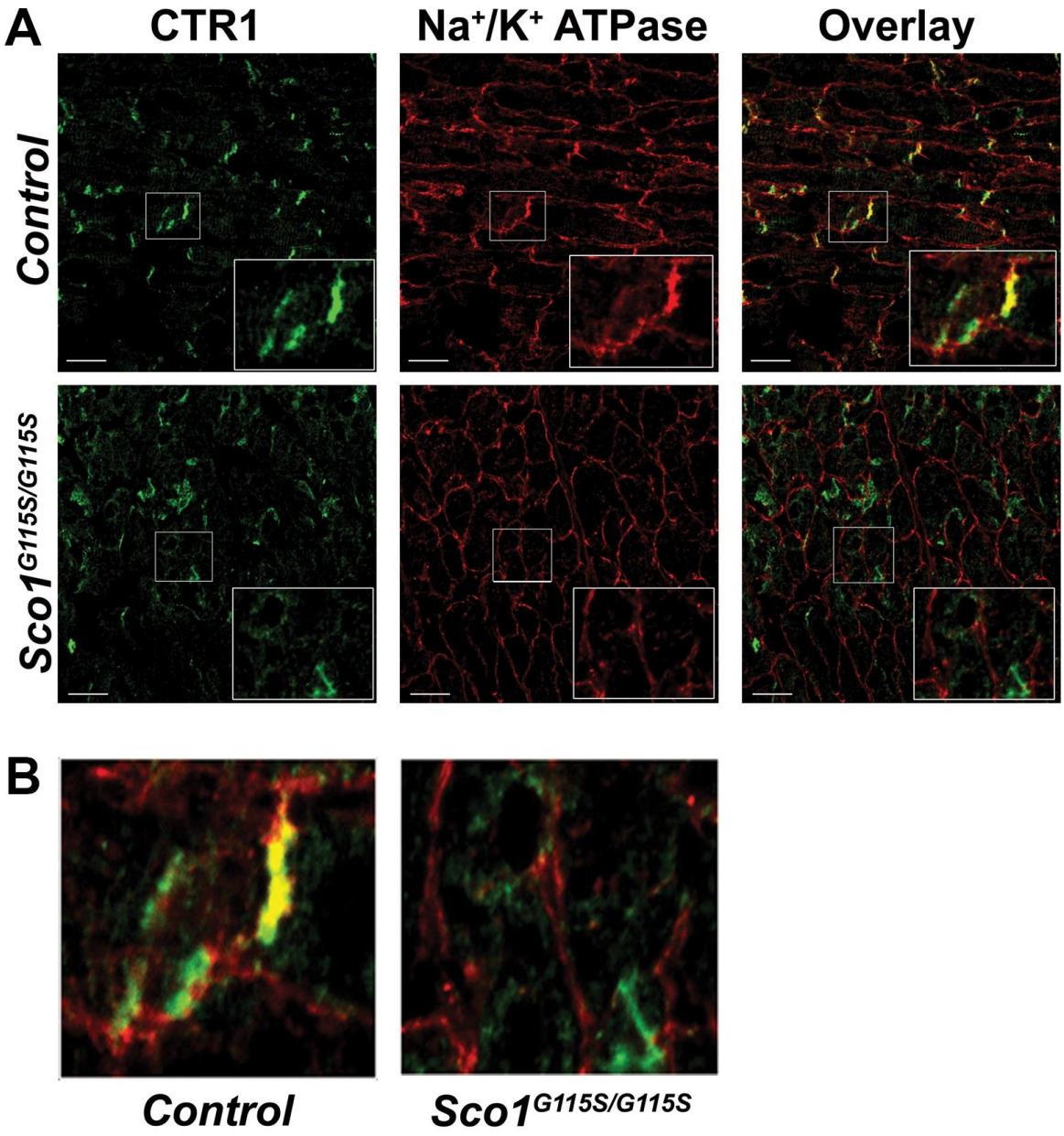


**Figure 4.20: CTR1 in G115S homozygous knock-in mice is mislocalized from plasma membrane** (A) Immunofluorescence analysis of CTR1 (green) localization in hearts of wild-type (*Control*, top) and G115S *Sco1* knock-in (*Sco1*$^{G11S/G115S}$, bottom) mice at P120. $Na^+/K^+$ ATPase (red) was used as a positive control for plasma membrane. Images were taken at 40X and scale bar represents 20 μm. Co-stained signal in overlay is shown in yellow. Inset represents magnified image of region of interest (white box). (B) Enlarged image of region of interest from overlay in A.

## 5. Discussion

As SCO1 and SCO2 are both known COX assembly factors with essential roles in the metallation of the $Cu_A$ site of COX2, it is unsurprising that patients harbouring pathogenic mutations in either gene present with a severe COX deficiency in affected tissues. More surprising, however, is that affected *SCO* patient tissues also exhibit a significant reduction in total copper levels. How and why the disrupted function of two copper-binding proteins that are physically localized to the inner membrane of the mitochondrion has such a pronounced effect on copper homeostasis at the whole cell level remains a mystery. An understanding of how the organelle fits into the regulatory framework that governs copper homeostasis is challenged by the fact that little to nothing is known about the mechanisms cells and tissues employ to modulate the levels and bioavailabity of the metal ion. To begin to address this knowledge gap, we generated multiple mouse models in which SCO1 function was ablated or altered in a tissue-specific manner and used a number of approaches to characterize the relevant tissues at a biochemical, molecular, genetic and elemental level. We restricted our focus to the importance of SCO1 function to copper homeostasis in the liver and heart as these are two of the most severely affected tissues in *SCO1* patients that have been described to date.

All of our *Sco1* mouse models displayed profound, tissue-specific phenotypes that were ultimately lethal. *Sco1*$^{liv/liv}$ mice presented with a severe hepatopathy, characterized by hepatomegaly, marked steatosis, and release of enzymes into the serum indicative of liver failure. *Sco1* knockout hearts in both the heart- and striated muscle-specific models were markedly dilated with cardiomyocytes exhibiting altered architecture. Deletion of *Sco1* in the liver, heart or striated muscle was lethal arguing that, like in humans, SCO1 function is also essential to COX assembly and copper homeostasis in the mouse. While it is tempting to speculate that the different lifespan of each model reflects the relative importance of SCO1 to the integrity of these two pathways in each tissue, there are significant differences between models with respect to when the *Cre* transgene is turned on during development. In fact, it is likely that the early lethality observed in the *Sco1*$^{hrt/hrt}$ mice compared to the *Sco1*$^{stm/stm}$ mice is caused by the almost complete absence of SCO1 protein in the hearts of *Sco1*$^{hrt/hrt}$ mice as early as E15. Expression of the *Cre* transgene later on in heart development in the *Sco1*$^{stm/stm}$ mice allowed for wild-type levels of SCO1 until P1 with appreciable amounts of protein remaining until P9, suggesting that perhaps there is a perinatal window when SCO1 expression in the heart is absolutely critical for survival. Why the *Sco1*$^{stm/stm}$ mice continued to live for several months without *Sco1* expression in the cardiomyocytes is unknown. One possibility, supported by the *Sco1*$^{stm/stm}$ enzymology data, is that the half-life of the COX holoenzyme is relatively long in juvenile

and adult mice and sufficient residual COX activity remained to support normal heart function. Consistent with this idea, echocardiography revealed that heart function in *Sco1*$^{stm/stm}$ mice was equivalent to that of wild-type littermates at P60.

Our *Sco1* knockout and knockin mouse models exhibited a combined COX and copper deficiency and therefore phenocopied affected tissues of *SCO1* patients. Firstly, both the livers of *Sco1*$^{liv/liv}$ mice and hearts of *Sco1*$^{stm/stm}$ mice had significant, isolated COX deficiencies. Residual enzyme activity in *Sco1* knockout livers was comparable to that of fibroblasts from the *SCO1* patient who presented with a severe hepatopathy (Leary et al., 2007), and that of *Sco1* knockout hearts was similar to the muscle of the *SCO1* patient with a hypertrophic cardiomyopathy (Stiburek et al., 2009). Consistent with the reduction in enzymatic activity, *Sco1* knockout tissues also had reduced levels of both the COX holoenzyme and the structural subunit COX IV. Both the livers of *Sco1*$^{liv/liv}$ mice and the hearts of *Sco1*$^{stm/stm}$ mice also had a severe copper deficiency. The hearts of *Sco1*$^{G115S/G115S}$ knock-in mice mirrored those of the *Sco1*$^{stm/stm}$ mice, suggesting that mitochondrial signalling crucial to the regulation of copper homeostasis is similarly perturbed in animals expressing an allelic variant of *Sco1* that is pathogenic in humans. Taken together, these data suggest that these mouse models provide a robust avenue with which to explore the underlying etiology of human diseases caused by mutations in *SCO1*.

Interestingly, the livers of *Sco1*$^{liv/liv}$ mice further phenocopied the human patient condition in that the mitochondrial copper pool was preserved in spite of the severe global copper deficiency. *SCO1* and *SCO2* patient fibroblasts and liver also prioritize the preservation of their organelle copper pool (Dodani et al., 2010). These and other findings suggest that there may in fact be a hierarchy of copper homeostasis within the cell, and that delivery of copper to various organelles and, by extension, cuproproteins is prioritized in both healthy and disease states. The ability of the cell and even the organism to preferentially route copper to specific proteins or compartments has been observed in other model systems. When the zebrafish embryo is challenged with a copper deficiency, it routes copper to the pathways of highest priority in an effort to preserve the developmental program (Mendelsohn et al., 2006). The single-celled green algae *Chlamydomonas reinhardtii* preferentially shuttles copper to mitochondria at the expense of chloroplasts under copper-limiting conditions (Merchant and Bogorad, 1986). Finally, by altering the levels of the mitochondrial protein CMC1 one can shift the relative distribution of copper from IMS-localized SOD1 to COX (Horn et al., 2008), suggesting that even within an organelle signalling pathways exist to tightly control routing of the metal ion. How these signalling pathways function coordinately to regulate copper homeostasis at the

cellular level and how mitochondrial signalling contributes to this regulatory framework will be important questions to address in the future.

One of the major differences between our mouse models and *SCO1* patient fibroblasts is that mutations that alter SCO1 function have fundamentally different consequences on the abundance and localization of proteins involved in copper transport. In *SCO1* and *SCO2* patient fibroblasts the copper deficiency is caused by an increase in ATP7A-dependent copper export from the cells (Leary et al., 2007; Leary et al., 2013), similar to the increases in ATP7A abundance driving the copper deficiency in our liver-specific *Lrpprc* knockout mice. In contrast, we only observed an increase in ATP7A abundance in our *Sco1* models just prior to lethality, long after the copper deficiency was manifest. While ATP7A can effect changes in the rate of copper efflux without a change in its abundance (Petris et al., 1996), we did not investigate whether ATP7A or ATP7B localization were altered in tissues of interest. This choice reflects the profound changes we observed in both the abundance and localization of CTR1 in the *Sco1* knockout livers and hearts and in the $Sco1^{G115S/G115S}$ knock-in heart, which suggest that the copper import machinery is predominantly affected in these murine cell types upon perturbing SCO1 function. The root cause of the unique effects on the export and import machinery observed in *SCO1* patient fibroblasts relative to our mouse models is unknown. While it is admittedly difficult to directly compare results from a cell culture isolate to an organ *in situ*, it is also possible that distinct, cell-type specific effectors downstream of mitochondrial signalling dictate which arm of copper homeostasis is primarily affected by loss of SCO1 function.

Multiple lines of evidence from each of our mouse models strongly suggest that SCO1 has a role in maintaining the correct localization and, in some cases, the abundance of CTR1. The livers of $Sco1^{liv/liv}$ mice had a mild but significant copper deficiency as early as P18, and there was evidence shortly thereafter of CTR1 internalization from the plasma membrane. As the copper deficiency worsened with time, CTR1 abundance also decreased and the protein was eventually undetectable immunologically. CTR1 levels were also reduced in copper-deficient *Sco1* knockout MEFs and were rescued upon forced overexpression of SCO1 suggesting a direct role for the protein or the organelle in preserving cellular copper import competence. We determined that the decrease in CTR1 levels was due to the increased degradation of the protein, as *Ctr1* mRNA transcript abundance was unaffected in the *Sco1* knockout livers and CTR1 protein levels in *Sco1* knockout MEFs were rescued by inhibiting the proteasome. Consistent with this idea, forced overexpression of a *Ctr1* cDNA in *Sco1* knockout MEFs failed to increase the abundance of the mature, glycosylated CTR1 species. The degradation of CTR1 via the proteasome is an interesting result, as the canonical degradation pathway

of plasma membrane transporters typically occurs via endocytosis and eventual fusion of the resultant vesicles with lysosomes (MacGurn et al., 2012). It may be that the CTR1 protein is degraded through retrograde trafficking within the endoplasmic reticulum-associated degradation (ERAD) pathway, which has been found to digest some misfolded plasma membrane proteins in a proteasomal-dependent manner (Vembar and Brodsky, 2008). However, recent findings indicate that the iron transporter ZIP14 is also turned over by the proteasome following its endocytosis in HEK293 cells (Zhao et al., 2014). Thus, there is a precedent in the literature that supports our model of proteasomal degradation of CTR1 upon loss of SCO1 function. Interestingly, the copper deficiency in the livers of *Sco1*$^{hrt/hrt}$ mice was also caused by a decrease in the total abundance of CTR1, which seems to support the possibility that hepatocytes regulate cellular copper through this mechanism.

The cardiac copper deficiencies in our heart-specific *Sco1* knockout mouse models and the *Sco1*$^{G115S/G115S}$ knock-in mouse were also caused by post-translational modifications of CTR1 that reduced copper import. Like other nutrient transporters (Doria-Medina et al., 1993; Kleber and Saffitz, 2014), the majority of CTR1 in the wild-type heart was localized to the intercalated discs, at the cell-cell junctions between individual cardiomyocytes. This localization pattern has previously been reported for CTR1 (Kuo et al., 2006), and presumably represents the most ideal mechanism for copper to be transported between cardiomyocytes that are not immediately adjacent to the vasculature. In contrast, the hearts of both the *Sco1*$^{stm/stm}$ and *Sco1*$^{G115S/G115S}$ mice displayed intense intracellular localization of CTR1 that was coincident with the early endosomal marker Rab5. This suggests that, like the liver, CTR1 was internalized from the plasma membrane in response to altered SCO1 function. However, CTR1 did not co-localize with another early endosomal marker, EEA1, or with the late endosomal/lysosomal marker LAMP1.

The intracellular localization of CTR1 in the hearts of our *Sco1*$^{stm/stm}$ and *Sco1*$^{G115S/G115S}$ mice differs from an earlier report in the literature which found that internalized CTR1 co-localizes with Rab5, EEA1 and Rab7, all common markers for the early endosomal/recycling pathway (Clifford et al., 2016). These initial findings were made in cultured HEK293 cells in which mitochondrial signalling through SCO1 remained intact. However, it is plausible that the mechanisms that dictate sorting, trafficking and ultimately the fate of internalized CTR1 differ across cell types. The existence of such cell-type specific mechanisms is supported by the differences between our heart- and liver-specific *Sco1* mouse models with respect to CTR1 degradation. The exact function and significance of the Rab5-positive, EEA1-negative endosomes containing CTR1 in the *Sco1*$^{stm/stm}$ and *Sco1*$^{G115S/G115S}$ models remains unknown. It is possible that this subpopulation of endosomes is part

of a newly characterized, long-term recycling pathway containing the effectors APPL1 and APPL2 rather than EEA1 (Kalaidzidis et al., 2015; Urbanska et al., 2011). Although this possibility has yet to be confirmed, the presence of internalized CTR1 within this alternative recycling pathway raises the intriguing possibility that the cardiomyocyte and hepatocyte use different strategies to dynamically regulate copper import. Why the heart appears to preferentially store CTR1 in a long-term recycling pathway while the liver chooses to degrade the protein may be explained by the general copper requirement of the two tissues in question. Heart- and liver-specific deletion of *Ctr1* in mice has radically different consequences for animal viability. Deletion of *Ctr1* in either the developing or adult heart results in an early onset, fatal hypertrophic cardiomyopathy (Kim et al., 2010), suggesting that in cardiomyocytes there is a continuous need for CTR1-dependent copper import. In contrast, liver-specific *Ctr1* knockout mice have a relatively mild copper deficiency and a normal lifespan. Under normal physiological conditions, copper concentrations in the liver are much higher than that of the heart, particularly during development where copper stores in the liver are exported into the blood stream to support the growth of peripheral organs. Although the localization of CTR1 at the plasma membrane increases dramatically with time in hepatocytes, suggesting that the murine liver becomes more of a copper uptake organ later in life, intra-hepatic levels of the metal ion reflect a dynamic equilibrium between copper export into the general circulation and inclusion in the bile for excretion. Therefore, the degradation of CTR1 in liver under copper replete conditions may make the most sense, as there is less of a need for rapid copper uptake compared to the heart, should exogenous copper levels drop.

While it remains unclear why altered SCO1 function in cardiomyocytes led to mislocalization of the protein without its eventual degradation as we observed in the *Sco1* knockout liver, it may be that each tissue expresses unique effectors downstream of the mitochondrial copper signalling pathway. Certainly, it appears the cellular copper sensing machinery is differentially affected in the livers of $Sco1^{liv/liv}$ mice when compared to the hearts of $Sco1^{stm/stm}$ or $Sco1^{G115S/G115S}$ mice. The abundance of CCS, the most reliable biomarker of intracellular copper levels (Lassi and Prohaska, 2012), should increase in a copper-deficient state and decrease upon copper overload. However, CCS abundance decreases in the *Sco1* knockout liver while it remains unchanged in the *Sco1* transgenic heart, indicating that loss of SCO1 function in both model systems compromises the proper monitoring of cellular copper status. In fact, these findings argue that the liver of $Sco1^{liv/liv}$ mice is sensing a copper overload state during which the normal response is to rapidly turnover CTR1 (Petris et al., 2003). Why CCS levels remain unchanged in the copper-deficient *Sco1* null G115S heart is

unclear, although the internalization of the bulk of the CTR1 pool suggests that the cardiomyocytes also sense that they are copper replete. The differences in CCS abundance between the *Sco1* transgenic heart and liver may explain why CTR1 abundance only declined in the latter tissue, as the protein is known to be degraded under conditions of prolonged copper excess while it is only internalized under mild copper excess (Petris et al., 2003).

The upregulation of the metallothionein 1 gene further supports the argument that the *Sco1* null hepatocytes are sensing a state of copper overload, as this is a well established response to conditions of copper excess (Freedman et al., 1989; Fürst et al., 1988). Interestingly, an increase in the abundance of metallothionein would effectively exacerbate the copper deficiency because it would sequester the limiting amounts of bioavailable copper that remained in the cell. An increase in metallothionein expression is also observed in the livers of a mouse model of Wilson disease (Muchenditsi et al., 2017). Due to the deletion of *Atp7b* and the resultant dysregulation of biliary copper export, these mice hyperaccumulate copper in their livers. Liver-specific *Atp7b* knockout mice also develop a significant hepatic steatosis and upregulate the expression of genes involved in lipid biosynthesis (Muchenditsi et al., 2017), responses we also observed in our liver-specific *Sco1* knockout mice. Comparable compensatory responses in both the liver-specific *Atp7b* and liver-specific *Sco1* knockout mice further support the idea that the *Sco1* null hepatocyte is inappropriately sensing a state of copper overload and raise the possibility that the copper deficiency upon ablation of *Sco1* expression in the liver may be driven initially by the copper export system. Such a scenario is consistent with a transient spike in bioavailable copper within the cytosol, which would then be predicted to cause the internalization and degradation of CTR1. Whether this initial response is accompanied by aberrant mitochondrial signaling that stimulates copper efflux via the secretory pathway or by redistribution of ATP7A/B remains unknown.

Despite the modest copper deficiency in the hearts of *Sco1*$^{hrt/hrt}$ mice, we observed a significant copper deficiency in their livers pointing to the potential crosstalk between these two organs. A previous study of heart-specific *Ctr1* knockout mice supports the idea that the heart communicates its copper status to the liver (Kim et al., 2010). In the *Ctr1*$^{hrt/hrt}$ mice, the deletion of *Ctr1* in the heart with the same *Cre* driver we used to generate our *Sco1*$^{hrt/hrt}$ mouse results in a significant increase in CCS abundance, arguing that the cardiomyocytes are appropriately sensing a copper deficient state. This leads to a significant increase in ATP7A abundance in hepatocytes and an increased copper mobilization into the bloodstream, presumably in an effort to resupply the heart with copper. HepG2 cells exposed to serum isolated from *Ctr1*$^{hrt/hrt}$ mice expressed significantly more ATP7A, arguing

that the heart secretes a soluble factor into the plasma to communicate with the liver. Although we saw a similar reduction in hepatic copper levels in our *Sco1*$^{hrt/hrt}$ livers, we did not observe a concordant increase in serum copper levels or ATP7A abundance. CCS levels in the *Sco1* knockout and knock-in hearts were also unchanged. We therefore believe that unlike the *Ctr1* knockout heart, hearts of our *Sco1* transgenic models are incorrectly signalling a state of copper excess to the livers which in turn results in CTR1 degradation.

It is tempting to assume that the changes in CTR1 observed with perturbations in *Sco1* expression are a direct reflection of the isolated COX deficiency. All of our mouse models exhibited severe, combined copper and COX deficiencies, and affected tissues from many patients with pathogenic mutations in COX assembly factors including hearts from *SURF1* patients (Stiburek et al., 2009) and fibroblasts from both *COX10* and *COX15* patients (Leary et al., 2007) are also severely copper deficient; however, multiple lines of evidence argue against the COX deficiency being the primary driver of the copper deficient state in either organism. Overexpression of SCO2 in both *SCO1* and *COX15* patient fibroblasts functionally complements the copper deficiency without affecting an increase in residual COX activity (Leary et al, 2007). Rho$^0$ cells, which lack mitochondrial DNA and therefore are unable to assemble COX, only have a modest reduction in CTR1 levels. Finally, while *Cox10* and *Lrpprc* knockout livers exhibit COX and copper deficiencies of comparable severity, CTR1 abundance was markedly reduced in the *Cox10* knockout liver while ATP7A levels were significantly increased in the *Lrpprc* knockout liver in the absence of changes in CTR1. These observations collectively suggest that inputs other than the COX deficiency contribute critically to the transduction of signals that target the import or the export machinery in fundamentally different ways.

If the COX deficiency is not the primary cause of the copper deficiency than what is the nature of the signal that is released from the mitochondrion that regulates CTR1 function? One intriguing possibility is the contribution of oxidative biology to modulating the activity of this signalling pathway. The mitochondrial matrix is a relatively oxidizing environment, with the ratio of reduced to oxidized glutathione (GSH:GSSG) being significantly lower than that of the cytosol (Shen et al., 2005). The import of many proteins within the IMS relies on their oxidative folding, which involves the systematic oxidation of cysteinyl sulphur pairs through the MIA40-ERV1 disulphide relay (Mesecke et al., 2005). Mitochondria are also capable of generating reactive oxygen species through the electron transport chain. Therefore, reducing and oxidizing inputs offer a convenient means of regulating the generation and transduction of mitochondrial signals that ultimately affect CTR1 function. Post-translational modifications that result in the sulfenylation, glutathionylation or

nitrosylation of cysteinyl sulphurs in fact exert profound effects on protein function (Kim et al., 2002). It is thus possible that redox regulation of the cysteinyl sulphurs within the $Cx_3C$ motif of SCO1, or other cysteine-containing proteins known to interact with SCO1 within the IMS, directly contributes to modulating the activity of an organellar copper signalling pathway. Tissue-specific differences in the abundance of key players that orchestrate these reversible post-translational modifications may provide for relative enrichment for a particular redox species that in turn results in cell-type specific regulation of CTR1 function. However, it is just as likely that distinct, tissue-specific changes in CTR1 localization and/or abundance in response to loss of SCO1 function are mediated by unique effectors that are downstream of the initial copper sensing signal.

Although glutathione (GSH) is essential to maintaining redox balance, it also has a critical role in maintaining cellular copper homeostasis. GSH can bind copper and plays a critical role in protecting the cell during copper overload (Freedman et al., 1989). It is also required for CTR1 dependent copper import into the cell (Maryon et al., 2013b), as it binds the imported copper and passes the metal ion down an affinity gradient to metallochaperones like CCS and ATOX1 (Banci et al., 2010). Glutathionylation of ATOX1, ATP7A and ATP7B strongly inhibits the function of these proteins and as a result cellular copper efflux (Singleton et al., 2010). As such, it may be that GSH plays a similar role in copper signalling within the mitochondrion. The mitochondrial matrix contains 10-15% of the cellular GSH pool, presumably due to the oxidative nature of the organelle (Marí et al., 2009). Mitochondrial GSH acts as a buffer against deleterious side reactions driven by reactive oxygen species, yet mutations in ATP7A increase mitochondrial copper levels and disrupt redox balance within the organelle by saturating this buffering capacity (Bhattacharjee et al., 2016). It may be that alterations in mitochondrial copper cause changes within the redox state of the organelle and that this in turn is communicated to the rest of the cell in a SCO1-dependent manner through the regulation of its cysteinyl sulphurs. However, this possibility remains untested experimentally and warrants further investigations.

## 6. Conclusions

The work presented within this thesis has furthered the idea that the inner mitochondrial membrane protein SCO1 has an essential role in maintaining cellular copper homeostasis. Proving our hypothesis, we have shown that mice lacking SCO1 in both the liver and heart phenocopy *SCO1* patients and display a significant isolated COX deficiency as well as a severe copper deficiency. Contrary to the copper deficiency observed in human *SCO1* patients, the copper deficiency in our mouse models was caused by defects in the high-affinity copper import pathway, albeit by different mechanisms in different tissues (Figure 6.1). Livers lacking *Sco1* expression exhibited internalization and degradation of CTR1, whereas in hearts lacking *Sco1,* CTR1 abundance was maintained but the protein was mislocalized and maintained on endosomes. The exact cause and the proteins or genes responsible for these tissue-specific differences are unknown.

One of the main limitations in studying human disease states with knockout mouse models is that the absence of protein is not equivalent to the expression of a partially functional mutated protein. To mitigate this issue, we developed a knock-in mouse model with global expression of *G115S Sco1* pathogenic variant, analogous to the human *G132S* mutation that is known to cause hypertrophic cardiomyopathy. Examining the hearts of these mice, we found a similar phenotype to that of our heart specific knockout mice, with a severe copper deficiency and a mislocalization of CTR1 within the cardiac tissue. The fact that our knockout model so closely phenocopied the knock-in model analogous to the human condition provides support that these models are viable to studying *SCO1* human patients.

Finally, data presented within this thesis demonstrates that the deletion of SCO1 in the heart activated a systemic copper signalling pathway which resulted in a copper deficiency in the liver. This further establishes the existence of such a copper signalling pathway between the heart and liver, however, we observed minor differences compared to the previously reported pathway. The hepatic copper deficiency in the heart-specific SCO1 was caused by a decrease in the abundance of CTR1, compared to an increase in ATP7A expression observed in the livers of heart-specific CTR1 knockout mice. These differences perhaps suggest that our model represents the signalling of copper overload rather than copper deficiency.

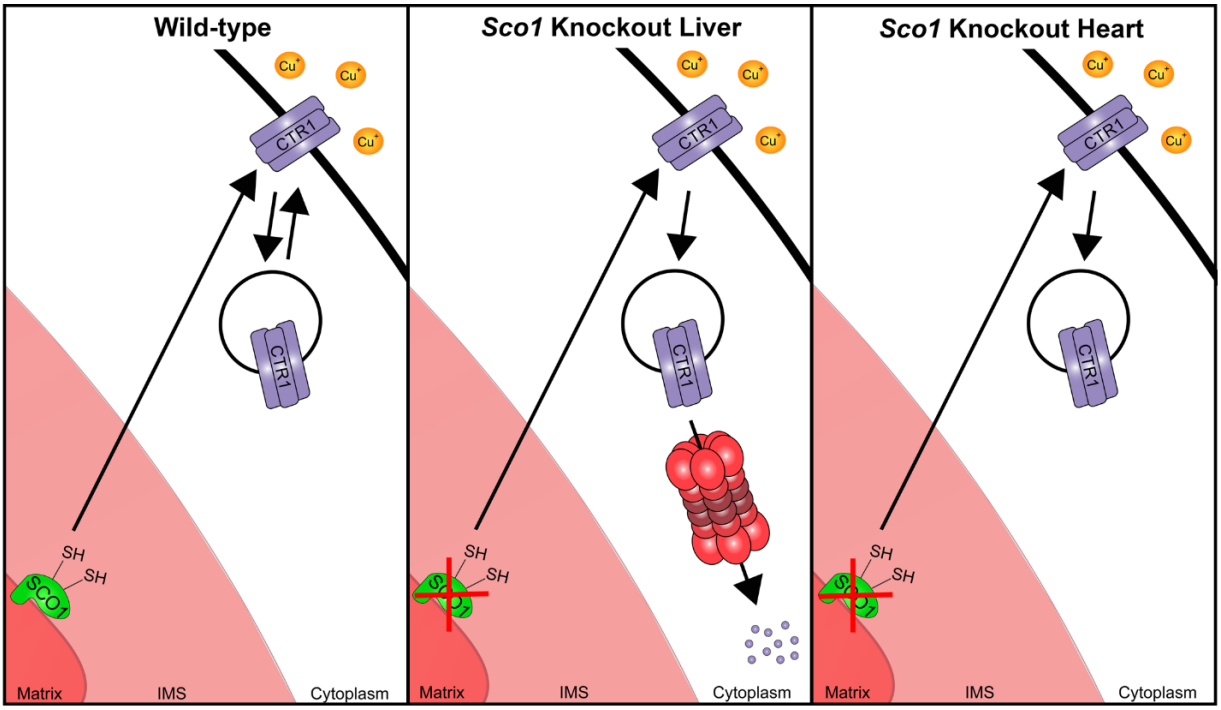


**Figure 6.1: Deletion of *Sco1* causes changes in CTR1 localization and abundance**

Wild-type SCO1 (left) maintains proper expression of CTR1 with the protein primarily being localized to the plasma membrane but being in dynamic equilibrium with the cytosol. Deletion of *Sco1* in the liver (middle) results in CTR1 being internalized from the plasma membrane and degraded via the proteasome. Deletion of *Sco1* in the cardiomyocytes (right) results in mislocalization of the protein from the intercalated discs onto endosomes while maintaining wild-type abundance of the protein.

## 7. Future Directions

We have shown that SCO1 has an essential role in maintaining both the localization and abundance of CTR1 in multiple tissues; however, this raises multiple questions with regards to how this system functions. Primarily, how does SCO1, a protein tethered to the inner mitochondrial membrane, communicate with the periphery of the cell to regulate the localization CTR1? It may be that SCO1 communicates though the use of a soluble secondary messenger with dual localization between the mitochondria and cytosol, analogous to the role COX19 plays in regulating copper efflux in the human *SCO1* patient fibroblasts (Leary et al., 2013b). However, a liver-specific COX19 knockout mouse has a significant hepatic copper deficiency (Leary lab unpublished data), suggesting that COX19 can not be the sole protein involved in emanating a signal from the mitochondria. Therefore, future work must be completed to determine the downstream proteins that are involved in transmitting the copper signal. Certainly, establishing primary tissue culture models from the *Sco1* knockout mice would aid in answering this question. Assuming such a model could be generated and validated to function the same as the knockout tissues, knockdown experiments could be performed to reduce the abundance of soluble proteins known to have dual localization between the mitochondria and cytosol to examine the role these proteins having in communicating mitochondrial copper signals.

Primary tissue culture models lacking *Sco1* would also aid in determining the tissue specific differences resulting in CTR1 being degraded in the liver but not in the heart, another question raised by the data in this thesis. Pull-down experiments in the hearts and livers of wild-type and *Sco1* tissue-specific knockout mice could determine potential interactors with CTR1 that may be targeting the protein for internalization or degradation, such as proteins involved in specific endocytic pathways or protein specific E3 ubiquitin ligases. If a list of potential proteins could be identified within the *Sco1* knockout tissues, these proteins could be knocked down in the primary cell models to determine if they are essential in maintaining the proper localization and abundance of CTR1.

The data presented within this thesis suggests that SCO1 may sit at the head of the copper sensing and signalling pathway; however, copper deficiencies were observed in all mouse models examined with isolated COX deficiencies. It may be that a separate process senses alterations of copper levels in the cell, e.g. the redox state of the mitochondrion, and this process acts through SCO1 to regulate cellular copper levels. The mitochondrial redox state is an intriguing possibility for this function as it is perturbed by genetic manipulations that cause copper overload (Bhattacharjee et al., 2016). Fittingly, it has also been shown that the redox state of the cysteinyl sulphurs of SCO1 change under copper replete or deficient conditions (Leary et al., 2013b). Experiments could be performed to

examine the redox state of the organelle upon deletion or perturbation of SCO1 function to determine if it is altered in a similar manner to cells under copper excess conditions, which would provide further evidence in support of our hypothesis that SCO1 perturbed cells are incorrectly signalling a copper overload.

The overexpression of SCO2 rescuing the copper deficiency in the SCO1 patient fibroblasts suggests that redox state of the mitochondria or at the very least SCO1 is central to the copper signalling mechanism (Leary et al., 2007). Further investigation should be performed into the role of SCO2 in these copper signalling pathways within the tissues of our knockout mice. Why is it that the overexpression of SCO2 results in the rescue of the copper phenotype while causing a dominant negative COX phenotype? Would over-expression of SCO2 in our knockout mouse or tissue culture models rescue copper levels in a similar fashion? Can we manipulate the redox state of these proteins without manipulating SCO2 abundance, e.g. by using antioxidants, and will that affect the levels of copper or CCS within the cell, possibly signalling a copper overload or deficient state?

Despite our validation and basic characterization of hearts of the *G115S* knock-in mouse, work remains to determine the cause of the tissue specific differences observed in human *SCO1* patients. Generation and characterization of knock-in mice harbouring the other human pathogenic *Sco1* alleles will be essential to answering these questions; however, this is made more difficult given that the P174L and M294V human pedigrees are both compound heterozygotes, necessitating the mice harbour both one knock-in and one deleted allele. Will expression of the other pathogenic alleles at appropriate levels result in a similar tissue specific phenotype in the mice? Will there be differences in the levels of COX activity or copper concentrations in the tissues of the mice expressing different pathogenic variants? If these differences do exist it may indicate why we see such stark differences in the human disease states.

## 8. References


Acin-Perez, R., Gatti, D.L., Bai, Y., and Manfredi, G. (2011). Protein phosphorylation and prevention of cytochrome oxidase inhibition by ATP: Coupled mechanisms of energy metabolism regulation. Cell Metab. *13*, 712–719.

Aller, S.G., and Unger, V.M. (2006). Projection structure of the human copper transporter CTR1 at 6-A resolution reveals a compact trimer with a novel channel-like architecture. Proc. Natl. Acad. Sci. U. S. A. *103*, 3627–3632.

Baertling, F., van den Brand, M., Hertecant, J.L., Al-Shamsi, A., van den Heuvel, L., Distelmaier, F., Mayatepek, E., Smeitink, J.A., Nijtmans, L.G., and Rodenburg, R.J. (2015). Mutations in COA6 cause cytochrome c oxidase deficiency and neonatal hypertrophic cardiomyopathy. Hum. Mutat. *36*, 34–38.

Baker, Z.N., Cobine, P.A., and Leary, S.C. (2017). The mitochondrion: a central architect of copper homeostasis. Metallomics *9*, 1501–1512.

Banci, L., Bertini, I., Ciofi-Baffoni, S., Leontari, I., Martinelli, M., Palumaa, P., Sillard, R., and Wang, S. (2007). Human Sco1 functional studies and pathological implications of the P174L mutant. Proc. Natl. Acad. Sci. U. S. A. *104*, 15–20.

Banci, L., Bertini, I., Ciofi-Baffoni, S., Hadjiloi, T., Martinelli, M., and Palumaa, P. (2008). Mitochondrial copper(I) transfer from Cox17 to Sco1 is coupled to electron transfer. Proc. Natl. Acad. Sci. U. S. A. *105*, 6803–6808.

Banci, L., Bertini, I., Ciofi-Baffoni, S., Kozyreva, T., Zovo, K., and Palumaa, P. (2010). Affinity gradients drive copper to cellular destinations. Nature *465*, 645–648.

Bandmann, O., Weiss, K.H., and Kaler, S.G. (2015). Wilson's disease and other neurological copper disorders. Lancet Neurol. *14*, 103–113.

Barros, M.H., Johnson, A., and Tzagoloff, A. (2004). COX23, a homologue of COX17, is required for cytochrome oxidase assembly. J. Biol. Chem. *279*, 31943–31947.

Bartnikas, T.B., and Gitlin, J.D. (2003). Mechanisms of biosynthesis of mammalian copper/zinc superoxide dismutase. J. Biol. Chem. *278*, 33602–33608.

Beers, J., Glerum, M.D., and Tzagoloff, A. (1997). Purification, characterization, and localization of yeast Cox17p, a mitochondrial copper shuttle. J. Biol. Chem. *272*, 33191–33196.

Bertinato, J., Iskandar, M., and L'Abbé, M.R. (2003). Copper deficiency induces the upregulation of the copper chaperone for Cu/Zn superoxide dismutase in weanling male rats. J. Nutr. *133*, 28–31.

Bhattacharjee, A., Yang, H., Duffy, M., Robinson, E., Conrad-Antoville, A., Lu, Y.W., Capps, T., Braiterman, L., Wolfgang, M., Murphy, M.P., et al. (2016). The activity of Menkes disease protein ATP7A is essential for redox balance in mitochondria. J. Biol. Chem. *291*, 16644–16658.

Boulet, A., Vest, K.E., Maynard, M.K., Gammon, M.G., Russell, A.C., Mathews, A.T., Cole, S.E., Zhu, X., Phillips, C.B., Kwong, J.Q., et al. (2017). The mammalian phosphate carrier SLC25A3 is a mitochondrial copper transporter required for cytochrome c oxidase biogenesis. J. Biol. Chem. jbc.RA117.000265.

Bourens, M., and Barrientos, A. (2017). Human mitochondrial cytochrome c oxidase assembly factor COX18 acts transiently as a membrane insertase within the subunit 2 maturation module. J. Biol. Chem. *292*, 7774–7783.

Brady, D.C., Crowe, M.S., Turski, M.L., Hobbs, G.A., Yao, X., Chaikuad, A., Knapp, S., Xiao, K., Campbell, S.L., Thiele, D.J., et al. (2014). Copper is required for oncogenic BRAF signalling and tumorigenesis. Nature *509*, 492–496.

Braiterman, L., Nyasae, L., Guo, Y., Bustos, R., Lutsenko, S., and Hubbard, A. (2009). Apical targeting and Golgi retention signals reside within a 9-amino acid sequence in the copper-ATPase, ATP7B. Am. J. Physiol. Gastrointest. Liver Physiol. *296*, G433-44.

Brancaccio, D., Gallo, A., Piccioli, M., Novellino, E., Ciofi-Baffoni, S., and Banci, L. (2017). [4Fe-4S] cluster assembly in mitochondria and its impairment by copper. J. Am. Chem. Soc. *139*, 719–730.

Caruano-Yzermans, A.L., Bartnikas, T.B., and Gitlin, J.D. (2006). Mechanisms of the copper-dependent turnover of the copper chaperone for superoxide dismutase. J. Biol. Chem. *281*, 13581–13587.

Chelly, J., Zeynep, T., Tonnesen, T., Petterson, A., Ishikawa-Brush, Y., Niels, T., Horn, N., and Monaco, A. (1993). Isolation of a candidate gene for Menkes disease that encodes a potetial heavy metal binding protein. Nat. Genet. *3*, 14–19.

Clifford, R.J., Maryon, E.B., and Kaplan, J.H. (2016). Dynamic internalization and recycling of a metal ion transporter: Cu homeostasis and CTR1, the human $Cu^{+}$ uptake system. J. Cell Sci. *129*,

1711–1721.

Cobine, P.A., Ojeda, L.D., Rigby, K.M., and Winge, D.R. (2004). Yeast contain a non-proteinaceous pool of copper in the mitochondrial matrix. J. Biol. Chem. *279*, 14447–14455.

Cobine, P.A., Pierrel, F., Bestwick, M.L., and Winge, D.R. (2006a). Mitochondrial matrix copper complex used in metallation of cytochrome oxidase and superoxide dismutase. J. Biol. Chem. *281*, 36552–36559.

Cobine, P.A., Pierrel, F., Leary, S.C., Sasarman, F., Horng, Y.C., Shoubridge, E.A., and Winge, D.R. (2006b). The P174L mutation in human Sco1 severely compromises Cox17-dependent metallation but does not impair copper binding. J. Biol. Chem. *281*, 12270–12276.

Culotta, V.C., Klomp, L.J., Strain, J., Casareno, R., Krems, B., and Gitlin, J.D. (1997). The copper chaperone for superoxide dismutase. J. Biol. Chem. *272*, 23469–23472.

Dancis, A., Yuan, D.S., Haile, D., Askwith, C., Eide, D., Moehle, C., Kaplan, J., and Klausner, R.D. (1994). Molecular characterization of a copper transport protein in S. cerevisiae: an unexpected role for copper in iron transport. Cell *76*, 393–402.

Danks, D.M., Cartwright, E., Stevens, B.J., and Townley, R.R. (1973). Menkes' kinky hair disease: further definition of the defect in copper transport. Science *179*, 1140–1142.

Dodani, S.C., Leary, S.C., Cobine, P.A., Winge, D.R., and Chang, C.J. (2011). A targetable fluorescent sensor reveals that copper-deficient SCO1 and SCO2 patient cells prioritize mitochondrial copper homeostasis. J. Am. Chem. Soc. *133*, 8606–8616.

Doria-Medina, C.L., Lund, D.D., Pasley, A., Sandra, A., and Sivitz, W.I. (1993). Immunolocalization of GLUT-1 glucose transporter in rat skeletal muscle and in normal and hypoxic cardiac tissue. Am. J. Physiol. Endocrinol. Metab. *265*, E454–E464.

De Feo, C.J., Aller, S.G., Siluvai, G.S., Blackburn, N.J., and Unger, V.M. (2009). Three-dimensional structure of the human copper transporter hCTR1. Proc. Natl. Acad. Sci. U. S. A. *106*, 4237–4242.

Festa, R.A., and Thiele, D.J. (2012). Copper at the front line of the host-pathogen battle. PLoS Pathog. *8*, e1002887.

Finney, J., Moon, H.J., Ronnebaum, T., Lantz, M., and Mure, M. (2014). Human copper-dependent amine oxidases. Arch. Biochem. Biophys. *546*, 19–32.

Freedman, J.H., Ciriolo, M.R., and Peisach, J. (1989). The role of glutathione in copper metabolism and toxicity. J. Biol. Chem. *264*, 5598–5605.

Fürst, P., Hu, S., Hackett, R., and Hamer, D. (1988). Copper activates metallothionein gene transcription by altering the conformation of a specific DNA binding protein. Cell *55*, 705–717.

Furukawa, Y., Torres, A.S., and O'Halloran, T. V (2004). Oxygen-induced maturation of SOD1: a key role for disulfide formation by the copper chaperone CCS. EMBO J *23*, 2872–2881.

Ghosh, A., Trivedi, P.P., Timbalia, S.A., Griffin, A.T., Rahn, J.J., Chan, S.S.L., and Gohil, V.M. (2014). Copper supplementation restores cytochrome c oxidase assembly defect in a mitochondrial disease model of COA6 deficiency. Hum. Mol. Genet. *23*, 3596–3606.

Ghosh, A., Pratt, A.T., Soma, S., Theriault, S.G., Griffin, A.T., Trivedi, P.P., and Gohil, V.M. (2016). Mitochondrial disease genes COA6, COX6B and SCO2 have overlapping roles in COX2 biogenesis. Hum. Mol. Genet. *25*, 660–671.

Glerum, M.D., Shtanko, A., and Tzagoloff, A. (1996a). Characterization of COX17 , a Yeast Gene Involved in Copper Metabolism and Assembly of Cytochrome Oxidase. J. Biol. Chem. *24*, 14504–14509.

Glerum, M.D., Shtanko, A., and Tzagoloff, A. (1996b). SCO1 and SCO2 act as high copy suppressors of a mitochondrial copper recruitment defect in Saccharomyces cerevisiae. J. Biol. Chem. *271*, 20531–20535.

Greenough, M. (2004). Signals regulating trafficking of Menkes (MNK; ATP7A) copper-translocating P-type ATPase in polarized MDCK cells. Am. J. Physiol. Cell Physiol. *287*, C1463–C1471.

Guo, Y., Smith, K., Lee, J., Thiele, D.J., and Petris, M.J. (2004). Identification of methionine-rich clusters that regulate copper-stimulated endocytosis of the human CTR1 copper transporter. J. Biol. Chem. *279*, 17428–17433.

Hamer, D.H. (1986). Metallothionein. Annu. Rev. Biochem. *55*, 913–951.

Hamza, I., Faisst, A., Prohaska, J., Chen, J., Gruss, P., and Gitlin, J.D. (2001). The metallochaperone Atox1 plays a critical role in perinatal copper homeostasis. Proc. Natl. Acad. Sci. U. S. A. *98*, 6848–6852.

Hatori, Y., Clasen, S., Hasan, N.M., Barry, A.N., and Lutsenko, S. (2012). Functional partnership of the copper export machinery and glutathione balance in human cells. J. Biol. Chem. *287*, 26678–26687.

Hlynialuk, C.J., Ling, B., Baker, Z.N., Cobine, P.A., Yu, L.D., Boulet, A., Wai, T., Hossain, A., El Zawily, A.M., McFie, P.J., et al. (2015). The mitochondrial metallochaperone SCO1 is required to sustain expression of the high-affinity copper transporter CTR1 and preserve copper homeostasis. Cell Rep. *10*, 933–943.

Holmes, D.T., Buhr, K.A. (2007). Error propagation in calculated ratios. Clin. Biochem. *40*, 728-734.

Horn, D., Al-Ali, H., and Barrientos, A. (2008). Cmc1p is a conserved mitochondrial twin CX9C protein involved in cytochrome c oxidase biogenesis. Mol. Cell. Biol. *28*, 4354–4364.

Horng, Y.C., Cobine, P.A., Maxfield, A.B., Carr, H.S., and Winge, D.R. (2004). Specific copper transfer from the Cox17 metallochaperone to both Sco1 and Cox11 in the assembly of yeast cytochrome c oxidase. J. Biol. Chem. *279*, 35334–35340.

Ikeda, K., Shiba, S., Horie-Inoue, K., Shimokata, K., and Inoue, S. (2013). A stabilizing factor for mitochondrial respiratory supercomplex assembly regulates energy metabolism in muscle. Nat. Commun. *4*. 2147.

Itoh, S., Kim, H.W., Nakagawa, O., Ozumi, K., Lessner, S.M., Aoki, H., Akram, K., McKinney, R.D., Ushio-Fukai, M., and Fukai, T. (2008). Novel role of antioxidant-1 (Atox1) as a copper-dependent transcription factor involved in cell proliferation. J. Biol. Chem. *283*, 9157–9167.

Itoh, S., Ozumi, K., Kim, H.W., Nakagawa, O., McKinney, R.D., Folz, R.J., Zelko, I.N., Ushio-Fukai, M., and Fukai, T. (2009). Novel mechanism for regulation of extracellular SOD transcription and activity by copper: Role of antioxidant-1. Free Radic. Biol. Med. *46*, 95–104.

Jaksch, M., Ogilvie, I., Yao, J., Kortenhaus, G., Bresser, H.G., Gerbitz, K.D., and Shoubridge, E.A. (2000). Mutations in SCO2 are associated with a distinct form of hypertrophic cardiomyopathy and cytochrome c oxidase deficiency. Hum. Mol. Genet. *9*, 795–801.

Jaksch, M., Horvath, R., Horn, N., Auer, D.P., Macmillan, C., Peters, J., Gerbitz, K.D., Kraegeloh-Mann, I., Muntau, A., Karcagi, V., et al. (2001). Homozygosity (E140K) in SCO2 causes delayed infantile onset of cardiomyopathy and neuropathy. Neurology *57*, 1440–1446.

Jomova, K., and Valko, M. (2011). Advances in metal-induced oxidative stress and human disease. Toxicology *283*, 65–87.

Kadenbach, B., and Hüttemann, M. (2015). The subunit composition and function of mammalian cytochrome c oxidase. Mitochondrion *24*, 64–76.

Kalaidzidis, I., Miaczynska, M., Brewinska-Olchowik, M., Hupalowska, A., Ferguson, C., Parton, R.G., Kalaidzidis, Y., and Zerial, M. (2015). APPL endosomes are not obligatory endocytic intermediates but act as stable cargo-sorting compartments. J. Cell Biol. *211*, 123–144.

Kaler, S.G. (2013). Inborn errors of copper metabolism. Handb. Clin. Neurol. *113*, 1745–1754.

Kaler, S.G., Holmes, C.S., Goldstein, D.S., Tang, J., Godwin, S.C., Donsante, A., Liew, C.J., Sato, S., and Patronas, N. (2008). Neonatal diagnosis and treatment of Menkes disease. N. Engl. J. Med. *358*, 605–614.

Kidane, T.Z., Farhad, R., Lee, K.J., Santos, A., Russo, E., and Linder, M.C. (2012). Uptake of copper from plasma proteins in cells where expression of CTR1 has been modulated. BioMetals *25*, 697–709.

Kim, B.E., Nevitt, T., and Thiele, D.J. (2008). Mechanisms for copper acquisition, distribution and regulation. Nat Chem Biol *4*, 176–185.

Kim, B.E., Turski, M.L., Nose, Y., Casad, M., Rockman, H.A., and Thiele, D.J. (2010). Cardiac copper deficiency activates a systemic signaling mechanism that communicates with the copper acquisition and storage organs. Cell Metab. *11*, 353–363.

Kim, S.O., Merchant, K., Nudelman, R., Beyer, W.F., Keng, T., DeAngelo, J., Hausladen, A., and Stamler, J.S. (2002). OxyR: A molecular code for redox-related signaling. Cell *109*, 383–396.

Kleber, A.G., and Saffitz, J.E. (2014). Role of the intercalated disc in cardiac propagation and arrhythmogenesis. Front. Physiol. *5*, 404.

Klomp, A.E., Tops, B.B., Van Denberg, I., Berger, R., and Klomp, L.J. (2002). Biochemical characterization and subcellular localization of human copper transporter 1 (hCTR1). Biochem. J. *364*, 497–505.

Klomp, A.E., Juijn, J.A., van der Gun, L.T., van den Berg, I.E., Berger, R., and Klomp, L.J. (2003). The N-terminus of the human copper transporter 1 (hCTR1) is localized extracellularly, and interacts

with itself. Biochem. J. *370*, 881–889.

Klomp, L., Lin, S., Yuan, D., Klausner, R., Culotta, V., and Gitlin, J. (1997). Identification and functional expression of HAH1, a novel human gene involved in copper homeostasis. J. Biol. Chem. *272*, 9221–9226.

Krishnamoorthy, L., Cotruvo, J.A., Chan, J., Kaluarachchi, H., Muchenditsi, A., Pendyala, V.S., Jia, S., Aron, A.T., Ackerman, C.M., Wal, M.N.V., et al. (2016). Copper regulates cyclic-AMP-dependent lipolysis. Nat. Chem. Biol. *12*, 586–592.

Kuo, Y.-M., Gybina, A.A., Pyatskowit, J.W., Gitschier, J., and Prohaska, J.R. (2006). Copper transport protein (Ctr1) levels in mice are tissue specific and dependent on copper status. J. Nutr. *136*, 21–26.

Lassi, K.C., and Prohaska, J.R. (2011). Rapid alteration in rat red blood cell copper chaperone for superoxide dismutase after marginal copper deficiency and repletion. Nutr. Res. *31*, 698–706.

Lassi, K.C., and Prohaska, J.R. (2012). Erythrocyte copper chaperone for superoxide dismutase is increased following marginal copper deficiency in adult and postweanling mice. J. Nutr. *142*, 292–297.

Leary, S.C., Kaufman, B.A., Pellecchia, G., Guercin, G.H., Mattman, A., Jaksch, M., and Shoubridge, E.A. (2004). Human SCO1 and SCO2 have independent, cooperative functions in copper delivery to cytochrome c oxidase. Hum. Mol. Genet. *13*, 1839–1848.

Leary, S.C., Cobine, P.A., Kaufman, B.A., Guercin, G.H., Mattman, A., Palaty, J., Lockitch, G., Winge, D.R., Rustin, P., Horvath, R., et al. (2007). The human cytochrome c oxidase assembly factors SCO1 and SCO2 have regulatory roles in the maintenance of cellular copper homeostasis. Cell Metab. *5*, 9–20.

Leary, S.C., Winge, D.R., and Cobine, P.A. (2009). "Pulling the plug" on cellular copper: The role of mitochondria in copper export. Biochim. Biophys. Acta Mol. Cell Res. *1793*, 146–153.

Leary, S.C., Antonicka, H., Sasarman, F., Weraarpachai, W., Cobine, P.A., Pan, M., Brown, G.K., Brown, R., Majewski, J., Ha, K.C.H., et al. (2013a). Novel mutations in SCO1 as a cause of fatal infantile encephalopathy and lactic acidosis. Hum. Mutat. *34*, 1366–1370.

Leary, S.C., Cobine, P.A., Nishimura, T., Verdijk, R.M., de Krijger, R., de Coo, R., Tarnopolsky,

M.A., Winge, D.R., and Shoubridge, E.A. (2013b). COX19 mediates the transduction of a mitochondrial redox signal from SCO1 that regulates ATP7A-mediated cellular copper efflux. Mol. Biol. Cell *24*, 683–691.

Lee, J., Prohaska, J.R., and Thiele, D.J. (2001). Essential role for mammalian copper transporter Ctr1 in copper homeostasis and embryonic development. Proc. Natl. Acad. Sci. U. S. A. *98*, 6842–6847.

Lee, J., Peña, M.M., Nose, Y., and Thiele, D.J. (2002). Biochemical characterization of the human copper transporter Ctr1. J. Biol. Chem. *277*, 4380–4387.

Lichtmannegger, J., Leitzinger, C., Wimmer, R., Schmitt, S., Schulz, S., Kabiri, Y., Eberhagen, C., Rieder, T., Janik, D., Neff, F., et al. (2016). Methanobactin reverses acute liver failure in a rat model of Wilson disease. J. Clin. Invest. *126*, 2721–2735.

Lill, R. (2009). Function and biogenesis of iron-sulphur proteins. Nature *460*, 831–838.

Lin, S.J., and Culotta, V.C. (1995). The ATX1 gene of Saccharomyces cerevisiae encodes a small metal homeostasis factor that protects cells against reactive oxygen toxicity. Proc. Natl. Acad. Sci. U. S. A. *92*, 3784–3788.

Lin, S.J., Pufahl, R.A., Dancis, A., O'Halloran, T. V., and Culotta, V.C. (1997). A role for the Saccharomyces cerevisiae ATX1 gene in copper trafficking and iron transport. J. Biol. Chem. *272*, 9215–9220.

Lode, A., Kuschel, M., Paret, C., and Rödel, G. (2000). Mitochondrial copper metabolism in yeast: Interaction between Sco1p and Cox2p. FEBS Lett. *485*, 19–24.

Lutsenko, S., Barnes, N.L., Bartee, M.Y., and Dmitriev, O.Y. (2007). Function and regulation of human copper-transporting ATPases. Physiol. Rev. *87*, 1011–1046.

Lutsenko, S., Bhattacharjee, A., and Hubbard, A.L. (2010). Copper handling machinery of the brain. Metallomics *2*, 596.

Lyons, A.M., Ardissone, A., Reyes, A., Robinson, A.J., Moroni, I., Ghezzi, D., Fernandez-Vizarra, E., and Zeviani, M. (2016). COA7 (C1orf163/RESA1) mutations associated with mitochondrial leukoencephalopathy and cytochrome c oxidase deficiency. J. Med. Genet. *53*, 846–849.

MacGurn, J.A., Hsu, P.-C., and Emr, S.D. (2012). Ubiquitin and membrane protein turnover: from cradle to grave. Annu. Rev. Biochem. *81*, 231–259.

Macomber, L., and Imlay, J.A. (2009). The iron-sulfur clusters of dehydratases are primary intracellular targets of copper toxicity. Proc. Natl. Acad. Sci. U. S. A. *106*, 8344–8349.

Marí, M., Morales, A., Colell, A., García-Ruiz, C., and Fernández-Checa, J.C. (2009). Mitochondrial glutathione, a key survival antioxidant. Antioxid. Redox Signal. *11*, 2685–2700.

Maryon, E.B., Molloy, S.A., and Kaplan, J.H. (2007). O-linked glycosylation at threonine 27 protects the copper transporter hCTR1 from proteolytic cleavage in mammalian cells. J. Biol. Chem. *282*, 20376–20387.

Maryon, E.B., Zhang, J., Jellison, J.W., and Kaplan, J.H. (2009). Human copper transporter 1 lacking O-linked glycosylation is proteolytically cleaved in a Rab9-positive endosomal compartment. J. Biol. Chem. *284*, 28104–28114.

Maryon, E.B., Molloy, S.A., Ivy, K., Yu, H., and Kaplan, J.H. (2013a). Rate and regulation of copper transport by human copper transporter 1 (hCTR1). J. Biol. Chem. *288*, 18035–18046.

Maryon, E.B., Molloy, S.A., and Kaplan, J.H. (2013b). Cellular glutathione plays a key role in copper uptake mediated by human copper transporter 1. Am. J. Physiol. Cell Physiol. *304*, C768–C779.

Maxfield, A.B., Heaton, D.N., and Winge, D.R. (2004). Cox17 Is Functional When Tethered to the Mitochondrial Inner Membrane. J. Biol. Chem. *279*, 5072–5080.

McCord, J.M., and Fridovich, I. (1969). Superoxide dismutase. An enzymic function for erythrocuprein (hemocuprein). J. Biol. Chem. *244*, 6049–6055.

McEwen, J.E., Ko, C., Kloeckner-Gruissem, B., and Poyton, R.O. (1986). Nuclear functions required for cytochrome c oxidase biogenesis in Saccharomyces cerevisiae. Characterization of mutants in 34 complementation groups. J. Biol. Chem. *261*, 11872–11879.

McKenzie, M., Lazarou, M., Thorburn, D.R., and Ryan, M.T. (2007). Analysis of mitochondrial subunit assembly into respiratory chain complexes using Blue Native polyacrylamide gel electrophoresis. Anal. Biochem. *364*, 128–137.

Mendelsohn, B.A., Yin, C., Johnson, S.L., Wilm, T.P., Solnica-Krezel, L., and Gitlin, J.D. (2006). Atp7a determines a hierarchy of copper metabolism essential for notochord development. Cell Metab. *4*, 155–162.

Mercer, J.F.B., Livingston, J., Hall, B., Paynter, J.A., Begy, C., Chandrasekharappa, S., Lockhart, P.,

Grimes, A., Bhave, M., Siemieniak, D., et al. (1993). Isolation of a partial candidate gene for Menkes disease by positional cloning. Nat. Genet. *3*, 20–25.

Mercer, S.W., La Fontaine, S., Warr, C.G., and Burke, R. (2016). Reduced glutathione biosynthesis in Drosophila melanogaster causes neuronal defects linked to copper deficiency. J. Neurochem. *137*, 360–370.

Merchant, S., and Bogorad, L. (1986). Rapid degradation of apoplastocyanin in Cu(II)-deficient cells of Chlamydomonas reinhardtii. J. Biol. Chem. *261*, 15850–15853.

Merchant, S.S., Allen, M.D., Kropat, J., Moseley, J.L., Long, J.C., Tottey, S., and Terauchi, A.M. (2006). Between a rock and a hard place: Trace element nutrition in Chlamydomonas. Biochim. Biophys. Acta Mol. Cell Res. *1763*, 578–594.

Mesecke, N., Terziyska, N., Kozany, C., Baumann, F., Neupert, W., Hell, K., and Herrmann, J.M. (2005). A disulfide relay system in the intermembrane space of mitochondria that mediates protein import. Cell *121*, 1059–1069.

Molloy, S.A., and Kaplan, J.H. (2009). Copper-dependent recycling of hCTR1, the human high affinity copper transporter. J. Biol. Chem. *284*, 29704–29713.

Morgada, M.N., Abriata, L.A., Cefaro, C., Gajda, K., Banci, L., and Vila, A.J. (2015). Loop recognition and copper-mediated disulfide reduction underpin metal site assembly of Cu A in human cytochrome oxidase. Proc. Natl. Acad. Sci. U. S. A. *112*, 11771–11776.

Muchenditsi, A., Yang, H., Hamilton, J.P., Koganti, L., Housseau, F., Aronov, L., Fan, H., Pierson, H., Bhattacharjee, A., Murphy, R., Sears, C., Potter, J., Wooton-Kee, C.R., Lutsenko, S. (2017). Targeted inactivation of copper transporter Atp7b in hepatocytes causes liver steatosis and obesity in mice. Am. J. Physiol. Gastrointest. Liver Physiol. *313*, G39-G49

Muller, P.J., and Klomp, L.J. (2009). ATOX1: A novel copper-responsive transcription factor in mammals? Int. J. Biochem. Cell Biol. *41*, 1233–1236.

Nevitt, T., Öhrvik, H., and Thiele, D.J. (2012). Charting the travels of copper in eukaryotes from yeast to mammals. Biochim. Biophys. Acta Mol. Cell Res. *1823*, 1580–1593.

Nittis, T., George, G.N., and Winge, D.R. (2001). Yeast Sco1, a Protein Essential for Cytochrome c Oxidase Function Is a Cu(I)-binding Protein. J. Biol. Chem. *276*, 42520–42526.

Öhrvik, H., Nose, Y., Wood, L.K., Kim, B.-E., Gleber, S.-C., Ralle, M., and Thiele, D.J. (2013). Ctr2 regulates biogenesis of a cleaved form of mammalian Ctr1 metal transporter lacking the copper- and cisplatin-binding ecto-domain. Proc. Natl. Acad. Sci. U. S. A. *110*, E4279–E4288.

Öhrvik, H., Logeman, B., Turk, B., Reinheckel, T., and Thiele, D.J. (2016). Cathepsin protease controls copper and cisplatin accumulation via cleavage of the Ctr1 Metal-binding ectodomain. J. Biol. Chem. *291*, 13905–13916.

Oswald, C., Krause-Buchholz, U., and Rödel, G. (2009). Knockdown of human COX17 affects assembly and supramolecular organization of cytochrome c oxidase. J. Mol. Biol. *389*, 470–479.

Pacheu-Grau, D., Bareth, B., Dudek, J., Juris, L., Vögtle, F.N., Wissel, M., Leary, S.C., Dennerlein, S., Rehling, P., and Deckers, M. (2015). Cooperation between COA6 and SCO2 in COX2 maturation during cytochrome c oxidase assembly links two mitochondrial cardiomyopathies. Cell Metab. *21*, 823–833.

Papadopoulou, L.C., Sue M, C., Davidson, M.M., Tanji, K., Nishino, I., Sadlock, J.E., Krishna, S., Walker, W., Selby, J., Glerum, D.M., et al. (1999). Fatal infantile cardioencephalomyopathy with COX deficiency and mutations in SCO2, a COX assembly gene. Nat. Genet. *23*, 333–337.

Park, J.D., Liu, Y., and Klaassen, C.D. (2001). Protective effect of metallothionein against the toxicity of cadmium and other metals. Toxicology *163*, 93–100.

Petris, M.J., and Mercer, J.F.B. (1999). The Menkes protein (ATP7A; MNK) cycles via the plasma membrane both in basal and elevated extracellular copper using a C-terminal di-leucine endocytic signal. Hum. Mol. Genet. *8*, 2107–2115.

Petris, M.J., Mercer, J.F.B., Culvenor, J.G., Lockhart, P., Gleeson, P.A., and Camakaris, J. (1996). Ligand-regulated transport of the Menkes copper P-type ATPase efflux pump from the Golgi apparatus to the plasma membrane: a novel mechanism of regulated trafficking. EMBO J. *15*, 6084–6095.

Petris, M.J., Voskoboinik, I., Cater, M., Smith, K., Kim, B.E., Llanos, R.M., Strausak, D., Camakaris, J., and Mercer, J.F. (2002). Copper-regulated trafficking of the Menkes disease copper ATPase is associated with formation of a phosphorylated catalytic intermediate. J. Biol. Chem. *277*, 46736–46742.

Petris, M.J., Smith, K., Lee, J., and Thiele, D.J. (2003). Copper-stimulated endocytosis and degradation of the human copper transporter, hCtr1. J. Biol. Chem. *278*, 9639–9646.

Petrukhin, K., Lutsenko, S., Chernov, I., Ross, B.M., Kaplan, J.H., and Gilliam, T.C. (1994). Characterization of the wilson disease gene encoding a P-type copper transporting ATPase: Genomic organization, alternative splicing, and structure/function predictions. Hum. Mol. Genet. *3*, 1647–1656.

Polishchuk, E. V., Concilli, M., Iacobacci, S., Chesi, G., Pastore, N., Piccolo, P., Paladino, S., Baldantoni, D., van Ijzendoorn, S.C., Chan, J., et al. (2014). Wilson disease protein ATP7B utilized lysosomal exocytosis to maintain copper homeostasis. Dev Cell *29*, 686–700.

Prohaska, J.R., and Gybina, A.A. (2004). Intracellular copper transport in mammals. J. Nutr. *134*, 1003–1006.

Prohaska, J.R., Broderius, M., and Brokate, B. (2003). Metallochaperone for Cu,Zn-superoxide dismutase (CCS) protein but not mRNA is higher in organs from copper-deficient mice and rats. Arch. Biochem. Biophys. *417*, 227–234.

Pronicka, E., Piekutowska-Abramczuk, D., Szymańska-Debińska, T., Bielecka, L., Kowalski, P., Łuczak, S., Karkucińska-Wieckowska, A., Migdał, M., Kubalska, J., Zimowski, J., et al. (2013). The natural history of SCO2 deficiency in 36 Polish children confirmed the genotype-phenotype correlation. Mitochondrion *13*, 810–816.

Puig, S., Lee, J., Lau, M., and Thiele, D.J. (2002). Biochemical and genetic analyses of yeast and human high affinity copper transporters suggest a conserved mechanism for copper uptake. J. Biol. Chem. *277*, 26021–26030.

Rae, T.D., Schmidt, P.J., Pufahl, R.A., Culotta, V.C., and O'Halloran, T. V (1999). Undetectable intracellular free copper: the requirement of a copper chaperone for superoxidedismutase. Science *284*, 805–808.

Ramsden, C.A., and Riley, P.A. (2014). Tyrosinase: The four oxidation states of the active site and their relevance to enzymatic activation, oxidation and inactivation. Bioorganic Med. Chem. *22*, 2388–2395.

Rigby, K., Cobine, P.A., Khalimonchuk, O., and Winge, D.R. (2008). Mapping the functional interaction of Sco1 and Cox2 in cytochrome oxidase biogenesis. J. Biol. Chem. *283*, 15015–15022.

Roberts, E.A., Robinson, B.H., and Yang, S. (2008). Mitochondrial structure and function in the untreated Jackson toxic milk (tx-j) mouse, a model for Wilson disease. Mol. Genet. Metab. *93*, 54–65.

Robinson, N.J., and Winge D.R. (2010) Copper Metallochaperones. Annu. Rev. Biochem. *79*. 537-562.

Schaefer, M., Hopkins, R.G., Failla, M.L., and Gitlin, J.D. (1999). Hepatocyte-specific localization and copper-dependent trafficking of the Wilson's disease protein in the liver. Am. J. Physiol. *276*, G639–G646.

Schushan, M., Barkan, Y., Haliloglu, T., Ben-Tal, N. (2010). Cα-trace model of the transmembrane domain of human copper transporter 1, motion and functional implications. Proc. Natl. Acad. Sci. U.S.A. *107*, 10908-10913.

Shen, D., Dalton, T.P., Nebert, D.W., and Shertzer, H.G. (2005). Glutathione redox state regulates mitochondrial reactive oxygen production. J. Biol. Chem. *280*, 25305–25312.

Singleton, W.C.J., McInnes, K.T., Cater, M.A., Winnall, W.R., McKirdy, R., Yu, Y., Taylor, P.E., Ke, B.X., Richardson, D.R., Mercer, J.F.B., et al. (2010). Role of glutaredoxin1 and glutathione in regulating the activity of the copper-transporting P-type ATPases, ATP7A and ATP7B. J. Biol. Chem. *285*, 27111–27121.

Speno, H., Taheri, M.R., Sieburth, D., and Martin, C.T. (1995). Identification of essential amino acids within the proposed CuA binding site in subunit II of Cytochrome c oxidase. J. Biol. Chem. *270*, 25363–25369.

Sternlieb, I. (1968). Mitochondrial and fatty changes in hepatocytes of patients with Wilson's disease. Gastroenterology *55*, 354–367.

Stiburek, L., Vesela, K., Hansikova, H., Hulkova, H., and Zeman, J. (2009). Loss of function of Sco1 and its interaction with cytochrome c oxidase. Am. J. Physiol. Cell Physiol. *296*, C1218–C1226.

Stohs, S.J., and Bagchi, D. (1995). Oxidative Mechanisms in the Toxcity of Metal Ions. Free Radic. Biol. Med. *18*, 321–336.

Stone, S.J., Myers, H.M., Watkins, S.M., Brown, B.E., Feingold, K.R., Elias, P.M., Farese, R.V. Jr. (2004) Lipopenia and skin barrier abnormalities in DGAT2-deficient mice. J. Biol. Chem. *279*. 11767-

11776.

Strausak, D., La Fontaine, S., Hill, J., Firth, S.D., Lockhart, P.J., and Mercer, J.F. (1999). The role of GMXCXXC metal binding sites in the copper-induced redistribution of the menkes protein. J. Biol. Chem. *274*, 11170–11177.

Stroud, D.A., Maher, M.J., Lindau, C., Vögtle, F.N., Frazier, A.E., Surgenor, E., Mountford, H., Singh, A.P., Bonas, M., Oeljeklaus, S., et al. (2015). COA6 is a mitochondrial complex IV assembly factor critical for biogenesis of mtDNA-encoded COX2. Hum. Mol. Genet. *24*, 5404–5415.

Sturtz, L.A., Diekert, K., Jensen, L.T., Lill, R., and Culotta, V.C. (2001). A fraction of yeast Cu,Zn-superoxide dismutase and its metallochaperone, CCS, localize to the intermembrane space of mitochondria. A physiological role for SOD1 in guarding against mitochondrial oxidative damage. J. Biol. Chem. *276*, 38084–38089.

Timón-Gómez, A., Nývltová, E., Abriata, L.A., Vila, A.J., Hosler, J., and Barrientos, A. (2018). Mitochondrial cytochrome c oxidase biogenesis: Recent developments. Semin. Cell Dev. Biol. *76*, 163-178.

Tiranti, V., Hoertnagel, K., Carrozzo, R., Galimberti, C., Munaro, M., Granatiero, M., Zelante, L., Gasparini, P., Marzella, R., Rocchi, M., et al. (1998). Mutations of SURF-1 in Leigh Disease Associated with Cytochrome c Oxidase Deficiency. Am. J. Hum. Genet. *63*, 1609–1621.

Tzagoloff, A., and Dieckmann, C.L. (1990). PET Genes of Saccharomyces cerevisiae. Microbiol. Rev. *54*, 211–225.

Urbanska, A., Sadowski, L., Kalaidzidis, Y., and Miaczynska, M. (2011). Biochemical characterization of APPL Endosomes: The role of annexin A2 in APPL membrane recruitment. Traffic *12*, 1227–1241.

Valko, M., Rhodes, C.J., Moncol, J., Izakovic, M., and Mazur, M. (2006). Free radicals, metals and antioxidants in oxidative stress-induced cancer. Chem. Biol. Interact. *160*, 1–40.

Valnot, I., Osmond, S., Gigarel, N., Mehaye, B., Amiel, J., Cormier-Daire, V., Munnich, A., Bonnefont, J.P., Rustin, P., and Rötig, A. (2000). Mutations of the SCO1 gene in mitochondrial cytochrome c oxidase deficiency with neonatal-onset hepatic failure and encephalopathy. Am. J. Hum. Genet. *67*, 1104–1109.

Vashchenko, G., and MacGillivray, R.T.A. (2013). Multi-copper oxidases and human iron metabolism. Nutrients *5*, 2289–2313.

Vembar, S.S., and Brodsky, J.L. (2008). One step at a time: Endoplasmic reticulum-associated degradation. Nat. Rev. Mol. Cell Biol. *9*, 944–957.

Vesela, K., Hansikova, H., Tesarova, M., Martasek, P., Elleder, M., Houstek, J., and Zeman, J. (2004). Clinical, biochemical and molecular analyses of six patients with isolated cytochrome c oxidase deficiency due to mutations in the SCO2 gene. Acta Paediatr. *93*, 1312–1317.

Vest, K.E., Leary, S.C., Winge, D.R., and Cobine, P.A. (2013). Copper import into the mitochondrial matrix in Saccharomyces cerevisiae is mediated by Pic2, a mitochondrial carrier family protein. J. Biol. Chem. *288*, 23884–23892.

Vest, K.E., Wang, J., Gammon, M.G., Maynard, M.K., White, O.L., Cobine, J.A., Mahone, W.K., and Cobine, P.A. (2016). Overlap of copper and iron uptake systems in mitochondria in Saccharomyces cerevisiae. Open Biol. *6*, 150223.

Vidoni, S., Harbour, M.E., Guerrero-Castillo, S., Signes, A., Ding, S., Fearnley, I.M., Taylor, R.W., Tiranti, V., Arnold, S., Fernandez-Vizarra, E., et al. (2017). MR-1S Interacts with PET100 and PET117 in Module-Based Assembly of Human Cytochrome c Oxidase. Cell Rep. *18*, 1727–1738.

Voskoboinik, I., Mar, J., and Camakaris, J. (2003). Mutational analysis of the Menkes copper P-type ATPase (ATP7A). Biochem. Biophys. Res. Commun. *301*, 488–494.

Vulpe, C., Levinson, B., Whitney, S., Packman, S., and Gitschier, J. (1993). Isolation of a candidate gene for Menkes disease and evidence that it encodes a copper-transporting ATPase. Nat Genet *3*, 7–13.

Wang, R., and Brattain, M.G. (2007). The maximal size of protein to diffuse through the nuclear pore is larger than 60kDa. FEBS Lett. *581*. 3164–3170.

Wang, Y., Hodgkinson, V., Zhu, S., Weisman, G.A., and Petris, M.J. (2011). Advances in the understanding of mammalian copper transporters. Adv. Nutr. An Int. Rev. J. *2*, 129–137.

West, E.C., and Prohaska, J.R. (2004). Cu,Zn-superoxide dismutase is lower and copper chaperone CCS is higher in erythrocytes of copper-deficient rats and mice. Exp. Biol. Med. (Maywood). *229*, 756–764.

Wortmann, S.B., Koolen, D.A., Smeitink, J.A., van den Heuvel, L., and Rodenburg, R.J. (2015). Whole exome sequencing of suspected mitochondrial patients in clinical practice. J. Inherit. Metab. Dis. *38*, 437–443.

Yamaguchi, Y., Heiny, M.E.., Suzuki, M., and Gitlin, J.D. (1996). Biochemical characterization and intracellular localization of the menkes disease protein. Proc. Natl. Acad. Sci. U. S. A. *93*, 14030–14035.

Yoshimura, N., Kida, K., Usutani, S., and Nishimura, M. (1995). Histochemical localization of copper in various organs of brindled mice after copper therapy. Pathol. Int. *45*, 10–18.

Zhao, N., Zhang, A.-S., Worthen, C., Knutson, M.D., and Enns, C.A. (2014). An iron-regulated and glycosylation-dependent proteasomal degradation pathway for the plasma membrane metal transporter ZIP14. Proc. Natl. Acad. Sci. U. S. A. *111*, 9175–9180.

Zhou, B., and Gitschier, J. (1997). hCTR1: A human gene for copper uptake identified by complementation in yeast. Proc. Natl. Acad. Sci. U. S. A. *94*, 7481–7486.

Zhu, Z., Yao, J., Johns, T., Fu, K., De Bie, I., Macmillan, C., Cuthbert, A.P., Newbold, R.F., Wang, J.C., Chevrette, M., et al. (1998). SURF1, encoding a factor involved in the biogenesis of cytochrome c oxidase, is mutated in Leigh syndrome. Nat. Genet. *20*, 337–343.

Zischka, H., and Lichtmannegger, J. (2014). Pathological mitochondrial copper overload in livers of Wilson's disease patients and related animal models. Ann. N. Y. Acad. Sci. *1315*, 6–15.